

1 Pliocene-Quaternary volcanic rocks of NW Armenia:
2 magmatism and lithospheric dynamics within an active
3 orogenic plateau

4
5 **I. Neill^{1*}, Kh. Meliksetian², M.B. Allen¹, G. Navarsardyan², S. Karapetyan²**

6
7 ¹Department of Earth Sciences, Durham University, Science Site, DH1 3LE, Durham, UK

8 ²Institute of Geological Sciences, National Academy of Sciences of Armenia, Marshal
9 Baghramian Avenue, Yerevan 0019, Armenia

10

11 *Corresponding author. E-mail: iain.neill@durham.ac.uk. Phone: +44 1913 342356.

12

13 ***Abstract***

14

15 *The Pliocene-Quaternary volcanic rocks of Armenia are a key component of the Arabia-*
16 *Eurasia collision, representing intense magmatism within the Turkish-Iranian plateau, tens*
17 *of millions of years after the onset of continental collision. Here we present whole rock*
18 *elemental and Nd-Sr isotope data from mafic, intermediate, and felsic lava flows and cinder*
19 *cones in Shirak and Lori provinces, NW Armenia. Magmatism appears to be controlled*
20 *locally by extension related to major strike-slip faults within the plateau. Major and trace*
21 *element results show that the three series – valley-filling medium-K alkali basalt flows, ridge-*
22 *forming andesite to rhyolite flows, and andesitic cinder cones – form a compositional*
23 *continuum linked by a crystallisation sequence dominated by two pyroxenes, plagioclase and*
24 *amphibole. There is petrographic and major and trace element evidence for magma mixing*

25 *processes and potentially crustal contamination by Mesozoic-early Cenozoic arc-related*
26 *rocks, which has not significantly affected the isotopic signature. Modelling of the basaltic*
27 *rocks indicates that they formed by moderate degrees of partial melting (~3-4 %) of an*
28 *incompatible element enriched, subduction-modified, lithospheric mantle source. Samples*
29 *have a distinctive high Zr/Hf ratio and high Zr concentrations, which are an intrinsic part of*
30 *the source or the melting process, and are much more commonly found in ocean island*
31 *basalts. Regional models for magmatism often argue for whole-scale delamination of the*
32 *mantle lithosphere beneath Eastern Anatolia and the Lesser Caucasus, but this scenario is*
33 *hard to reconcile with limited crustal signatures and the apparent lack of asthenospheric*
34 *components within many studied centres.*

35

36 ***Highlights***

37

- 38 - Whole-rock study of Pliocene-Quaternary lavas from the Armenian Highlands
- 39 - Compositional range controlled by fractional crystallisation, magma mixing and
40 possible crustal contamination
- 41 - Low-degree melting of a shallow metasomatised lithospheric mantle source
- 42 - Exploring triggers for <10 Myr increase in magmatic activity in the Arabia-Eurasia
43 collision zone

44

45 ***Keywords***

46

47 *Armenia; geochemistry; petrogenesis; orogenic plateau*

48

49 **1. Introduction**

50

51 Orogenic plateaus such as the modern Turkish-Iranian, Bolivian Altiplano-Puna and Tibetan
52 plateaus form in response to plate convergence and collision, and represent a primary
53 topographic feature of the continents. In spite of their thickened crust, plateaus are also sites
54 of intense, ultimately mantle-derived magmatism (e.g. Williams et al., 2004; Mo et al., 2007).
55 Such magmatism is often attributed to asthenospheric upwelling following the break-off of
56 the subducted oceanic slab (e.g. Keskin, 2003), or the delamination of the lithosphere inboard
57 of the plate suture (e.g. Kay and Kay, 1993).

58

59 The Turkish-Iranian plateau (Fig. 1) is a product of the Cenozoic Arabia-Eurasia
60 collision, and magmatism post-dating initial collision is particularly voluminous from the
61 Late Miocene until the present day, in numerous locations across eastern Turkey, Armenia,
62 and much of Iran (Fig. 1). Erupted products range from mafic to felsic, and sodic to
63 ultrapotassic (Pearce et al., 1990; Karapetian et al., 2001; Davidson et al., 2004; Azizi and
64 Moinevaziri, 2009; Saadat et al., 2011; Saadat and Stern, 2012; Allen et al., 2013). In nearby
65 Georgia and the Greater Caucasus, the most recent magmatism appears to have started
66 slightly earlier, in the Middle Miocene, and continued with some gaps in the record until
67 recent times (Lebedev et al., 2006a,b; 2007; 2008a,b; Adamia et al., 2011).

68

69 This plateau-wide ‘recent’ magmatism may be only partly explained by partial
70 melting of asthenospheric or mantle lithosphere sources due to break-off of the southern Neo-
71 Tethys slab (e.g. Keskin, 2003; 2007; Şengör et al., 2008; Dilek et al., 2010; van Hunen and
72 Allen, 2011). Miocene to recent magmatism extends to at least 500 km from the Bitlis-Zagros
73 suture zone, a spatial scale akin to the Cenozoic ‘ignimbrite flare-up’ of the western United
74 States (Johnson, 1991). The wide extent of Miocene-Quaternary magmatism hundreds of

75 kilometres from the suture zone indicates that whole-scale lithospheric delamination (Pearce
76 et al., 1990), or other unrecognised processes may be collectively responsible for magmatism
77 in this region.

78

79 To further consider the origin of such magmatism, this paper focuses on Armenia
80 (Fig. 1), where recent volcanism has been under-represented in the international literature.
81 We present whole rock elemental and Nd-Sr isotope data from three series of mafic to felsic
82 Pliocene-Quaternary volcanic rocks in the north of Shirak and west of Lori administrative
83 provinces in the northwest of the country (herein referred to as 'Shirak') (Fig. 2). The local
84 tectonic setting and relationship to magmatism is highlighted, alongside discussion on
85 magmatic evolution, mantle sources and partial melting. We finish by assessing how the
86 results fit with regional geodynamic models.

87

88 **2. Geological setting, structure, and petrography**

89

90 2.1. The Turkish-Iranian plateau

91

92 The Turkish-Iranian orogenic plateau (Fig. 1) developed following the closure of the Neo-
93 Tethys Ocean (Şengör and Kidd, 1979). The basement of the plateau consists of Mesozoic to
94 Early Cenozoic accretionary belts and arc rocks and also older, Gondwanaland-related micro-
95 continental fragments that all accreted to the southern margin of Eurasia. It is widely assumed
96 that the Neo-Tethys oceanic crust was divided into a northern and a southern segment; the
97 former closed either during the Late Cretaceous (Lordkinpanidze, 1980; Keskin, 2008) or the
98 Paleocene-Early Eocene (Sosson et al., 2010). The two segments of Neo-Tethys were
99 separated by micro-continental fragments such as the South Armenian Block and Tauride-

100 Anatolide terranes (Sosson et al., 2010). Destruction of the southern segment of Neo-Tethys
101 brought Arabia and Eurasia together along the Bitlis-Zagros suture zone (Fig. 1).

102

103 The timing of initial collision between Arabia and Eurasia is debated, although most
104 estimates range between 35 and 20 Ma (Agard et al., 2005; Allen and Armstrong, 2008;
105 Morley et al., 2009; Okay et al., 2010; Ballato et al., 2011; McQuarrie and van Hinsbergen,
106 2013). Marine carbonates deposited across much of central Iran and eastern Turkey in the
107 Early Miocene indicate that growth of the orogenic plateau is a later phenomenon (Bottrill et
108 al., 2012). Deformation is presently focussed on the plateau margins, from the Greater
109 Caucasus and Alborz in the north to the Zagros in the south, with no active crustal thickening
110 or thinning occurring between (Jackson et al., 1995; Allen et al., 2011). Lithospheric
111 thickness is highly variable, from >200 km in Iran near the Zagros suture, to only 60 km or
112 less in eastern Anatolia (Priestley and McKenzie, 2006; Angus et al., 2006). The current
113 height of the plateau, ~1750 m above sea level, has been attributed to a combination of Late
114 Cenozoic crustal shortening, and also to the detachment of mantle lithosphere and/or
115 subducted Tethyan slabs beneath the plateau, allowing the upwelling of hot, buoyant
116 asthenosphere beneath the region (Keskin, 2003).

117

118 The Cenozoic magmatic record of the plateau is divided into several stages (see Dilek
119 et al., 2010; Chiu et al., 2013 for reviews). First is an Eocene ‘flare-up’ of arc magmatism
120 immediately prior to the onset of continental collision, focussed predominantly on the
121 Urumieh-Dokhtar arc in southwest Iran, the Lut Block, Kopeh Dag and Alborz regions of
122 eastern and northern Iran (Verdel et al., 2011), and also in Armenia (Lordkinpanidze et al.,
123 1988). The flare-up has been attributed to back-arc extension (Vincent et al., 2005), an
124 episode of flat subduction (Berberian and Berberian, 1981), perhaps coupled with enhanced

125 slab roll-back (Verdel et al., 2011), or break-off of the northern Neo-Tethyan slab in Armenia
126 and North-Central Turkey (Keskin et al., 2008; Sosson et al., 2010). The second stage is a
127 magmatic ‘gap’ which comprised some 20-30 Myr of limited magmatic activity between the
128 Eocene and the Late Miocene as continental collision proceeded (Verdel et al., 2011;
129 Richards et al., 2011). The third and final stage is the aforementioned upsurge of mantle-
130 derived volcanism from the Middle to Late Miocene until the present day (Chiu et al., 2013),
131 which forms the basis of this study.

132

133 2.2. Basement and structure in Armenia

134

135 Armenia, including the Lesser Caucasus mountain range, lies at the northern side of the
136 plateau (Figs. 1, 2). Southern Armenia is underlain by the aforementioned South Armenian
137 Block (SAB), a micro-continental fragment rifted during the early Mesozoic, separating the
138 northern and southern branches of the Neo-Tethyan seaway (Stampfli, 2000). The SAB
139 consists of Proterozoic gneisses, mica schists and amphibolites partially overlain by
140 Devonian to Jurassic sediments, Jurassic and younger ophiolitic material, and Paleocene to
141 Early Oligocene volcanic rocks related to subduction of the southern branch of Neo-Tethys
142 (Rolland et al., 2009). In the north of Armenia, the Armenian Highlands represent the former
143 active continental margin of Eurasia and contain arc and discontinuous ophiolite sequences
144 formed during the closure of the northern branch of the Neo-Tethyan seaway (Adamia et al.,
145 1981; 2011). The largest tract of ophiolitic material in Armenia forms the Sevan-Akera suture
146 zone, a 400 km-long boundary between the SAB and the Mesozoic arc of the Lesser
147 Caucasus to the north. Immediately south of our field area, between Amasia and Stepanavan,
148 is a belt of blueschist-facies mélangé (part of the Sevan-Akera ophiolite suite), tectonically

149 overlain by Jurassic to Cretaceous mafic rocks, and two sequences of Cretaceous to Early
150 Oligocene subduction-related volcano-sedimentary rocks (Rolland et al., 2009).

151

152 Following the Eocene amalgamation of the Armenian crustal blocks (Rolland et al.,
153 2009), north-directed subduction of the southern Neo-Tethys terminated along the Bitlis-
154 Zagros suture, some 300 km south of Armenia. After the last subduction-related magmatism,
155 the magmatic ‘gap’ in Armenia extended until the Late Miocene (~10 Ma), based on
156 groundmass and mineral K-Ar ages from the oldest volcanic rocks of the Gegham Highlands
157 (Arutyunyan et al., 2007). The most voluminous volcanism is of Pliocene-Quaternary age,
158 covering much of Aragatsotn, Shirak, Kotayk, Gegharkunik, and Syunik provinces, an area
159 >10,000 km² (Mitchell and Westaway, 1999; Karapetian et al., 2001; Lebedev et al., 2011)
160 (Fig. 2).

161

162 2.3. Pliocene - Quaternary magma series

163

164 The geology of NW Armenia was first studied in detail during Soviet times (Kharazyan,
165 1983). The oldest Pliocene – Quaternary volcanism is represented by poorly-exposed
166 rhyolites and obsidians at Aghvorik (Fig. 2), covered by dolerites which drape much of the
167 lowest topography in Shirak, often part-filling river valleys for tens of kilometers.
168 Relationships with sedimentary deposits dated using mammalian fossils lead authors to
169 conclude that these mafic lavas were of Late Pliocene age (Kharazyan, 1983 and references
170 therein). A K-Ar age determination from dolerite from the Akhurian river basin within our
171 study area gave a result of 2.5 ± 0.2 Ma (Chernyshev et al., 2002). Groundmass K-Ar results
172 from numerous mafic to felsic volcanic rocks across the Javakheti Highlands in southern
173 Georgia gave ages of 4.6 ± 0.2 to 1.54 ± 0.10 Ma (Late Pliocene to Quaternary) (Lebedev et

174 al., 2008a,b). The mafic rocks in Armenia and southern Georgia may have resulted from
175 fissure eruptions (Jrbashyan et al., 1996), but the actual source of these lavas has never been
176 found, and may be buried by younger flows.

177

178 On top of the plateau-like topography formed by the mafic flows in Shirak, are hills of
179 intermediate-felsic composition of up to 600 m prominence, including the north-south
180 trending Javakheti, or Kechut, ridge (Fig. 2). Kharazyan (1983) distinguished two units
181 within the Armenian part of the Javakheti ridge. The first unit (Lower Kechut Suite) is said to
182 contain two-pyroxene basaltic andesites, andesites and hornblende andesites which cover the
183 valley series and are thus assumed to be of Early Pleistocene age (Kharazyan, 2005).
184 SHRIMP U-Pb zircon dating of andesitic vent-proximal ash and breccia layers deposited on
185 the eastern flank of the Javakheti ridge in Lori province at the Karakhach archaeological site
186 (Fig. 2) gives maximum eruption ages of 1.94 ± 0.05 to 1.80 ± 0.03 Ma (Presnyakov et al.,
187 2012). This study also noted two Eocene zircons (40-50 Ma) consistent with Eocene arc
188 rocks found to the east of the study area, plus five Proterozoic grains, consistent with an
189 origin in the underthrust SAB. It is uncertain whether or not these old grains were from
190 xenoliths ripped up during explosive volcanism or zircons assimilated during magma ascent.
191 The Javakheti Ridge extends into southern Georgia, where it is higher and has a sharp little
192 denuded topographic profile compared to further south. Groundmass K-Ar dating revealed
193 younger ages of <1 Ma for the Samsari volcanic centre to the north of the Javakheti Ridge
194 (Chernyshev et al., 2006). Kharazyan (1983) also defined an Upper Kechut Suite supposedly
195 containing lavas erupted from cinder cones on the western part of the ridge, and considered to
196 be of Middle Pleistocene age (Kharazyan, 2005). We did not find clear evidence of this unit
197 during our studies. The only other Pliocene-Quaternary volcanic products in this part of
198 Shirak are cinder cones to the west of the Javakheti Ridge around Lake Arpi (Fig. 2), which

199 are estimated to be of Early-Middle Pleistocene age, based on relationships with the mafic
200 rocks and some river terraces (Kharazyan, 1983).

201

202 Overall there have been no comprehensive geochronological studies carried out in
203 Shirak using a single reliable technique, unlike those for similar sequences in Georgia
204 (Lebedev et al., 2008a,b). A lack of continuous exposure hampers judgement of the relative
205 age of the different lavas. We have decided to sub-divide the entire Pliocene-Quaternary suite
206 close to the Javakheti Ridge into three components: mafic flows (the dolerites) largely
207 covering the topography developed on the basement (herein termed the *Valley Series*); more
208 evolved flows built up into hills above the mafic flows (*Ridge Series*); and scattered cinder
209 cones (*Cone Series*) (Fig. 2).

210

211 2.3.1. *Valley Series*

212

213 The Valley Series consists of mafic flows with a maximum cumulative thickness of 200 m in
214 eastern Lori province (Fig. 2). In the study area, the exposed sequence comprises at most four
215 or five stacked flows up to 40 m thick in total, and directly overlies the Sevan-Akera suture
216 and ophiolite sequence in the Dzoraged gorge and near Amasia (Fig. 2). We have collected
217 samples from these locations, as well as from Lake Arpi and near Tashir in western Lori
218 Province (Fig. 2). Valley Series samples collected from near Lake Arpi, Amasia, and Tashir
219 (Fig. 2), consist of vesicular sub-ophitic dolerites with rare clinopyroxene or optically zoned
220 plagioclase phenocrysts, set in a groundmass of 1-2 mm grain size consisting of
221 clinopyroxene, plagioclase and oxides (see Supplementary Item 1). Clinopyroxene is
222 commonly rimmed or almost totally replaced by red-brown amphibole, and there is
223 occasional interstitial quartz and rare rounded quartz blebs. Some samples contain very rare

224 iddingsite crystals, and the few olivines found in thin section are rounded and <0.5 mm in
225 diameter.

226

227 2.3.2. Ridge Series

228

229 Magmatism in this series is restricted to intermediate to felsic lavas built up into prominent
230 topographic features. The highest of these is the north to south-trending Javakheti Ridge (Fig.
231 2), consisting of rounded and glacially eroded peaks reaching ~3100 m above sea level,
232 following a clear north-south trend running north into Georgia (Fig. 2). A second series of
233 hills lie north of the Akhuryan River parallel to the Georgian border, but these are more
234 topographically muted, reaching a maximum elevation of ~2400 m. Rock types from both
235 ridges are almost exclusively andesitic to dacitic flows, with rare black dacites and rhyolitic
236 obsidians (Karapetian et al., 2001). Analysed flows range from basaltic trachyandesites to
237 dacites, and there is much compositional and textural variation. Some of the least evolved
238 samples (<60 wt.% SiO₂) contain 1-3 mm phenocrysts and glomerocrysts of clinopyroxene
239 (rarely orthopyroxene) and plagioclase, set in a flow-banded groundmass of plagioclase,
240 clinopyroxene and Fe-Ti oxides, with accessory apatite and zircon. More evolved samples
241 tend to contain significantly more plagioclase phenocrysts, and several have abundant 1-3
242 mm euhedral green-brown pleochroic amphiboles, but the presence of amphibole is not
243 ubiquitous even in samples of similar SiO₂ and MgO concentrations. Many plagioclase
244 crystals are sieve-textured and some have corroded margins, usually taken to imply the
245 occurrence of magma mixing processes (Tsuchiyama, 1985; Tepley et al., 1999), and many
246 crystals are also optically zoned. Other evidence for magma mixing is the common
247 occurrence of rounded quartz blebs with dark reaction coronas, and ubiquitous opaque rims
248 on primary hornblende crystals (Tepley et al., 1999; Supplementary Item 1). A black dacite

249 contains a few clinopyroxene glomerocrysts, but mostly consists of a fine-grained
250 groundmass dominated by prismatic to acicular feldspars. The Ridge Series includes the only
251 crustal xenoliths noted from our sampling, at a single site near Darik, north of Lake Arpi
252 (Fig. 2). The xenoliths consist of a coarse-grained groundmass of plagioclase, clinopyroxene,
253 oxide, and rare iddingsite after olivine; and 2-3 mm phenocrysts of clinopyroxene and
254 plagioclase, most consistent with inclusion of material from the Valley Series. A slight
255 chilled margin is observed within the host.

256

257 *2.3.3. Cone Series*

258

259 Scattered cinder cones are present in the Akhuryan valley near Lake Arpi (Fig. 2), often tens
260 of metres high and several hundred metres across. We have collected samples from Sepasar,
261 Eznasar, and Kaputkogh cones (Fig. 2). Most are composed of poorly welded unsorted glass
262 or scoria fragments, and more coherent scoria bombs reaching a few tens of centimetres in
263 diameter. The Cone Series compositions mirror the least evolved of the ridge series, the
264 majority of samples containing differing proportions of plagioclase and clinopyroxene as
265 phenocrysts and groundmass (Supplementary Item 1). Bombs from Kaputkogh and Eznasar
266 contain ubiquitous mm-scale rounded quartz xenocrysts, whereas those at Sepasar appear
267 more mafic, and devoid of foreign material.

268

269 **3. Analytical methods**

270

271 Samples were powdered in an agate ball mill at Durham University. Major element analysis
272 was conducted on fused glass beads using a PANalytical Axios Advanced X-Ray
273 Fluorescence (XRF) spectrometer at the University of Leicester. Leftover fractions of the

274 powder from XRF analysis were digested using a standard HF and HNO₃ technique prior to
275 trace element analysis. Solutions were run on a Thermo X2 inductively-coupled plasma mass
276 spectrometer (ICP-MS) at the Northern Centre for Isotopic and Elemental Tracing (NCIET)
277 at Durham University. Accuracy, precision, and reproducibility were monitored using blanks,
278 multi-run and within-run duplicates, Re-Rh spike solutions, and five international reference
279 standards. Standard W2 (n = 15) gave first relative standard deviations of 5% or better for
280 most transition metals (excepting 10% for Sc, 12% for Cr, 6% for Ni), the large ion lithophile
281 elements (LILE) and the rare earth elements (REE) (7% for La, 6% for Ce). Elemental results
282 are recorded in Table 1 and Supplementary Item 2, the latter also containing standard results.

283

284 Radiogenic Nd and Sr isotope analysis was conducted at NCIET, with column
285 chemistry for elemental pre-concentration based on the method of Dowall et al. (2007).
286 Powders were digested in HF and HNO₃, and solutions run through 1 ml pipettes containing
287 several drops of dilute Sr-spec resin to collect the Sr-bearing fraction. The high field strength
288 element (HFSE)- and rare earth element (REE)-bearing fraction from these columns was run
289 through 10 ml Bio-Rad polypropylene columns containing 1 ml of Bio-Rad AG1-X8 200-400
290 mesh anion-exchange resin. Neodymium was collected as part of a general rare earth element
291 fraction. Analysis was conducted on a Thermo Neptune Mass Collector ICP-MS. Strontium
292 was run in a single batch during which time blanks averaged 88 pg Sr (n = 6). International
293 reference standard NBS987 gave a mean of $^{87}\text{Sr}/^{86}\text{Sr} = 0.710263 \pm 0.000012$ (2σ , n = 12),
294 comparable to a preferred value of 0.710240, and providing a minimum uncertainty of
295 16 ppm (2σ). No correction was applied to the final results. Neodymium was run in two
296 separate batches, with blanks averaging 10 pg Nd (n = 6). During the first run, a combination
297 of the J&M standard and a Sm-doped version gave a mean $^{143}\text{Nd}/^{144}\text{Nd} = 0.511098 \pm$
298 0.000007 (2σ , n = 13), and a minimum uncertainty of 13 ppm (2σ). During the second run,

299 $^{143}\text{Nd}/^{144}\text{Nd} = 0.511100 \pm 0.000007$ (2σ , $n = 13$), giving an uncertainty of 14 ppm (2σ). For
300 consistency between the runs, all results were normalised to a preferred value of 0.511110.
301 Results are presented in Table 2.

302

303 **4. Geochemistry**

304

305 4.1. Sample freshness

306

307 We collected the freshest available samples at each locality, and this is reflected in loss-on-
308 ignition (LOI) values typically <1 wt.%, mostly un-weathered feldspars and mafic minerals,
309 and an overall lack of sericite and chlorite in thin section. Major and trace element data,
310 particularly element vs. SiO_2 plots (see Section 4.2), have trends consistent with magmatic
311 processes, particularly for CaO, MgO, K_2O , and Na_2O , as opposed to the widespread scatter
312 expected during sub-solidus alteration which easily mobilises these elements (e.g. Cann,
313 1970; Pearce, 1996). $^{87}\text{Sr}/^{86}\text{Sr}$ isotope results are commonly affected by hydrothermal
314 alteration, but here are depleted with no sign of a trend towards high $^{87}\text{Sr}/^{86}\text{Sr}$ at constant
315 $^{144}\text{Nd}/^{143}\text{Nd}$ (Table 2); nor is there a correlation between LOI and isotopic ratios.
316 Furthermore, the samples were erupted in an intra-continental high plateau so have not
317 interacted with high $^{87}\text{Sr}/^{86}\text{Sr}$ seawater or been exposed to tropical weathering.

318

319 4.2. Major and trace element characteristics

320

321 4.2.1. Valley Series

322

323 The Valley Series lavas (~49-55 wt.% SiO₂) are mostly mildly alkaline trachybasalts based
324 on the total alkali-silica classification (Le Bas et al., 1986; Fig. 3a), and belong to the
325 medium-K series of Peccerillo and Taylor (1976; Fig. 3b). They are evolved, with 4-7 wt.%
326 MgO and low molar Mg# from 46 to 58. Overall the samples have low TiO₂, moderate-high
327 Al₂O₃, and a sodic character (Na₂O/K₂O = 2.7-4.1) (Fig. 4). Trace element abundances and
328 trends can be seen on Figure 5. Also, the lavas have low Sc (<25 ppm), moderate Cr, Ni, and
329 large ion lithophile element (LILE) abundances (e.g. Ba = 280-450 ppm and Sr = 540-720
330 ppm). Chondrite-normalised (CN) REE abundances are light REE (LREE) enriched
331 (La/Yb_{CN} = 5-9; calc-alkaline), with flat heavy REE (HREE) patterns around 15-20 times
332 chondritic abundances (Fig. 6a). The patterns are split into two groups, one with lower LREE
333 and higher HREE concentrations and vice versa, the patterns crossing over at around Pr-Nd.
334 There are some very slight negative Eu anomalies relative to the MREE. The extended
335 Primitive Mantle-normalised (PMN) plot (Fig. 6b) shows that the samples have spiky LILE
336 patterns (modest positive Ba, Rb, Th, Sr anomalies), prominent negative K, Nb-Ta, and Ti
337 anomalies and positive Zr-Hf anomalies relative to the REE, with super-chondritic Zr/Hf
338 ratios of 47-55.

339

340 4.2.2. Ridge Series

341

342 The more evolved Ridge Series (~57-68 wt.% SiO₂, 2-5 wt.% MgO, Mg# = 41-55) has a
343 wide range of sub-alkaline compositions from basaltic trachy-andesite through to dacite (Fig.
344 3a). Samples largely belong to the medium-K series, although two plot in the high-K field
345 (Fig. 3b). They have noticeably lower TiO₂, Fe₂O_{3(t)} and P₂O₅ concentrations compared to the
346 valley series, and are slightly less sodic (Na₂O/K₂O = 1.4-2.5) (Fig. 4). Transition metal
347 abundances are lower than the Valley Series, but the Ridge Series has higher Ba and Zr and

348 lower Sr and Nb concentrations compared to the mafic lavas (Fig. 5). Chondrite-normalised
349 LREE patterns (Fig. 6c) are similar to the Valley Series, again splitting into two groups with
350 higher or lower LREE concentrations. Ridge samples have La/Yb_{CN} from 8 to 18, with a
351 highly fractionated M-HREE distribution such that some samples have a U-shaped pattern.
352 There are small negative Eu anomalies. Primitive Mantle-normalised patterns (Fig. 6d) differ
353 slightly from the Valley Series in having positive Rb spikes, and more pronounced negative
354 Nb-Ta, P and Ti anomalies.

355

356 *4.2.3. Cone Series*

357

358 The Cone Series splits into three groups, the most mafic being the two cones at Sepasar (58
359 wt.% SiO_2 , but low Mg# = 43), and the most felsic at Eznasar (62 wt.% SiO_2 , Mg# = 52). The
360 large cone at Kaputkogh has intermediate silica content relative to the other cones, although it
361 has the highest Mg# of 54. The cones have higher Nb and Zr concentrations relative to the
362 other series (Fig. 5); REE patterns for the Cone Series are clearly bimodal (Fig. 6e), whilst
363 the Primitive Mantle-normalised plots look similar to the Valley Series (Fig. 6f).

364

365 *4.3. Radiogenic isotope geochemistry*

366

367 Most samples span a narrow range from $^{87}Sr/^{86}Sr = 0.70416$ to 0.70446 and $^{143}Nd/^{144}Nd =$
368 0.51280 to 0.51287 , giving a range of values in epsilon notation from $\epsilon Nd = +3.1$ to $+4.6$. No
369 age corrections were applied owing to the young age of the rocks. On Figure 7a, there is
370 overlap between samples from the Valley, Ridge, and Cone series, and the samples display
371 only a little isotopic enrichment with major element evolution (Fig. 7b). Overall, the samples
372 lie on the mantle array between bulk silicate earth and depleted MORB mantle, and there is

373 no clear evidence of any trends which might be related to mixing of different mantle end
374 members (e.g. EMI or EMII) or old, isotopically enriched crustal contaminants. The Cone
375 and Ridge Series samples containing quartz xenocrysts are not isotopically different from the
376 other samples.

377

378 Regionally, the samples are significantly more depleted than most Pliocene-
379 Quaternary centres in north-west Iran and Mount Damavand (Alborz), and Tendürek volcano
380 in Eastern Anatolia (Fig. 7a). The Iranian volcanic rocks were erupted through thicker
381 lithosphere than beneath Armenia (e.g. Liotard et al., 2008; Kheirkhah et al., 2009; Mirnejad
382 et al., 2010; Davidson et al., unpublished data; Allen et al., 2013). Samples are also more
383 depleted than asthenospheric melts from eastern Iran which have trends towards the EM-II
384 mantle end member (Saadat et al., 2011; Saadat and Stern, 2012). Instead, results are closest
385 to the few analyses conducted on the large stratovolcano, Mount Ararat, close to the
386 Armenian border (Pearce et al., 1990; Kheirkhah et al., 2009), and nearly identical in terms of
387 $^{143}\text{Nd}/^{144}\text{Nd}$ to six analyses of the ~3.25-2.05 Ma valley series lavas from southern Georgia,
388 and from eight Late Miocene sub-alkaline basalts in central Georgia (Lebedev et al., 2006;
389 2007). Radiogenic isotope results are not yet widely published from other Armenian
390 Pliocene-Quaternary centres, but Savov et al. (2007) and Lin et al. (2011) reported values
391 from $^{87}\text{Sr}/^{86}\text{Sr} = 0.7041$ to 0.7051 and $^{143}\text{Nd}/^{144}\text{Nd} = 0.5128$ to 0.5129 from various locations.

392

393 **5. Discussion**

394

395 5.1. Volcano-tectonic interaction

396

397 Before considering the petrogenesis of the magma series, we first address the location of
398 volcanic activity with respect to major crustal structures. The internal part of the orogenic
399 plateau is not undergoing contractile deformation (Jackson et al., 1995; Vernant et al., 2004),
400 but internal reorganisation of the plateau during the on-going convergence between Arabia
401 and Eurasia means that Eastern Anatolia, the Lesser Caucasus, and northwest Iran are criss-
402 crossed by numerous active strike-slip fault systems (Rebaï et al., 1993; Koçyiğit et al.,
403 2001). These systems, which often tally with pre-existing crustal discontinuities, have been
404 widely implicated in providing a locus for Quaternary magmatic activity through the
405 production of highly localised pull-apart zones (Dewey et al., 1986; Karakhanian et al., 1997,
406 2002; Avagyan et al., 2010; Shabanian et al., 2012).

407

408 In Armenia, the active Pambak-Sevan-Syunik right-lateral strike-slip fault system is
409 one such structure exploiting the existing discontinuity of the Sevan-Akera suture zone (Fig.
410 2). All of the magmatism described in this study originated just to the north of the fault zone,
411 and so we propose that this location sat over a region of localised upper crustal extension at
412 the time of magmatism. No active extension is recorded from the Shirak region from
413 earthquake focal mechanisms or geomorphic features. Blanket coverage of most pre-existing
414 fault structures by the Valley Series, and the absence of linear arrays of cinder cones (e.g.
415 Dewey et al., 1986), may have helped obscure this association between faulting and
416 magmatism. The south-eastern termination of the Pambak-Sevan-Syunik fault in the Syunik
417 region is characterised by widespread volcanism in the area south of the fault, with little
418 volcanism to the north (Kharakhanian et al., 2004). The Syunik centres therefore appear to
419 have developed along the complementary trailing imbricate fan (Woodcock and Fischer,
420 1986) to the Shirak volcanic rocks. The north-south trending volcanism along the Javakheti
421 Ridge is consistent with this idea.

422

423 Not all young Armenian centres fit a simple fault-control hypothesis: Aragats
424 volcano, the largest centre in the country, is situated in a region apparently not crossed by
425 presently-active faults (Kharakhanian et al., 2004). It is possible that older faults may be
426 obscured by lava flows, or that some other control on the location of Aragats may apply, such
427 as a local thin-spot in the lithosphere which focussed melting beneath the plateau.

428

429 5.2. Fractionation and contamination processes

430

431 *5.2.1. Fractional crystallisation – minerals involved*

432

433 No sample from the mafic Valley Series lavas is close to a primary melt (MgO is typically <
434 7 wt.%), so it is assumed that they have already evolved at depth involving a typical
435 fractionation assemblage of olivine and spinel. In the major element data, clear falling trends
436 for the Valley Series against typical indices of fractionation, such as SiO₂, TiO₂, MgO, and
437 CaO (Fig. 4), corroborate with the observed mineral assemblages in confirming that clino-
438 and orthopyroxene and Fe-Ti oxides were important in Valley Series evolution. Al₂O₃
439 concentrations cover a narrow range with no trends, indicating that feldspar fractionation was
440 not an important feature of the Valley Series; likewise with P₂O₅ concentrations and apatite.
441 Trace element abundances, such as Ba, Th, and La, display rising trends against SiO₂ in the
442 Valley Series, which confirms their incompatible behaviour (Fig. 5). In the more evolved
443 Ridge and Cone Series, clear falling trends emerge against SiO₂ for Al₂O₃, P₂O₅, Sr, Nb, Zr
444 and La, pointing to addition of plagioclase, along with small proportions of zircon and
445 apatite, to the fractionating assemblage.

446

447 The overall pattern of Shirak magmatism can be compared with Eastern Anatolia.
448 Volcanic centres that display either high- or low-Y trends relative to Rb, are associated with
449 fractionation of anhydrous (plagioclase, olivine, pyroxenes, and magnetite), or hydrous
450 assemblages (including amphibole, which is compatible with Y) respectively (Pearce et al.,
451 1990) (Fig. 8). The mafic Valley Series rocks in Shirak follow the same moderate to low-Y
452 trend as the Kars plateau/Mt. Ararat systems, which may indicate amphibole fractionation has
453 taken place at depth, given that amphibole is not seen in any of the Valley Series thin
454 sections. Another indication of amphibole fractionation is the compatible middle to heavy
455 REE (Sm-Lu) showing falling trends as the three series evolve (Fig. 6). The ridge series lavas
456 have a steeply falling trend for Y against Rb, which may reflect increased partition
457 coefficients for both clinopyroxene and amphibole for Y as these minerals fractionate from
458 more evolved rocks (Pearce et al., 1990).

459

460 *5.2.2. Magma mixing*

461

462 The petrographic evidence for magma mixing (zoned plagioclases, sieve textures,
463 reaction rims and quartz blebs) also needs to be reconciled with geochemical data. Major
464 element plots, especially TiO₂, CaO and MgO vs. SiO₂ (Fig. 4) have straight line trends
465 which are widely associated with mixing of two compositionally distinct magmas (Langmuir
466 et al., 1978), rather than the curved trends associated with fractional crystallisation. In the
467 field, the key observation is that the most evolved rocks found in the area, the obsidians at
468 Agvorik, underlie the mafic Valley Series, so felsic magmas had already been erupted by the
469 time of mafic magma injection.

470

471 *5.2.3. Crustal contamination*

472

473 Many models (e.g. Keskin et al., 1998) consider assimilation-fractional crystallisation (AFC)
474 processes to be important in magma genesis in the plateau. Keskin et al. (1998) argue that
475 recent mafic to felsic samples from Eastern Anatolia have undergone significant amounts of
476 AFC coinciding with enriched $^{87}\text{Sr}/^{86}\text{Sr}$ ratios up to 0.7065 (Pearce et al., 1990). In Shirak,
477 samples have only a slight variation in isotope ratios relative to SiO_2 (Fig. 7b), and samples
478 containing quartz xenocrysts do not have different isotopic ratios to the other lavas - a feature
479 that should strongly support the hypothesis that fractionation and magma mixing were the
480 dominant processes. Also, preliminary results from elsewhere in Armenia, including the
481 Aragats volcanic system, show little clear isotopic evidence for contamination (Savov et al.,
482 2007; Lin et al., 2011) in spite of Aragats erupting through the SAB basement which has
483 enriched $^{87}\text{Sr}/^{86}\text{Sr}$ ratios of up to 0.7303 - any contamination should be easily identified
484 (Bagdasaryan and Gukasyan, 1985). However, along-strike from Shirak at Artvin in eastern
485 Turkey, Eocene rocks have measured $^{143}\text{Nd}/^{144}\text{Nd}$ of 0.512663 - 0.512854 and $^{87}\text{Sr}/^{86}\text{Sr}$ of
486 0.705148 - 0.704233 (Aydınçakır and Şen, in press). These values are very similar to the
487 Shirak lavas (Fig. 7), so partial melting or assimilation of similar Eocene crust may be very
488 difficult to decipher geochemically.

489

490 On a Th/Yb vs. Ta/Yb plot (Pearce, 1983) (Fig. 9), the three series form a consistent
491 linear trend sub-parallel to the mantle array, with the felsic rocks having compositions more
492 enriched than those of typical continental crust (Rudnick and Gao, 2003). On this diagram,
493 the fractional crystallisation trend for a typical amphibole-bearing assemblage is shown. The
494 samples plot to the left of the fractionation trend which suggests that AFC processes may be
495 operating - although choice of mineral assemblages and partition coefficients can easily affect
496 the FC trend. AFC modelling (Powell, 1984) using the average composition of the Artvin

497 rocks (Aydinçakir and Şen, in press) quite reasonably reproduces the trend of the Shirak
498 lavas, but the ratio of assimilation to fractionation is high at 0.8. Modelling thus shows that
499 large volumes of isotopically similar material can be incorporated into the Shirak lavas
500 without a significant effect on trace element evolution. Studies of disequilibrium textures and
501 mineral chemistry might better elucidate the processes involved in magma evolution.

502

503 5.3. Mantle source and partial melting

504

505 *5.3.1. Mantle source of the Valley Series*

506

507 The presence of LILE and HFSE anomalies on normalised plots of mafic rocks (Fig. 6b) are
508 normally taken to indicate a subduction-modified mantle source owing to the retention of
509 HFSE in the slab, and the comparative mobility of the LILE/REE during slab heating and
510 dewatering into the overlying mantle wedge (e.g. Pearce and Peate, 1995). We have already
511 introduced the Th/Yb vs. Ta/Yb diagram (Fig. 9). The alkali basalts from Shirak plot above
512 the mantle array which is commonly taken to indicate the presence of a subduction-modified
513 source. However, they also have very much higher Ta/Yb ratios than many subduction-
514 related rocks. The Shirak lavas are therefore derived from an incompatible element-enriched
515 mantle source, or are derived from a limited degree of melt extraction. As these lavas erupted
516 >20 Myr after the end of Neo-Tethyan subduction, and there is no evidence for a slab at
517 shallow depths beneath Eastern Anatolia and Armenia at the present day (Zor et al., 2008), it
518 is improbable that a normal supra-subduction zone hydrated asthenospheric mantle wedge
519 was involved in the origin of the Shirak lavas. Therefore, the subduction-like characteristics
520 are likely to be derived from a fertile source within the mantle that had been inherited its
521 slab-related geochemical component from earlier Neo-Tethyan subduction. Crustal

522 contamination is unlikely be responsible for the subduction-like characteristics of the Shirak
523 lavas, as LILE and HFSE anomalies are significant in even the most mafic samples.

524

525 Some of the trace element characteristics of the valley series may help constrain the
526 mineralogy of the mantle source. Overall, the flat normalised HREE patterns (Fig. 6a)
527 indicate a spinel-facies mantle source at <70 km, unless the degree of partial melting was
528 very high (>25%) in order to completely consume any garnet present at depths of >70 km.
529 This is unlikely given the overall LREE-enriched and Nb-Ta/HREE-enriched trace element
530 patterns (Fig. 6b) which point towards modest degrees of partial melting of an enriched
531 source. Low Sc concentrations (<25 ppm) in all Valley Series samples may indicate residual
532 clinopyroxene, another indicator of a low degree of partial melting, but it is also possible that
533 extensive pyroxene fractionation prior to eruption has resulted in these low values. Intra-
534 LILE variations, including low Ba/Rb (<25) and Rb/Sr ratios (<0.05), do not point towards
535 amphiboles or phlogopite playing an important role during melting (e.g. Furman and Graham,
536 1999). Melting therefore took place beneath the Armenian crust at depths of ~45-70 km.

537

538 One unusual feature of the Shirak lavas is high ocean island basalt (OIB)-like Zr
539 concentrations (~200 ppm) and Zr/Hf ratios (41-52) relative to MOR and arc basalts, the
540 latter having chondritic Zr/Hf ratios of 35-39 (Weaver et al., 1987; David et al., 2000;
541 Pfänder et al., 2007). Nb/Ta ratios range from 16-22 relative to the chondritic ratio of 19.9
542 (Pfänder et al., 2007). Mafic samples from other nearby centres in the plateau, including
543 Tendürek and Ararat, show similar features (Fig. 10). Lower ratios in the Ridge Series
544 compared to the Valley Series might be explained by contamination with crustal material
545 such as the Eocene basement (Fig. 10). However, the high Zr/Hf ratios of 47-52 in the less
546 evolved Valley Series are a primary feature of the magmas.

547

548 There is little correlation between Zr and Zr/Hf ratios (not shown), indicating that
549 zircon accumulation cannot be directly responsible for the high Zr-Zr/Hf character of the
550 Shirak lavas. HFSE fractionation in OIBs may be due to: (1) residual or fractionating
551 clinopyroxene (David et al., 2000); (2) fractionation of Ti-bearing phases such as rutile,
552 ilmenite, and amphibole (Foley et al., 2000; Tiepolo et al., 2001); (3) melting of recycled
553 eclogite or garnet pyroxenite (Pfänder et al., 2007); or (4) the occurrence of carbonate
554 metasomatism (Dupuy et al., 1992). For option (1), fractionation of clinopyroxene only has a
555 modest effect upon Zr/Hf ratios (Pfänder et al., 2000). Our modelling of pure clinopyroxene
556 fractional crystallisation from a starting composition with Zr/Hf and Nb/Ta of primitive
557 mantle shows that unrealistic amounts of fractionation are required to generate the Shirak
558 samples (Fig. 10). In option (2), fractionation of titanate phases such as rutile and ilmenite
559 can generate very high Zr/Hf and Nb/Ta ratios, with $D_{\text{Zr/Hf}}$ and $D_{\text{Nb/Ta}}$ both <1 (Pfänder et al.,
560 2000); however, titanate fractionation would also strongly reduce overall Nb concentrations,
561 a feature not seen in the Valley Series. Partial melting of garnet-bearing lithologies (option 3)
562 is invoked in many OIB examples (see Pfänder et al., 2007) but can be ruled out here on the
563 basis of flat normalised HREE patterns in the Shirak lavas – these are not OIB-like magmas
564 (Fig. 6b). Where carbonates are invoked in the mantle source (e.g. Dupuy et al., 1992;
565 Hoernle et al., 2002) (option 4), resultant alkaline melts or mantle xenoliths have very high Sr
566 and Ba of $\gg 1000$ ppm, and in spite of high Zr/Hf ratios many carbonatites have very low
567 concentrations of these elements (Ionov et al., 1993). This is not the signature of the Shirak
568 samples hence carbonate metasomatism is unlikely in this case. Several studies have shown
569 that amphibole and phlogopite fractionate the HFSE (Moine et al., 2001; Tiepolo et al., 2001;
570 Chakhmouradian, 2006), with Chakhmouradian (2006) demonstrating that low-Ti amphiboles
571 have high Zr/Hf ratios of ~ 60 -200. Hence these minerals can impart high Zr/Hf on a melt; but

572 it is still unclear what the high overall Zr concentrations in the Shirak lavas are caused by -
573 this feature is normally attributed to ancient recycled oceanic crust in OIBs (Weaver, 1991).

574

575 *5.3.2. Modelling of partial melting*

576

577 Any model of partial melting conditions for Shirak has to be based on the HREE and HFSE,
578 making the assumption that neither set of elements were transported into the lithospheric
579 mantle source in a slab-derived fluid (Pearce and Peate, 1995). Therefore, we have
580 constructed non-modal batch melting curves using Dy, Yb and Nb (ignoring Zr owing to its
581 anomalous behaviour), in order to constrain the degree of partial melting needed to form the
582 Valley Series. We have taken the approach of Pearce et al. (1990) in assuming that hydrous
583 phases such as amphibole and phlogopite (if present) are completely consumed during
584 melting and do not contribute to the melt model. Given the high Ta/Yb ratios of even the least
585 evolved Valley Series samples (Fig. 9), it is reasonable to compare the melting of depleted
586 MORB mantle (DMM) (Workman and Hart, 2005) with a more incompatible-element
587 enriched source, in this case primitive mantle with 1% bulk continental crust extracted, as
588 used by Fitton and Godard (2004) for the Ontong Java oceanic plateau.

589

590 Although we can easily model HREE and HFSE ratios (see below), fractional
591 crystallisation of olivine, spinel, plagioclase and pyroxene versus fractionation of amphibole
592 from primary magma have competing effects on absolute REE and HFSE concentrations.
593 Often, elemental values for basalts in modelling are back-calculated to 9 wt.% MgO to negate
594 the effects of plagioclase and pyroxene crystallisation (Pearce & Parkinson, 1993). However,
595 valley series Dy and Yb concentrations are near-constant in spite of varying MgO and SiO₂
596 (Fig. 6a), probably due to the competing effects of amphibole and clinopyroxene

597 fractionation, so no realistic back-calculation can be applied. Therefore, we simply attempt to
598 model the elemental ratios of the last-evolved Valley Series lava (7 wt.% MgO) and assume
599 that this best reflects the conditions of partial melting.

600

601 Modelling results (Fig. 11) indicate that melting of a garnet peridotite cannot
602 reproduce the compositions of the Valley Series lavas, a finding consistent with the flat
603 normalised HREE patterns (Fig. 6a). Spinel peridotite partial melting curves do intersect the
604 valley series at low degrees of melting, with the DMM melting curve on Figure 11 giving
605 0.1-0.5% melting. In contrast the more fertile source gives 2-5% melting, which is perhaps
606 more realistic than the tiny proportion of melting required from a DMM source and the
607 difficulties of extracting such a small volume of melt (e.g. Hirth and Kohlstedt, 1995). This
608 spinel peridotite melting outcome is also consistent with geophysical surveys indicating a
609 seismically slow mantle at depths of ~50 km beneath Armenia (e.g. Koulakov et al., 2012).

610

611 5.4. Reconciliation with geophysical and geodynamic models

612

613 *5.4.1. Extent of lithospheric delamination*

614

615 Debate exists over the extent of lithospheric delamination beneath Eastern Anatolia following
616 the cessation of subduction beneath the Bitlis-Zagros suture (e.g. Keskin, 2003). Seismic
617 surveys indicate a crustal thickness of ~40-45 km, but with significant negative P- and S-
618 wave seismic velocity anomalies beneath, extending from ~50 to ~250 km depth, between
619 eastern Turkey, Armenia, the Black Sea and northwest Iran, concurrent with many Pliocene-
620 Quaternary volcanic centres (e.g. Piromallo and Morelli, 2003; Maggi & Priestley, 2005; Zor
621 et al., 2008; Koulakov et al., 2012). The anomaly has been used by these authors to argue for

622 the presence of hot, perhaps partially molten, asthenosphere, but several authors extend these
623 conclusions to the possibility that there is also no mantle lithosphere ‘lid’ beneath the
624 Anatolian crust (e.g. Keskin, 2003; Zor et al., 2008) and the Caucasus (Koulakov et al.,
625 2012). In this case, mafic magmatism in Shirak would have to have an asthenospheric source.

626

627 There are significant implications for magmatism in this scenario. The impact of hot
628 upwelling asthenosphere on the thickened Lesser Caucasus arc crust should result in
629 extensive lower crustal melting, as observed in the Puna Plateau of the Andes, and the Great
630 Basin Altiplano in the western U.S. (Allmendinger et al., 1997; Babeyko et al., 2002; Best et
631 al., 2009). Going back to our geochemical results, this model of whole-scale lithospheric
632 delamination proposed for the Puna Plateau is incompatible with the observed silica-
633 undersaturated magmatism in Shirak, which bears little evidence for large-scale crustal
634 interaction. We conclude that there is sufficient lithospheric mantle beneath the Armenian
635 crust to act as a thermal barrier between the asthenosphere and crust (Fig. 12), protecting the
636 crust from melting and infiltration by hot asthenospheric melts in the manner described by
637 Babeyko et al. (2002). An asthenospheric source for the Shirak magmas cannot have been
638 influenced by a subducting slab, because subduction processes ended prior to the Miocene.
639 Hence the Shirak magmas would not have subduction-like trace element characteristics, and
640 instead should closely resemble OIB. There are asthenosphere-derived OIB-like lavas
641 without subduction-related geochemical signatures in Eastern Iran (Saadat et al., 2010;
642 Saadat and Stern, 2012) and in the Arabian foreland (Lustrino et al., 2010). The Iranian alkali
643 olivine basalts show trends towards an EMII-like isotope signature (particularly with respect
644 to Pb isotope ratios) (Zindler and Hart, 1986). They also contain pyroxenite xenoliths
645 from the lithospheric mantle, plagioclase megacrysts of uncertain origin, and some lower
646 crustal gabbroic xenoliths (Saadat and Stern, 2012). These lavas are distinct in terms of

647 xenolith content, trace element signatures and isotope geochemistry from those erupted in
648 Shirak.

649

650 *5.4.2. Geodynamic model*

651

652 Our geodynamic model is presented schematically in Figure 12. We propose that, upon the
653 termination of Neo-Tethyan subduction along the Bitlis-Zagros suture during the Oligocene,
654 Armenia lay in a continental back-arc position relative to the former subducting slab and
655 mantle wedge. Modelling studies have suggested that an old slab may be able to persist or
656 ‘stall’ in the upper mantle without breaking off for up to 20 Myr after terminal collision (van
657 Hunen and Allen, 2011). Delayed break-off of the Neo-Tethyan slab from Arabia beneath
658 Eurasia may thus be responsible for the upsurge in magmatism since 10 Ma, and particularly
659 in the Pliocene-Quaternary, across the orogenic plateau (e.g. Keskin, 2003), concurrent with
660 the influx of hot asthenosphere into the region the slab once occupied. In Eastern Anatolia,
661 the region immediately above the detached slab might lack mantle lithosphere, and
662 asthenospheric and crustal melting would combine to produce arc-like magmas (Fig. 12)
663 (Keskin, 2003). However, as we have already discussed, it is improbable that whole-scale
664 lithospheric mantle delamination occurred beneath Armenia because we do not see attendant
665 whole-scale lower crustal melting. The former asthenospheric mantle wedge of the Neo-
666 Tethyan arc system would be refrigerated by the presence of a stalled slab, and rapidly
667 converted into lithospheric mantle over the 15-25 Myr following terminal collision (c.f. Holt
668 et al., 2010). This depleted lithospheric mantle could be stable and buoyant enough to be at
669 least partially preserved following the eventual detachment of the underlying oceanic slab,
670 whilst the aforementioned influx of convecting asthenosphere would trigger partial melting in

671 the overlying lithospheric mantle, as well as providing a thermal support for the orogenic
672 plateau (Fig. 12).

673

674 Another potentially important consideration is that, although much of the LILE and
675 LREE budget of the southern Neo-Tethyan slab may have been delivered to the lithosphere
676 before continental collision, a stalled slab and associated sediments would continue
677 dewatering before break-off. This would contribute to the subduction-like signature on the
678 mantle frozen-in beneath Armenia. Other Pliocene-Quaternary centres in the collision zone,
679 such as the foreland volcanic system at Karacadağ, may result from asthenospheric melting
680 beneath thin spots in the lithosphere (Lustrino et al., 2010; Ekici et al., 2012). Mantle-derived
681 volcanism is also apparent even in the 50+ km thick crust of the Elbrus region of the Greater
682 Caucasus (Lebedev et al., 2006b; Koulakov et al., 2012), and it is here that magmatism may
683 be related to melting during collisional thickening of lithospheric mantle and the breakdown
684 of hydrous mineral phases such as micas and amphiboles (e.g. Pearce et al., 1990; Allen et
685 al., 2013) or to asthenospheric upwelling during lithospheric dripping (see Sosson et al.,
686 2010) (Fig. 12).

687

688 **6. Conclusions**

689

- 690 • Mafic and more evolved Pliocene-Quaternary lavas in Shirak, NW Armenia, were
691 emplaced through a former continental margin arc sequence as a result of localised
692 extensional tectonics within the present-day Arabia-Eurasia collision zone.
- 693 • Magmas evolved from mafic through to dacitic compositions by fractional
694 crystallisation dominated by pyroxene, amphibole and plagioclase; and although
695 evolved samples contain quartz xenocrysts, none preserves clear isotopic evidence for

696 large-scale crustal assimilation - magma mixing appears to be the dominant
697 petrogenetic process. We conclude that if assimilation did occur, it was of local arc-
698 related crust of a similar isotopic composition to the Shirak melts.

- 699 • The least-evolved magmas preserve trace element evidence for derivation by
700 moderate degrees of melting (~3-4%) from a shallow, spinel-facies lithospheric
701 mantle source with an inherited subduction component probably related to earlier
702 Tethyan subduction processes. They contain high Zr concentrations and high Zr/Hf
703 ratios which are an intrinsic feature of the source or partial melting process.
- 704 • The presence of lithospheric mantle beneath Armenia is a requirement for
705 geodynamic models of the region in order to prevent the occurrence of whole-scale
706 lower crustal melting.

707

708 **Acknowledgements**

709

710 This work is funded by the Natural Environment Research Council project, ‘Orogenic Plateau
711 Magmatism’ [NE/H021620/1]. Nick Marsh conducted the XRF analyses; Geoff Nowell and
712 Chris Ottley assisted with, and partly conducted, radiogenic isotope and trace element
713 analyses, respectively. We are grateful to *Lithos* guest editor Ioan Seghedi, along with
714 Evgenii Sharkov and an anonymous reviewer for their constructive comments. Ivan Savov
715 and Douwe van Hinsbergen are thanked for discussion on some of the ideas presented within.

716

717 **References**

718

719 Adamia, S.A., Chkhotua, T., Kekelia, M., Lordkipanidze, M., Shavishvili, I., 1981. Tectonics
720 of the Caucasus and adjoining regions: implications for the evolution of the Tethys ocean.
721 *Journal of Structural Geology* 3, 437-447.

722

723 Adamia, S.A., Zakariadze, G., Chkhotua, T., Sadradze, N., Tsereteli, N., Chabukiani, A.,
724 Gventsadze, S., 2011. Geology of the Caucasus: A Review. *Turkish Journal of Earth Sciences*
725 20, 489-544.

726

727 Agard, P., Omrani, J., Jolivet, L., Mouthereau, F., 2005. Convergence history across Zagros
728 (Iran): constraints from collisional and earlier deformation. *International Journal of Earth*
729 *Sciences* 94, 401-419.

730

731 Allen, M.B., Armstrong, H.A., 2008. Arabia-Eurasia collision and the forcing of mid
732 Cenozoic global cooling. *Palaeontology Palaeoclimatology Palaeoecology* 265, 52-58.

733

734 Allen, M.B., Kheirkhah, M., Emami, M.H., Jones, S.J., 2011. Right-lateral shear across Iran
735 and kinematic change in the Arabia-Eurasia collision zone. *Geophysical Journal International*
736 184, 555-574.

737

738 Allen, M.B., Kheirkhah, M., Neill, I., Emami, M.H., McLeod, C.L., 2013. Generation of arc
739 and within-plate chemical signatures in collision zone magmatism: Quaternary lavas from
740 Kurdistan Province, Iran. *Journal of Petrology* 54, 887-911.

741

742 Allmendinger, R.W., Isacks, B.L., Jordan, T.E., Kay, S.M., 1997. The evolution of the
743 Altiplano-Puna plateau of the Central Andes. *Annual Reviews of Earth Science* 25, 139-174.

744

745 Angus, D.A., Wilson, D.C., Sandvol, E., Ni, J.F., 2006. Lithospheric structure of the Arabian
746 and Eurasian collision zone in eastern Turkey from S-wave receiver functions. *Geophysical*
747 *Journal International* 166, 1335-1346.

748

749 Avagyan, A., Sosson, M., Karakhanian, A., Philip, H., Rebai, S., Rolland, Y., Melkonyan, R.,
750 Davtyan, V., 2010. Recent tectonic stress evolution in the Lesser Caucasus and adjacent
751 regions. In: Sosson, M., Kaymakci, N., Stephenson, R.A., Bergerat, F., Starostenko, V.
752 (Eds.). *Sedimentary Basin Tectonics from the Black Sea and Caucasus to the Arabian*
753 *Platform*. Geological Society of London Special Publications, v. 340, p.p. 393-408.

754

755 Aydınçakır, E., Şen, C, in press. Petrogenesis of the post-collisional volcanic rocks from the
756 Borçka (Artvin) area: Implications for the evolution of the Eocene magmatism in the Eastern
757 Pontides (NE Turkey). *Lithos*, doi:10.1016/j.lithos.2013.04.007.

758

759 Azizi, H., Moinevaziri, H., 2009. Review of the tectonic setting of Cretaceous to Quaternary
760 volcanism in northwestern Iran. *Journal of Geodynamics* 47, 167-179.

761

762 Babeyko, A.Yu., Sobolev, S.V., Trumbull, R.B., Oncken, O., Lavier, L.L., 2002. Numerical
763 models of crustal-scale convection and partial melting beneath the Altiplano-Puna plateau.
764 *Earth and Planetary Science Letters* 199, 373-388.

765

766 Baghdasaryan, G.P., Ghukasyan, R.Kh., 1985. Geochronology of magmatic, metamorphic
767 and ore formations of Armenian SSR. Publication of the Academy of Sciences of Armenian
768 Soviet Socialist Republic (in Russian).

769

770 Ballatto, P., Uba, C.E., Landgraf, A., Strecker, M.R., Sudo, M., Stockli, D.F., Friedrich, A.,
771 Tabatabaei, S.H., 2011. Arabia-Eurasia continental collision: Insights from late Tertiary
772 foreland-basin evolution in the Alborz Mountains, northern Iran. *Geological Society of
773 America Bulletin* 123, 106-131.

774

775 Berberian, F., Berberian M., 1981. Tectono-plutonic episodes in Iran. In: Gupta, H.K.,
776 Delany, F.M. (Eds.). *Zagros, Hindu Kush, Himalaya Geodynamic Evolution*. American
777 Geophysical Union Geodynamic Series v. 3, p.p. 5-32.

778

779 Best, M.G., Barr, D.L., Christiansen, E.H., Gromme, S., Deino, A.L., Tingey, D.G., 2009.
780 The Great Basin Altiplano during the middle Cenozoic ignimbrite flareup: insights from
781 volcanic rocks. *International Geology Review* 51, 589-633.

782

783 Bottrill, A.D., van Hunen, J., Allen, M.B., 2012. Insight into collision zone dynamics from
784 topography: numerical modelling results and observations. *Solid Earth* 3, 387-399.

785

786 Cann, J.R., 1970. Rb, Sr, Zr and Nb in some ocean floor basaltic rocks. *Earth and Planetary
787 Science Letters* 10, 7-11.

788

789 Chakhmouradian, A., 2006. High-field-strength elements in carbonatitic rocks:
790 Geochemistry, crystal chemistry and significance for constraining the source of carbonatites.
791 *Chemical Geology* 235, 138-160.

792

793 Chernyshev, I.V., Lebedev, V.A., Arakelyants, M.M., Jrbashyan, R.T., Ghukasyan, Y.G.,
794 2002. Geochronology of the Aragats volcanic centre, Armenia: Evidence from K-Ar dating.
795 Doklady Earth Sciences 384, 393-398 (in Russian).
796

797 Chernyshev, I.V., Lebedev, V.A., Arakelyants, M.M., 2006. K-Ar dating of Quaternary
798 volcanics: Methodology and interpretation of results. Petrologiya (Petrology) 14, 69-89.
799

800 Chiu, H.-Y., Chung, S.-L., Zarrinkoub, M.H., Mohammadi, S.S., Khatib, M.M., Iizuka, Y.,
801 2013. Zircon U-Pb constraints from Iran on the magmatic evolution related to Neotethyan
802 subduction and Zagros orogeny. Lithos 162, 70-87.
803

804 David, K., Schiano, P., Allégre, C.J., 2000. Assessment of the Zr/Hf fractionation in oceanic
805 basalts and continental materials during petrogenetic processes. Earth and Planetary Science
806 Letters 178, 285-301.
807

808 Davidson, J.P., Hassanzadeh, J., Berzins, R., Stockli, D.F., Bashukooh, B., Turrin, B.,
809 Pandamouz, A., 2004. The geology of Damavand volcano, Alborz Mountains, northern Iran.
810 Geological Society of America Bulletin 116, 16-29.
811

812 Dewey, J.F., Hempton, M.R., Kidd, W.S.F., Saroglu, F., Şengör, A.M.C., 1986. Shortening
813 of continental lithosphere: the neotectonics of Eastern Anatolia – a young collision zone. In:
814 Coward, M.P., Ries, A.C. (Eds.). Collision Tectonics. Geological Society of London Special
815 Publication, v. 19, p.p. 3-36.
816

817 Dilek, Y., Imamverdiyev, N., Altunkaynak, Ş., 2010. Geochemistry and tectonics of
818 Cenozoic volcanism in the Lesser Caucasus (Azerbaijan) and the peri-Arabian region:
819 collision-induced mantle dynamics and its magmatic signature. *International Geology Review*
820 52, 536-578.

821

822 Dowall, D.P., Nowell, G.M., Pearson, D.G., 2007. Chemical pre-concentration procedures for
823 high-precision analysis of Hf-Nd-Sr isotopes in geological materials by plasma ionisation
824 multi-collector mass spectrometry (PIMMS) techniques. In: Holland, J.G., Tanner, S.D.
825 (Eds.) *Plasma Source Mass Spectrometry: Applications and Emerging Technologies*.
826 Cambridge: The Royal Society of Chemistry, p.p. 321-337.

827

828 Drew, S.T., Ducea, M.N., Schoenbohm, L.M., 2009. Mafic volcanism on the Puna Plateau,
829 NW Argentina: Implications for lithospheric composition and evolution with an emphasis on
830 lithospheric foundering. *Lithosphere* 1, 305-318.

831

832 Dupuy, C., Liotard, J.M., Dostal, J., 1992. Zr/Hf fractionation in intraplate basaltic rocks:
833 Carbonate metasomatism in the mantle source. *Geochimica et Cosmochimica Acta* 56, 2417-
834 2423.

835

836 Ekici, T., Macpherson, C.G., Otlu, N., 2012. Polybaric melting of a single mantle source
837 during the Neogene Siverek phase of the Karacadağ Volcanic Complex, SE Turkey. *Lithos*
838 146, 152-163.

839

840 Fitton, J.G., Godard, M., 2004. Origin and evolution of magmas on the Ontong Java Plateau.
841 In: Fitton, J.G., Mahoney, J.J., Wallace, P.J., Saunders, A.D. (Eds.). *Origin and Evolution of*

842 the Ontong Java Plateau. Geological Society of London Special Publication, v. 229, p.p. 151-
843 178.

844

845 Foley, S.F., Barth, M.G., Jenner, G.A., 2000. Rutile/melt partition coefficients for trace
846 elements and an assessment of the influence of rutile on the trace element characteristics of
847 subduction zone magmas. *Geochimica et Cosmochimica Acta* 64, 933-939.

848

849 Furman, T., Graham, D., 1999. Erosion of lithospheric mantle beneath the East African Rift
850 System: geochemical evidence from the Kivu volcanic province. *Lithos* 48, 237-262.

851

852 Jackson, J., Haines, J., Holt, W., 1995. The accommodation of Arabia-Euasia Plate
853 convergence in Iran. *Journal of Geophysical Research* 100, B8, P15205.

854

855 Johnson, C.M., 1991. Large-scale crust formation and lithosphere modification beneath
856 middle to late Cenozoic calderas and volcanic fields, western North America. *Journal of*
857 *Geophysical Research* 96, 13485-13507.

858

859 Jrbashian, R.T., Kazarian, G.A., Karapetian, S.G., Meliksetian, Kh.B., Mnatsakanian, A.,
860 Shirinian, K.G., 1996. Meso-Cenozoic basaltic volcanism in the northeastern part of
861 Armenian Highland. *Letters of the Armenian Academy of Sciences, Earth Sciences* 49, 19-32
862 (in Russian).

863

864 Hirth, G., Kohlstedt, D.L., 1995. Experimental constraints on the dynamics of the partially
865 molten upper mantle: deformation in diffusion creep regime. *Journal of Geophysical*
866 *Research* 100, 1981-2001.

867

868 Hoernle, K., Tilton, G., Le Bas, M.J., Duggan, S., Garbe-Schönberg, D., 2002. Geochemistry
869 of oceanic carbonatites compared with continental carbonatites: mantle recycling of oceanic
870 crustal carbonate. *Contributions to Mineralogy and Petrology* 142, 520-542.

871

872 Holt, P.J., Allen, M.B., van Hunen, J., Bjørnseth, H.M., 2010. Lithospheric cooling and
873 thickening as a basin forming mechanism. *Tectonophysics* 495, 184-194.

874

875 Ionov, D.A., Dupuy, C., O'Reilly, S.Y., Kopylova, M.G., Genshaft, Y.S., 1993. Carbonated
876 peridotite xenoliths from Spitsbergen: implications for trace element signature of mantle
877 carbonate metasomatism. *Earth and Planetary Science Letters* 119, 283-297.

878

879 Karapetian, S.G., Jrbashian, R.T., Mnatsakanian, A.Kh., 2001. Late collision rhyolitic
880 volcanism in the north-eastern part of the Armenian Highland. *Journal of Volcanology and*
881 *Geothermal Research* 112, 189-220.

882

883 Kharazyan, E.Kh., 1983. Geology of recent volcanism of north-west part of Armenian SSR
884 (basins of rivers Dzoraget and Akhuryan). PhD thesis, unpublished, ArmGeologia, Yerevan,
885 55 pp.

886

887 Kharazyan, E.Kh., 2005. Geological Map of Armenia. Ministry of Nature Protection of
888 Republic of Armenia.

889

890 Keskin, M., Pearce, J.A., Mitchell, J.G., 1998. Volcano-stratigraphy and geochemistry of
891 collision-related volcanism on the Erzurum-Kars Plateau, northeastern Turkey. *Journal of*
892 *Volcanology and Geothermal Research* 85, 355-405.

893

894 Keskin, M., 2003. Magma generation by slab steepening and breakoff beneath and
895 subduction-accretion complex: An alternative model for collision-related volcanism in
896 Eastern Anatolia, Turkey. *Geophysical Research Letters* 30, 1-4.

897

898 Keskin, M., 2007. Eastern Anatolia: a hot spot in a collision zone without a mantle plume. In:
899 Foulger, G.R., Jurdy, D.M. (Eds.) *Plates, Plumes, and Planetary Processes*. Geological
900 Society of America Special Paper, vol. 409, p.p. 1-25.

901

902 Keskin, M., Can Genç, Ş, Tüysüz, O., 2008. Petrology and geochemistry of post-collisional
903 Middle Eocene volcanic units in North-Central Turkey: Evidence for magma generation by
904 slab breakoff following the closure of the Northern Neotethys Ocean. *Lithos* 104, 267-305.

905

906 Karakhanian, A.S., Trifonov, V.G., Azizbekian, O.G., Hondkarian, D.G., 1997. Relationship
907 of late Quaternary tectonics and volcanism in the Khanarassar active fault zone, the
908 Armenian Upland. *Terra Nova* 9, 131-134.

909

910 Karakhanian, A., Djrashian, R., Trifonov, V., Philip, H., Arakelian, S., Avagian, A., 2002.
911 Holocene-historical volcanism and active faults as natural risk factors for Armenia and
912 adjacent countries. *Journal of Volcanology and Geothermal Research* 113, 319-344.

913

914 Karakhanian, A., Abgaryan, Y., 2004. Evidence of historical seismicity and volcanism in the
915 Armenian Highland (from Armenian and other sources). *Annals of Geophysics* 47, 793-810.
916

917 Kay, R.W., Kay, S.M., 1993. Delamination and delamination magmatism. *Tectonophysics*
918 219, 177-189.
919

920 Kheirkhah, M., Allen, M.B., Emami, M.H., 2009. Quaternary syn-collision magmatism from
921 the Iran/Turkey borderlands. *Journal of Volcanology and Geothermal Research* 182, 1-12.
922

923 Koçyiğit, A., Yilmaz, A., Adamia, S., Kuloshvili, S., 2001. Neotectonics of East Anatolian
924 Plateau (Turkey) and Lesser Caucasus: implications for transition from thrusting to strike-slip
925 faulting. *Geodinamica Acta* 14, 177-195.
926

927 Langmuir, C.H., Vocke, R.D., Hanson, G.N., Hart, S.R., 1978. A general mixing equation
928 with applications to Icelandic basalts. *Earth and Planetary Science Letters* 37, 380-392.
929

930 Koulakov, I., Zabelina, I., Amanatashvili, I., Meskhia, V., 2012. Nature of orogenesis and
931 volcanism in the Caucasus region based on results of regional tomography. *Solid Earth* 3,
932 327-337.
933

934 Lebedev, V.A., Chernyshev, I.V., Chugaev, A.V., Dudaury, O.Z., Vashakidze, G.T., 2006a.
935 K-Ar age and Sr-Nd characteristics of subalkali basalts in the Central Georgian neovolcanic
936 region. *Doklady Earth Sciences* 408, 657-661.
937

938 Lebedev, V.A., Bubnov, S.N., Chernyshev, I.V., Gol'tsman, Y.V., 2006b. Basic magmatism
939 in the geological history of the Elbrus neovolcanic area, Greater Caucasus: Evidence from K-
940 Ar and Sr-Nd isotope data. *Doklady Earth Sciences* 406, 37-44.

941

942 Lebedev, V.A., Bubnov, S.N., Chernyshev, I.V., Chugaev, A.V., Dudaury, O.Z., Vashakidze,
943 G.T., 2007. Geochronology and genesis of subalkaline basaltic lava rivers at the Dzhavakheti
944 Highland, Lesser Caucasus: K-Ar and Sr-Nd isotopic data. *Geochemistry International* 45,
945 211-225.

946

947 Lebedev, V.A., Bubnov, S.N., Dudaury, O.Z., Vashakidze, G.T., 2008a. Geochronology of
948 Pliocene volcanism in the Dzhavakheti Highland (the Lesser Caucasus). Part 1: Western part
949 of the Dzhavakheti Highland. *Stratigraphy and Geological Correlation* 16, 204-224.

950

951 Lebedev, V.A., Bubnov, S.N., Dudaury, O.Z., Vashakidze, G.T., 2008b. Geochronology of
952 Pliocene volcanism in the Dzhavakheti Highland (the Lesser Caucasus). Part 2: Eastern part
953 of the Dzhavakheti Highland. Regional geological correlation. *Stratigraphy and Geological*
954 *Correlation* 16, 553-574.

955

956 Lebedev, V.A., Chernyshev, I.V., Chugaev, A.V., Gol'tsman, Y.V., Bairova, E.D., 2010.
957 Geochronology of eruptions and parental magma sources of Elbrus volcano, the Greater
958 Caucasus: K-Ar and Sr-Nd-Pb isotope data. *Geochemistry International* 48, 41-67.

959

960 Lebedev, V.A., Chernyshev, I.V., Yakushev, A.I., 2011. Initial time and duration of
961 Quaternary magmatism in the Aragats neovolcanic area (Lesser Caucasus, Armenia).
962 *Doklady Earth Sciences* 437, 532-536.

963

964 Le Bas, M.J., Le Maitre, R.W., Streckeisen, A., Zanettin, B., 1986. A chemical classification
965 of volcanic rocks based on the total alkali-silica diagram. *Journal of Petrology* 27, 745-750.

966

967 Lin, Y.C., Chung, S.L., Karakhanian, A., Jrbashyan, R., Navasardyan, G., Galoyan, G., Chiu,
968 H.Y., Lin, I.J., Chu, C.H., Lee, H.Y., 2011. Geochemical and Sr-Nd isotopic constraints on
969 the petrogenesis of pre- to post-collisional volcanic rocks in Armenia. *Geophysical Research*
970 *Abstracts* 13, EU2011-5422.

971

972 Liotard, J.M., Dautria, J.M., Bosch, D., Condomines, M., Mehdizadeh, H., Ritz, J.F., 2008.
973 Origin of the absarokite-banakite association of the Damavand volcano (Iran): trace elements
974 and Sr, Nd, Pb isotope constraints. *International Journal of Earth Sciences* 97, 89-102.

975

976 Lordkipanidze, M., 1980. Alpine volcanism and geodynamics of the central segment of the
977 Mediterranean belt. *Metsniereba, Tbilisi* (in Russian).

978

979 Lordkipanidze, M., Meliksetian, B., Jrbashian, R., 1988. Mesozoic-Cenozoic magmatic
980 evolution of the Pontian-Crimean-Caucasian region. *Mémoire de la Société Géologique de*
981 *France* 154, 103-124.

982

983 Lustrino, M., Keskin, M., Mattioli, M., Lebedev, V.A., Chugaev, A., Sharkov, E., Kavak, O.,
984 2010. Early activity of the largest Cenozoic shield volcano in the circum-Mediterranean area:
985 Mt. Karacadağ, SE Turkey. *European Journal of Mineralogy* 22, 343-362.

986

987 Maggi, A., Priestley, K., 2005. Surface waveform tomography of the Turkish-Iranian plateau.
988 Geophysical Journal International 160, 1068-1080.
989

990 McDonough, W.F., Sun, S.-S., 1995. The composition of the Earth. Chemical Geology 120,
991 223-253.
992

993 McQuarrie, N., van Hinsbergen, D.J.J., 2013. Retrodeforming the Arabia-Eurasia collision
994 zone: Age of collision versus magnitude of continental subduction. Geology 41, 315-318.
995

996 Mirnejad, H., Hassanzadeh, J., Cousens, B.J., Taylor, B.E., 2010. Geochemical evidence for
997 deep mantle melting and lithospheric delamination as the origin of the inland Damavand
998 volcanic rocks of northern Iran. Journal of Volcanology and Geothermal Research 198, 288-
999 296.
1000

1001 Mitchell, J., Westaway, R., 1999. Chronology of Neogene and Quaternary uplift and
1002 magmatism in the Caucasus: constraints from K-Ar dating of volcanism in Armenia.
1003 Tectonophysics 304, 157-186.
1004

1005 Mo, X., Hou, Z., Niu, Y., Dong, G., Qu, X., Zhao, Z., Yang, Z., 2007. Mantle contributions
1006 to crustal thickening during continental collision: Evidence from Cenozoic igneous rocks in
1007 southern Tibet. Lithos 96, 225-242.
1008

1009 Moine, B.N., Grégoire, M., O'Reilly, S.Y., Sheppard, S.M.F., Cottin, J.Y., 2001. High field
1010 strength element fractionation in the upper mantle: evidence from amphibole-rich composite

1011 mantle xenoliths from the Kerguelen Islands (Indian Ocean). *Journal of Petrology* 42, 2145-
1012 2167.

1013

1014 Morley, C.K., Kongwung, B., Julapour, A.A., Abdolghafourian, M., Hajian, M., Waples, D.,
1015 Warren, J., Otterdoom, H., Srisuriyon, K., Kazemi, H., 2009. Structural development of a
1016 major late Cenozoic basin and transpressional belt in central Iran: The Central Basin in the
1017 Qom-Saveh area. *Geosphere* 5, 325-362.

1018

1019 Okay, A.I., Zattin, M., Cavazza, W., 2010. Apatite fission-track data for the Miocene Arabia-
1020 Eurasia collision. *Geology* 38, 35-38.

1021

1022 Pagé, P., Bédard, J.H., Tremblay, A., 2009. Geochemical variations in a depleted fore-arc
1023 mantle: The Ordovician Thetford Mines Ophiolite. *Lithos* 113, 21-47.

1024

1025 Pearce, J.A., 1983. Role of the sub-continental lithosphere in magma genesis at active
1026 continental margins. In: Hawkesworth, C.J., Norry, M.J. (Eds.). *Continental Basalts and*
1027 *Mantle Xenoliths*. Shiva, Natwich, p.p. 230-249.

1028

1029 Pearce, J.A., Bender, J.F., Delong, S.E., Kidd, W.S.F., Low, P.J., Guner, Y., Sargolu, F.,
1030 Yilmaz, Y., Moorbath, S., Mitchell, J.G., 1990. Genesis of collision volcanism in eastern
1031 Anatolia, Turkey. *Journal of Volcanology and Geothermal Research* 44, 189-229.

1032

1033 Pearce, J.A., Parkinson, I.J., 1993. Trace element models for mantle melting: application to
1034 volcanic arc petrogenesis. In: Prichard, H.M., Alabaster, T., Harris, N.B.W., Neary, C.R.
1035 (Eds.). *Geological Society Special Publication* 76, 373-403.

1036

1037 Pearce, J.A., Peate, D.W., 1995. Tectonic implications of the composition of volcanic arc
1038 magmas. *Annual Review of Earth and Planetary Sciences* 23, 251-285.

1039

1040 Pearce, J.A., 1996. A users guide to basalt discrimination diagrams. In: Wyman, D.A. (Ed.).
1041 Trace Element Geochemistry of Volcanic Rocks: Applications for Massive Sulphide
1042 Exploration. Geological Association of Canada Short Course Notes 12, 79-113.

1043

1044 Peccerillo, R., Taylor, S.R., 1976. Geochemistry of Eocene calc-alkaline volcanic rocks from
1045 the Kastamonu area, northern Turkey. *Contributions to Mineralogy and Petrology* 58, 63-81.

1046

1047 Pfänder, J.A., Münker, C., Stracke, A., Mezger, K., 2007. Na/Ta and Zr/Hf in ocean island
1048 basalts – Implications for crust-mantle differentiation and the fate of Niobium. *Earth and*
1049 *Planetary Science Letters* 254, 158-172.

1050

1051 Piromallo, C., Morelli, A., 2003. P-wave tomography of the mantle under the Alpine-
1052 Mediterranean area. *Journal of Geophysical Research* 108, B2, doi:10.1029/2002JB001757.

1053

1054 Powell, R., 1984. Inversion of the assimilation and fractional crystallisation (AFC) equations;
1055 characterisation of contaminants from isotope and trace element relationships in volcanic
1056 suites. *Journal of the Geological Society of London* 141, 447-452.

1057

1058 Presnyakov, S.L., Belyaeva, E.V., Lyubin, V.P., Rodionov, N.V., Antonov, A.V., Saltykova,
1059 A.K., Berezhnaya, N.G., Sergeev, S.A., 2012. Age of the earliest Paleolithic sites in the

1060 northern part of the Armenian Highland by SHRIMP-II U-Pb geochronology of zircons from
1061 volcanic ashes. *Gondwana Research* 21, 929-938.

1062

1063 Priestley, K.F., McKenzie, D.P., 2006. The thermal structure of the literature from shear
1064 wave velocities. *Earth and Planetary Science Letters* 244, 285-301.

1065

1066 Rebaï, S., Philip, H., Dorbath, L., Borissoff, B., Haessler, H., Cisternas, A., 1993. Active
1067 tectonics in the Lesser Caucasus: coexistence of compressive and extensional structures.
1068 *Tectonics* 12, 1089-1114.

1069

1070 Richards, J.P., Spell, T., Rameh, E., Razique, A., Fletcher, T., 2012. High Sr/Y magmas
1071 reflect arc maturity, high magmatic water content, and porphyry Cu ± Mo ± Au potential:
1072 examples from the Tethyan arcs of central and eastern Iran and western Pakistan. *Economic*
1073 *Geology* 107, 295-332.

1074

1075 Rolland, Y., Billo, S., Corsini, M., Sosson, M., Galoyan, G., 2009. Blueschists of the
1076 Amassia-Stepanavan suture zone (Armenia): linking Tethys subduction history from E-
1077 Turkey to W-Iran. *International Journal of Earth Sciences* 98, 533-550.

1078

1079 Saadat, S., Karimpour, M.H., Stern, C., 2010. Petrochemical characteristics of Neogene and
1080 Quaternary alkali olivine basalts from the western margin of the Lut Block, eastern Iran.
1081 *Iranian Journal of Earth Sciences* 2, 87-106.

1082

1083 Saadat, S., Stern, C.R., 2012. Petrochemistry of a xenolith-bearing Neogene alkali olivine
1084 basalt from northeastern Iran. *Journal of Volcanology and Geothermal Research* 225, 13-29.

1085

1086 Savov, I.P., Luhr, J., D'Antonio, M., Connor, C., Karakhanian, A., Ghukasyan, Y.,
1087 Djrbashian, R., 2007. Variable slab and subarc mantle signatures within dying arc setting –
1088 clues from the volcanology and geochemistry of Quaternary volcanic rocks from Armenia.
1089 American Geophysical Union Spring Meeting Abstracts, V53A-02.

1090

1091 Sen, P.A., Temel, A., Gourgaud, A., 2004. Petrogenetic modelling of Quaternary post-
1092 collisional volcanism: a case study of central and eastern Anatolia. *Geological Magazine* 141,
1093 81-98.

1094

1095 Şengör, A.M.C., Kidd, W.S.F., 1979. Post-collisional tectonics of the Turkish-Iranian plateau
1096 and a comparison with Tibet. *Tectonophysics* 55, 361-376.

1097

1098 Şengör, A.M.C., Özeren, M.S., Keskin, M., Sakiñç, M., Özbakir, A.D., Kayan, I., 2008.
1099 Eastern Turkish high plateau as a small Turkic-type orogen: Implications for post-collisional
1100 crust-forming processes in Turkic-type orogens. *Earth Science Reviews* 90, 1-48.

1101

1102 Shabaniyan, E., Acocella, V., Gioncada, A., Ghasemi, H., Bellier, O., 2012. Structural control
1103 on volcanism in intraplate post collisional settings: Late Cenozoic to Quaternary examples of
1104 Iran and Eastern Turkey. *Tectonics* 31, TC3013, doi:10.1029/2011TC003042.

1105

1106 Skhirtladse, N.N., 1958. Post-Paleogene Volcanism in Georgia (Postpaleogenovyi effuzivnyi
1107 vulkanizm Gruzii). Report of the Georgian Soviet Socialist Republic Academy of Sciences,
1108 Tblisi, 368 pp (in Russian).

1109

1110 Sosson, M., Rolland, Y., Müller, C., Danelian, T., Melkonyan, R., Kekelia, S., Adamia, A.,
1111 Babazadeh, V., Kangarli, T., Avagyan, A., Galoyan, G., Mosar, J., 2010. Subductions,
1112 obduction and collision in the Lesser Caucasus (Armenia, Azerbaijan, Georgia), new insights.
1113 In: Sosson, M., Kaymakci, N., Stephenson, R.A., Bergerat, F., Starostenko, V. (Eds.).
1114 Sedimentary Basin Tectonics from the Black Sea and Caucasus to the Arabian Platform.
1115 Geological Society of London Special Publications 340, 329-352.
1116
1117 Stampfli, G.M., 2000. Tethyan oceans. In: Bozkurt, E., Winchester, J.A., Piper, J.D.A. (Eds.).
1118 Tectonics and Magmatism in Turkey and the Surrounding Area. Geological Society of
1119 London Special Publications 173, 1-23.
1120
1121 Sun, S.-S., McDonough, W.F., 1989. Chemical and isotopic systematics of oceanic basalts:
1122 implications for mantle composition and processes. In: Saunders, A.D., Norry, M.J. (Eds.)
1123 Magmatism in the Ocean Basins. Geological Society of London Special Publication, vol.42,
1124 p.p. 313-345.
1125
1126 Tepley, F.J., Davidson, J.P., Clyne, M.A., 1999. Magmatic interactions as recorded in
1127 plagioclase phenocrysts of Chaos Crags, Lassen Volcanic Centre, California. Journal of
1128 Petrology 40, 787-806.
1129
1130 Tiepolo, M., Bottazzi, P., Foley, S.F., Oberti, R., Vannucci, R., Zanetti, A., 2001.
1131 Fractionation of Nb and Ta from Zr and Hf at mantle depths: the role of Titanian pargasite
1132 and kaersutite. Journal of Petrology 42, 221-232.
1133

1134 Tsachiyama, A., 1985. Dissolution kinetics of plagioclase in the melt system diopside-albite-
1135 anorthite, and origin of dusty plagioclase in andesites. *Contributions to Mineralogy and*
1136 *Petrology* 89, 1-16.

1137

1138 van Hunen, J., Allen, M.B., 2011. Continental collision and slab break-off: A comparison of
1139 3-D numerical models with observations. *Earth and Planetary Science Letters* 302, 27-37.

1140

1141 Verdel, C., Wernicke, B.P., Hassanzadeh, J., Guest, B., 2011. A Paleogene extensional arc
1142 flare-up in Iran. *Tectonics* 30, TC3008, doi:10.1029/2010TC002809.

1143

1144 Vernant, P., Nilforoushan, F., Hatzfeld, D., Abbassi, M., Vigny, C., Masson, F., Nankali, H.,
1145 Martinod, J., Ashtiani, A., Bayer, R., Tavakoli, F., Chery, J., 2004. Contemporary crustal
1146 deformation and plate kinematics in Middle East constraints by GPS measurements in Iran
1147 and northern Iran. *Geophysical Journal International* 157, 381-398.

1148

1149 Vincent, S.B., Allen, M.B., Ismail-Zadeh, A.D., Flecker, R., Foland, K.A., Simmons, M.B.,
1150 2005. Insights from the Talysh of Azerbaijan into the Paleogene evolution of the South
1151 Caspian region. *Geological Society of America Bulletin* 117, 1513-1533.

1152

1153 Weaver, B.L., Wood, D.A., Tarney, J., Joron, J.L., 1987. Geochemistry of ocean island
1154 basalts from the South Atlantic: Ascension, St. Helena, Gough and Tristan da Cunha. In:
1155 Fitton, J.G., Upton, B.G.J. (Eds.). *Alkaline Igneous Rocks*. Geological Society of London
1156 *Special Publications* 30, 253-267.

1157

1158 Weaver, B.L., 1991. The origin of ocean island basalt end-member compositions: trace
1159 element and isotope constraints. *Earth and Planetary Science Letters* 104, 381-397.
1160

1161 Williams, H.M., Turner, S.P., Pearce, J.A., Kelley, S.P., Harris, N.B.W., 2004. Nature of the
1162 source regions for post-collisional, potassic magmatism in southern and northern Tibet from
1163 geochemical variations and inverse trace element modelling. *Journal of Petrology* 45, 555-
1164 607.
1165

1166 Woodcock, N.H., Fischer, M., 1986. Strike-slip duplexes. *Journal of Structural Geology* 8,
1167 725-735.
1168

1169 Workman, R.K., Hart, S.R., 2005. Major and trace element composition of the depleted
1170 MORB mantle (DMM). *Earth and Planetary Science Letters* 231, 53-72.
1171

1172 Zindler, A., Hart, S., 1986. Chemical Geodynamics. *Annual Reviews in Earth and Planetary*
1173 *Sciences* 14, 493-571.
1174

1175 Zor, E., 2008. Tomographic evidence of slab detachment beneath eastern Turkey and the
1176 Caucasus. *Geophysical Journal International* 175, 1273-1282.
1177
1178

1179 **Table captions**

1180

1181 Table 1. Major and trace element data for selected samples from the valley, ridge, and cone
1182 series, Shirak. LOI = loss-on-ignition.

1183

1184 Table 2. Measured Nd and Sr isotope compositions of the valley, ridge, and cone series,
1185 Shirak.

1186

1187 **Supplementary Items**

1188

1189 Item 1. Selected photomicrographs of samples from the valley, ridge, and cone series, Shirak.

1190

1191 Item 2. Complete whole rock major and trace element data for the Shirak lavas, including
1192 trace element standards.

1193

1194

1195 **Figures**

1196

1197 Figure 1. Map of the Turkish- Iranian plateau with shaded digital topography, showing
1198 locations of Pliocene-Quaternary volcanic centres (cones) and the study area (rectangle).

1199

1200 Figure 2. Digital topography map of the study region with geological features simplified from
1201 work by Khachatur Meliksetian, Gevorg Navasardyan and Sergey Karapetyan of the Institute
1202 of Geology of the National Academy of Sciences of Armenia, plus outline map of Armenia
1203 showing administrative boundaries and regional coverage of Late Miocene-Quaternary
1204 magmatic products.

1205

1206 Figure 3. (a) Total alkali-silica classification (Le Bas et al., 1986) and (b) K_2O vs. SiO_2
1207 classification (Peccerillo and Taylor, 1976).

1208

1209 Figure 4. Major element variation diagrams for the Shirak lavas.

1210

1211 Figure 5. Minor and trace element variation in the Shirak lavas.

1212

1213 Figure 6. Rare earth element and extended trace element normalised plots. Chondrite
1214 normalisation values from McDonough and Sun (1995) and Primitive Mantle and OIB values
1215 from Sun and McDonough (1989).

1216

1217 Figure 7. (a) Nd-Sr isotope plot for Shirak lavas, compared to mafic centres within the
1218 collision zone. Pliocene-Pleistocene valley series in southern Georgia and Late Miocene
1219 mafic lavas from the Elbrus region of Southern Russia - Lebedev et al. (2007; 2010); NW

1220 Iran minor centres, Tendurek, Ararat, Kurkistan - Kheirkhah et al. (2009), Allen et al. (2013);
1221 Damavand - Davidson et al. (unpublished data), Mirnejad et al. (2010); Artvin, Eastern
1222 Turkey - Aydiçakir and Şen, in press). Mantle end members and array - Zindler & Hart
1223 (1986). (b) Variation of Nd and Sr isotopes as a function of magmatic evolution.

1224

1225 Figure 8. Fractional crystallisation (FC) trends within the Shirak lavas (symbols as per
1226 previous diagrams). Data and FC vectors for basic to acidic rocks for Eastern Anatolia are
1227 from Pearce et al. (1990). pl = plagioclase; o = olivine; opx = orthopyroxene; cpx =
1228 clinopyroxene; hb = hornblende; gnt = garnet.

1229

1230 Figure 9. Th/Yb vs. Ta/Yb diagram (Pearce, 1983) for the Shirak lavas, showing an FC
1231 vector for a hydrous assemblage, taking into account increasing partition coefficients during
1232 magmatic evolution (after Keskin et al., 1998), and an AFC vector as described on the figure.
1233 Eocene rocks from Eastern Turkey, likely to be similar to those directly underlying the Shirak
1234 lava series, are plotted (Aydiçakir and Şen, in press). Crust (UCC: upper continental crust;
1235 MCC: middle crust; LCC: lower crust; BCC: bulk continental crust, all from Rudnick and
1236 Gao, 2003). Active margins - Pearce (1983). See text for discussion.

1237

1238 Figure 10. Zr/Hf vs. Nb/Ta plot for Shirak lavas and selected mafic Pliocene-Quaternary
1239 lavas from the Arabia-Eurasia collision. Ararat and Tendürek are from lithospheric mantle
1240 sources, Karacadağ in southern Turkey has an OIB source. Sources: Tendürek, Ararat –
1241 Kheirkhah et al. (2009); Karacadağ - Sen et al. (2004), Lustrino et al. (2010); clinopyroxene
1242 fractionation based on partition coefficients of Pagé et al. (2009); other references as per
1243 Figure 9.

1244

1245 Figure 11. Non-modal batch partial melting models for the valley series lavas using depleted
1246 MORB mantle (Workman and Hart, 2005) and incompatible element enriched oceanic
1247 plateau (Fitton and Godard, 2004) sources. Source modes: spinel lherzolite - ol = 0.578, opx
1248 = 0.27, cpx = 0.119, sp = 0.033; garnet lherzolite - 0.598, 0.211, 0.076, gnt = 0.115. Melt
1249 modes: spinel lherzolite - 0.1, 0.27, 0.5, sp = 0.13; garnet lherzolite - 0.05, 0.2, 0.3, gnt =
1250 0.45. Partition coefficients are from the GERM Partition Coefficient Database
1251 (<http://earthref.org/KDD>).

1252

1253 Figure 12. A schematic cross-section through the present-day Arabia-Eurasia collision zone
1254 highlighting potential processes involved in Pliocene-Quaternary magmatism. Hatchings
1255 represent regions of partial melting. Crustal thicknesses estimated from Zor et al. (2008).

1 Pliocene-Quaternary volcanic rocks of NW Armenia:
2 magmatism and lithospheric dynamics within an active
3 orogenic plateau

4
5 **I. Neill^{1*}, Kh. Meliksetian², M.B. Allen¹, G. Navarsardyan², S. Karapetyan²**

6
7 ¹Department of Earth Sciences, Durham University, Science Site, DH1 3LE, Durham, UK

8 ²Institute of Geological Sciences, National Academy of Sciences of Armenia, Marshal
9 Baghramian Avenue, Yerevan 0019, Armenia

10

11 *Corresponding author. E-mail: iain.neill@durham.ac.uk. Phone: +44 1913 342356.

12

13 ***Abstract***

14

15 *The Pliocene-Quaternary volcanic rocks of Armenia are a key component of the Arabia-*
16 *Eurasia collision, representing intense magmatism within the Turkish-Iranian plateau, tens*
17 *of millions of years after the onset of continental collision. Here we present whole rock*
18 *elemental and Nd-Sr isotope data from mafic, intermediate, and felsic lava flows and cinder*
19 *cones in Shirak and Lori Provinces, NW Armenia. Magmatism appears to be controlled*
20 *locally by extension related to major strike-slip faults within the plateau. Major and trace*
21 *element results show that the three series – valley-filling medium-K alkali basalt flows, ridge-*
22 *forming andesite to rhyolite flows, and andesitic cinder cones – form a compositional*
23 *continuum linked by a crystallisation sequence dominated by two pyroxenes, plagioclase and*
24 *amphibole. There is some-petrographic and major and trace element evidence for magma*

25 | mixing processes and potentially crustal contamination by Mesozoic-early Cenozoic arc-
26 | related rocks, which has not significantly affected the isotopic signature. Modelling of the
27 | basaltic rocks indicates that they formed by moderate degrees of partial melting (~3-4 %) of
28 | an incompatible element enriched, subduction-modified, lithospheric mantle source. Samples
29 | have a distinctive high Zr/Hf ratio and high Zr concentrations, which are an intrinsic part of
30 | the source or the melting process, and are much more commonly found in ocean island
31 | basalts. Regional models for magmatism commonly-often argue for whole-scale delamination
32 | of the mantle lithosphere beneath Eastern Anatolia and the Lesser Caucasus, but this
33 | scenario is hard to reconcile with limited crustal signatures and the apparent lack of
34 | asthenospheric components within many studied centres.

35

36 | **Highlights**

37

- 38 | - Whole-rock study of Pliocene-Quaternary lavas from the Armenian Highlands
- 39 | - ~~Range of alkali basalts through to rhyolites~~ Compositional range controlled by
40 | fractional crystallisation, magma mixing and possible limited crustal contamination
- 41 | - Low-degree melting of a shallow metasomatised lithospheric mantle source
- 42 | - Exploring triggers for <10 Myr increase in magmatic activity in ~~Armenia and~~
43 | ~~elsewhere in~~ the Arabia-Eurasia collision zone

44

45 | **Keywords**

46

47 | *Armenia; geochemistry; petrogenesis; orogenic plateau*

48

49 | **1. Introduction**

50
51 Orogenic plateaus such as the modern Turkish-Iranian, Bolivian Altiplano-Puna and Tibetan
52 plateaus form in response to plate convergence and collision, and represent a primary
53 topographic feature of the continents. In spite of their thickened crust and compression
54 tectonics, plateaus are also sites of intense, ultimately mantle-derived magmatism (e.g.
55 Williams et al., 2004; Mo et al., 2007). Such magmatism is often attributed to asthenospheric
56 upwelling following the break-off of the subducting oceanic slab (e.g. Keskin, 2003), or the
57 delamination of the lithosphere inboard of the plate suture (e.g. Kay and Kay, 1993).
58

59 The Turkish-Iranian plateau (Fig. 1) is a product of the Cenozoic Arabia-Eurasia
60 collision, and magmatism post-dating initial collision is particularly voluminous from the
61 Late Miocene until the present day, in numerous locations across eastern Turkey, Armenia,
62 and much of Iran (Fig. 1). ~~Erupted products,~~ ranging in composition from mafic to felsic,
63 and sodic to ultrapotassic (Pearce et al., 1990; Karapetian et al., 2001; Davidson et al., 2004;
64 Azizi and Moinevaziri, 2009; Saadat et al., 2011; Saadat and Stern, 2012; Allen et al., 2013).
65 In nearby Georgia and the Greater Caucasus, the most recent magmatism appears to have
66 started slightly earlier, in the Middle Miocene, and continued with some gaps in the record
67 until recent times (Lebedev et al., 2006a,b; 2007; 2008a,b; Adamia et al., 2011).
68

69 This plateau-wide ‘recent’ magmatism may be only partly explained by partial
70 melting of asthenospheric ~~and-or~~ mantle lithosphere sources ~~resultant from~~ due to slab-break-
71 off of the southern Neo-Tethys slab (e.g. Keskin, 2003; 2007; Şengör et al., 2008; Dilek et
72 al., 2010; van Hunen and Allen, 2011). ~~Both the Eocene flare-up and~~ Miocene to recent
73 magmatism extends to at least 500 km from ~~their respective~~ the Bitlis-Zagros suture zones, ~~on~~
74 a spatial scale akin to the Cenozoic ‘ignimbrite flare-up’ of the western United States

75 | ([Johnson, 1991](#)), ~~with a remarkable co-incidence between the locations of the Eocene and~~
76 | ~~recent magmatism ([Verdel et al., 2011](#)).~~ The wide extent of Miocene-Quaternary magmatism
77 | hundreds of kilometres from the suture zone indicates that ~~slab break-off is not the sole~~
78 | ~~mantle melting trigger.~~ Whole-scale lithospheric delamination ([Pearce et al., 1990](#)), ~~on-~~
79 | ~~going under thrusting of Arabian crust ([Allen et al., in press](#)),~~ or other unrecognised
80 | processes may be collectively responsible for magmatism in this region.

81

82 | To further consider the origin of such magmatism, ~~we turn our attention~~ this paper
83 | focuses on Armenia ([Fig. 1](#)), where ~~the geochemistry of~~ recent volcanism has been under-
84 | represented in the international literature (~~[Karapetian et al., 2001](#); [Savov et al., 2007](#); [Lin et](#)~~
85 | ~~al., 2011~~). We present whole rock elemental and Nd-Sr isotope data from three series of
86 | mafic to felsic Pliocene-Quaternary volcanic rocks in the north of Shirak and west of Lori
87 | administrative provinces in the northwest of the country (herein referred to ~~simply~~ as 'Shirak')
88 | ([Fig. 2](#)). The local tectonic setting and relationship to magmatism is highlighted, alongside
89 | discussion on magmatic evolution ~~fractional crystallisation, crustal contamination,~~ mantle
90 | sources, and partial melting. We finish by assessing how the results fit with regional
91 | geodynamic models.

92

93 | **2. Geological setting, structure, and petrography**

94

95 | 2.1. The Turkish-Iranian plateau

96

97 | The Turkish-Armenian-Iranian orogenic plateau ([Fig. 1](#)), ~~itself a product of the Arabia-~~
98 | ~~Eurasia continental collision, and~~ developed following the closure of the Neo-Tethys Ocean
99 | ([Şengör and Kidd, 1979](#)). The basement of the plateau consists of Mesozoic to Early

100 Cenozoic accretionary belts and arc rocks and also older, Gondwanaland-related micro-
101 continental fragments that all accreted to the southern margin of Eurasia. It is widely assumed
102 that ~~in the region of study,~~ the Neo-Tethys oceanic crust~~Ocean~~ was divided into a northern
103 and a southern segment, the former closed ~~by collisions marked by the Sevan-Akera ophiolite~~
104 ~~suite (Fig. 2)~~ either during the Late Cretaceous (Lordkinpanidze, 1980; Keskin, 2008) or the
105 Paleocene-Early Eocene (Sosson et al., 2010). The ~~northern and southern~~two segments of
106 Neo-Tethys were separated by ~~rifted~~ micro-continental fragments such as the South
107 Armenian Block and Tauride-Anatolide terranes (Sosson et al., 2010). Destruction of the
108 southern segment of Neo-Tethys brought Arabia and Eurasia together along the Bitlis-Zagros
109 suture zone (Fig. 1).

110
111 The timing of initial collision between Arabia and Eurasia is debated, although ~~many~~
112 most estimates range between 35 and 20 Ma (Agard et al., 2005; Allen and Armstrong, 2008;
113 Morley et al., 2009; Okay et al., 2010; Ballato et al., 2011; McQuarrie and van Hinsbergen,
114 2013). ~~Furthermore, the timing of plateau growth from this point on is uncertain.~~ Marine
115 carbonates ~~were~~ deposited across much of central Iran and eastern Turkey in the Early
116 Miocene, ~~indicating~~indicate that surface uplift~~growth of the orogenic plateau~~ is a later
117 phenomenon (Bottrill et al., 2012). Deformation is ~~at~~presently focussed on the plateau
118 ~~margins of the plateau~~, from the Greater Caucasus and Alborz in the north to the Zagros in
119 the south, with no active crustal thickening or thinning occurring between (Jackson et al.,
120 1995; Allen et al., 2011). Lithospheric thickness is highly variable, from >200 km in Iran
121 near the Zagros suture, to only 60 km or less in eastern Anatolia (Priestley and McKenzie,
122 2006; Angus et al., 2006). The current height of the plateau, ~1750 m above sea level, has
123 been attributed to a combination of Late Cenozoic crustal shortening, and also to the

124 detachment of mantle lithosphere and/or subducted Tethyan slabs beneath the plateau,
125 allowing the upwelling of hot, buoyant asthenosphere beneath the region (Keskin, 2003).

126

127 ~~Plateau elevations in northern Armenia are approximately 2 km above sea level at~~
128 ~~present. Understanding the association between the growth of the plateau and partial melting~~
129 ~~processes, through interpreting the geochemical patterns of plateau magmatism, can provide~~
130 ~~key constraints on how the plateau has evolved through time, and give insights into orogenic~~
131 ~~plateaux in general.~~ The Cenozoic magmatic record ~~within the region of the present plateau of~~
132 ~~the plateau~~ is divided into several stages (see Dilek et al., 2010; [Chiu et al., 2013](#) for ~~reviews a~~
133 ~~review~~). First is an Eocene ‘flare-up’ of arc magmatism immediately prior to the onset of
134 continental collision, focussed predominantly on the Urumieh-Dokhtar arc in southwest Iran,
135 the Lut Block, Koppeh Dag and Alborz regions of eastern and northern Iran (Verdel et al.,
136 2011), and also in Armenia (Lordkinpanidze et al., 1988). The flare-up has been ~~variously~~
137 attributed to back-arc extension ~~behind the Iranian margin~~ (Vincent et al., 2005), an episode
138 of flat subduction (Berberian and Berberian, 1981), perhaps coupled with enhanced slab roll-
139 back (Verdel et al., 2011), or break-off of the northern Neo-Tethyan slab in Armenia and
140 North-Central Turkey (Keskin et al., 2008; Sosson et al., 2010). The second stage is a
141 magmatic ‘gap’ which comprised some 20-30 Myr of ~~very~~ limited magmatic activity between
142 the Eocene and the Late Miocene as continental collision proceeded (Verdel et al., 2011;
143 Richards et al., 2011). The third and final stage is the ~~resumption~~ ~~of the~~ ~~uplift~~ ~~of~~
144 ~~ultimately~~ mantle-derived volcanism from the ~~Late-Middle to Late~~ Miocene until the present
145 day ([Chiu et al., 2013](#)), ~~in numerous locations~~ ~~which forms the basis of this study.~~

146

147 2.24. Basement and structure [in Armenia](#)

148

149 Armenia, including the Lesser Caucasus mountain range, lies at the northern side of the
150 ~~Turkish-Iranian orogenic~~ plateau (Figs. 1, 2). Southern Armenia is underlain by the
151 aforementioned South Armenian Block (SAB), a micro-continental fragment rifted during the
152 early Mesozoic, separating the ~~During the early Mesozoic, the~~ northern and southern
153 branches of the Neo-Tethyan seaway ~~opened between Africa/Arabia and Eurasia, separated~~
154 ~~by micro-continental fragments of the former Gondawana supercontinent~~ (Stampfli, 2000).
155 ~~Much of southern Armenia is one such fragment, known as the South Armenian Block~~
156 ~~(SAB), which may link to the Tauride and Anatolide terranes to the west (Sosson et al.,~~
157 ~~2010). Where exposed beneath Pliocene-Quaternary rocks, t~~The SAB consists of Proterozoic
158 gneisses, mica schists, and amphibolites partially overlain by Devonian to Jurassic sediments,
159 Jurassic and younger ophiolitic material, and Paleocene to Early Oligocene volcanic rocks
160 related to subduction of the southern branch of Neo-Tethys (Rolland et al., 2009). ~~The~~ In the
161 north of Armenia, the Armenian Highlands represent the former active continental margin of
162 Eurasia and contains ~~island~~ arc and discontinuous ophiolite sequences formed during the
163 closure of the northern branch of the Neo-Tethyan seaway (Adamia et al., 1981; 2011). ~~There~~
164 ~~is significant debate over the mode of formation and location within the Neo-Tethyan realm~~
165 ~~of each ophiolite fragment (Sosson et al., 2010).~~The largest tract of ophiolitic material in
166 Armenia forms the Sevan-Akera suture zone, a 400 km-long boundary between the SAB and
167 the Mesozoic arc of the Lesser Caucasus to the north. Immediately south of our field area,
168 between Amasia and Stepanavan, is a belt of blueschist-facies mélange (part of the Sevan-
169 Akera ophiolite suite), tectonically overlain by Jurassic to Cretaceous mafic ~~oceanic~~ rocks,
170 ~~which are in turn overlain by~~ and two sequences of Cretaceous to Early Oligocene
171 subduction-related volcano-sedimentary rocks (Rolland et al., 2009). ~~⁴⁰Ar/³⁹Ar phengite ages~~
172 ~~from the blueschist suggest metamorphism took place during northwards Tethyan subduction~~
173 ~~in the Late Cretaceous (~95–91 Ma), followed by retrogression which started during collision~~

174 | ~~of the SAB with the Lesser Caucasus island are at ~74-71 Ma, and continued until terminal~~
175 | ~~collision with the Eurasian margin during the Eocene (Rolland et al., 2009).~~

176 |
177 | Following the Eocene amalgamation of the Armenian crustal blocks (Rolland et al.,
178 | 2009), north-directed subduction of the southern ~~branch of~~ Neo-Tethys terminated along the
179 | Bitlis-Zagros suture, (~~some 300 km south of Armenia~~). After the last ~~Eocene-Oligocene~~
180 | subduction-related magmatism, the magmatic ‘gap’ in Armenia extended until the Late
181 | Miocene (~<10 Ma), based on groundmass and mineral K-Ar ⁴⁰K-⁴⁰Ar ages from the oldest
182 | volcanic rocks of the Gegham Highlands (Arutyunyan et al., 2007). The most voluminous
183 | volcanism is ~~however~~ of Pliocene-Quaternary age, covering much of Aragatsotn, Shirak,
184 | Kotayk, Gegharkunik, and Syunik provinces, an area >10,000 km² (Mitchell and Westaway,
185 | 1999; Karapetian et al., 2001; Lebedev et al., 2011) (Fig. 2). ~~If interpretations of crustal~~
186 | ~~structure are correct, the magmas from Shirak in this study may have passed through a~~
187 | ~~complex series of interwoven crustal units including SAB basement, Jurassic arc material,~~
188 | ~~Jurassic-Early Oligocene arc rocks, flysch, and limestone (Sosson et al., 2010).~~

190 | 2.3.2. Pliocene - Quaternary magma series

191 |
192 | ~~Much of t~~The geology of NW Armenia was first studied in detail during Soviet times
193 | (Kharazyan, 1983). The oldest Pliocene – Quaternary volcanism is represented by poorly-
194 | exposed rhyolites and obsidians at Aghvorik (Fig. 2), covered by. ~~These felsic rocks are~~
195 | ~~covered by Upper Pliocene dolerites (see below). Aside from these felsic rocks, much of the~~
196 | ~~lowest topography in Shirak is covered by mafic rocks, traditionally named as doleritic~~
197 | ~~basalts or Pliocene plateau basalts in Armenian geological literature which drape much of the~~
198 | lowest topography in Shirak, often part-filling river valleys for tens of kilometers. These

199 | ~~flows form a stratigraphic horizon across much of northern and central Armenia, due to~~
200 | ~~presence of extended lava flows cropping out on plateaus and in cross-sections in many of the~~
201 | ~~river valleys. Some r~~Relationships with sedimentary deposits dated using mammalian fossils
202 | lead authors to conclude that these mafic lavas were of Late Pliocene age (Kharazyan, 1983
203 | and references therein). A ~~⁴⁰K-⁴⁰Ar~~ K-Ar age determination from dolerite from the Akhurian
204 | river basin within our study area gave a result of 2.5 ± 0.2 Ma (Chernyshev et al., 2002).
205 | Groundmass K-Ar ~~⁴⁰K-⁴⁰Ar~~ results from ~~a wide range of numerous~~ mafic to felsic volcanic
206 | rocks across the Javakheti Highlands in southern Georgia gave ages of 4.6 ± 0.2 to $1.54 \pm$
207 | 0.10 Ma (Late Pliocene to Quaternary) (Lebedev et al., 2008a,b). The mafic rocks in Armenia
208 | and southern Georgia ~~have been described as resulting~~ may have resulted from fissure
209 | eruptions (Jrbashyan et al., 1996), but the actual source of these lavas has never been found,
210 | and may be buried by younger, ~~more evolved~~ flows.

211 |
212 | ~~Also present~~ On top of the plateau-like topography formed by the mafic flows
213 | in Shirak, are ~~mountainous hills~~ areas of intermediate-felsic composition ~~extending of~~ up to
214 | 600 m ~~prominence above the plateau-like topography formed by the mafic flows~~, including
215 | the ~~prominent~~ north-south trending Javakheti, or Kechut, ridge (Fig. 2). ~~Prior to any~~
216 | ~~radiometric age determinations~~, Kharazyan (1983) distinguished two ~~age~~ units within the
217 | Armenian part of the Javakheti ridge. The first unit (Lower Kechut Suite) ~~is presented by~~ is
218 | said to contain two-pyroxene basaltic andesites, andesites and hornblende andesites which
219 | cover the valley series and are thus assumed to be of Early Pleistocene age (Kharazyan,
220 | 2005). SHRIMP U-Pb zircon dating of andesitic vent-proximal ash and breccia layers
221 | deposited on the eastern flank of the Javakheti ridge in Lori province at the Karakhach
222 | archaeological site (Fig. 2) ~~has gives~~ confirmed maximum eruption ages of 1.94 ± 0.05 to
223 | 1.80 ± 0.03 Ma, ~~giving a maximum eruption age~~ (Presnyakov et al., 2012). This study also

224 | noted ~~several older grains, two of Eocene age~~ two Eocene zircons (40-50 Ma) consistent with
225 | Eocene arc rocks found to the east of the study area, plus five Proterozoic grains, consistent
226 | with an origin in the underthrust SAB ~~(e.g. Rolland et al., 2009)~~. It is uncertain whether or
227 | not these old grains were from xenoliths ripped up during explosive volcanism or zircons
228 | assimilated during magma ascent. The Javakheti Ridge extends into southern Georgia, where
229 | it is higher and has a sharp little denuded topographic profile compared to further south.
230 | Groundmass ~~⁴⁰K-³⁹Ar~~ K-Ar dating revealed younger ages of $\ll 1$ Ma for the Samsari volcanic
231 | centre ~~which lies~~ to the north of the Javakheti Ridge (Chernyshev et al., 2006). Kharazyan
232 | (1983) also defined an Upper Kechut Suite ~~on the Javakheti Ridge,~~ supposedly containing
233 | lavas erupted from cinder cones on the western part of the ~~ridge-ridge covering eroded lavas~~
234 | ~~and pyroclastic material of the Lower Kechut Suite~~, and considered to be of Middle
235 | Pleistocene age (Kharazyan, 2005). We did not find clear evidence of this unit during our
236 | studies. The only other Pliocene-Quaternary volcanic products in this part of Shirak are
237 | cinder cones to the west of the Javakheti Ridge around Lake Arpi (Fig. 2), which are
238 | estimated to be of ~~Lower~~ Early-Middle Pleistocene age, based on relationships with ~~valley~~
239 | ~~series~~ the mafic rocks and some river terraces (Kharazyan, 1983).

240

241 | Overall ~~it is evident that~~ there have been no comprehensive geochronological studies
242 | carried out in ~~Armenia-Shirak~~ using a single reliable technique, unlike those ~~produced~~ for
243 | similar sequences in Georgia (Lebedev et al., 2008a,b). ~~Furthermore there is a~~ lack of
244 | continuous exposure, ~~which~~ hampers judgement of the relative age of the different lavas.
245 | ~~Hence, w~~ We have decided to ~~simplify the lavas, and~~ sub-divide the entire Pliocene-
246 | Quaternary suite close to the Javakheti Ridge into three ~~main~~ components: mafic flows (the
247 | dolerites) largely covering the topography developed on the ~~pre-existing Sevan-Akera~~
248 | ~~suture~~ basement (herein termed the *Valley Series*); more evolved flows built up into hills

249 | ~~rising up to 600 m~~ above the mafic flows (*Ridge Series*); and scattered cinder cones (*Cone*
250 | *Series*) (Fig. 2).

251

252 | 2.32.1. Valley Series

253

254 | The Valley Series consists of mafic flows ~~which reach with~~ a maximum cumulative thickness
255 | of 200 m in eastern Lori province (Fig. 2). In the study area, the exposed sequence ~~usually~~
256 | comprises at most four or five stacked flows up to 40 m thick in total, and directly overlies
257 | the Sevan-Akera suture and ophiolite sequence in the Dzoraged gorge and near Amasia (Fig.
258 | 2). We have collected samples from these locations, as well as from Lake Arpi and near
259 | Tashir in western Lori Province (Fig. 2). ~~Jrbashyan et al. (1996) suggested that these flows~~
260 | ~~are likely to have been fissure fed, and flowed from the north, before following the palaeo-~~
261 | ~~topography of the Debed and Akhuryan river valleys to the east and south.~~ Valley Series
262 | samples collected from near Lake Arpi, Amasia, and Tashir (Fig. 2), consist of vesicular sub-
263 | ophitic dolerites with rare clinopyroxene or optically zoned plagioclase phenocrysts, set in a
264 | groundmass of 1-2 mm grain size consisting of clinopyroxene, plagioclase, and oxides (see
265 | Supplementary Item 1). Clinopyroxene is commonly rimmed or almost totally replaced by
266 | red-brown amphibole, and there is occasional interstitial quartz and rare rounded quartz
267 | blebs. None of the samples contain any fresh olivine Some samples contain very rare
268 | iddingsite crystals, and the few olivines found in thin section are rounded and <0.5 mm in
269 | diameter. ~~although a number do have very rare 1-2 mm bright red cubic crystals, which may~~
270 | ~~be iddingsite replacing olivine. The vesicles in the selected samples do not contain secondary~~
271 | ~~infill.~~

272

273 | 2.32.2. Ridge Series

274

275 | Magmatism in this series is restricted to ~~more evolved~~ intermediate to felsic lavas ~~which have~~
276 | built up into prominent topographic features. The highest of these is the north to south-
277 | trending Javakheti Ridge (Fig. 2), consisting of ~~multiple~~ rounded and glacially eroded ~~centres~~
278 | peaks reaching ~3100 m above sea level, following a clear north-south trend running north
279 | into Georgia (Fig. 2). A second series of hills ~~and ridges~~ lie north of the Akhuryan River
280 | parallel to the Georgian border, but these are more topographically muted, reaching a
281 | maximum elevation of ~2400 m. Rock types from both ridges are almost exclusively ~~flows of~~
282 | andesitic to dacitic ~~composition~~flows, with ~~some~~ rare black dacites and rhyolitic obsidians
283 | (Karapetian et al., 2001). ~~The flows that we have analysed~~Analysed flows range from
284 | ~~evolved~~ basaltic trachyandesites to dacites, ~~but and they display there is~~ much compositional
285 | and textural variation. Some of the least evolved samples (<60 wt.% SiO₂) contain 1-3 mm
286 | phenocrysts and glomerocrysts of clinopyroxene (rarely orthopyroxene) and ~~some~~
287 | plagioclase, set in a flow-banded groundmass of plagioclase, clinopyroxene and Fe-Ti oxides,
288 | with accessory apatite and zircon. More evolved samples tend to contain significantly more
289 | plagioclase phenocrysts, and several have abundant 1-3 mm euhedral green-brown pleochroic
290 | amphiboles, but the presence of amphibole is not ubiquitous even in samples ~~containing of~~
291 | similar SiO₂ and MgO concentrations. Many plagioclase crystals ~~in either clinopyroxene or~~
292 | ~~amphibole dominated suites~~ are sieve-textured and some have corroded margins, implying
293 | usually taken to imply either the occurrence of magma mixing processes (Tsuchiyama, 1985;
294 | Tepley et al., 1999), ~~or rapid decompression during eruption (Nelson and Montana, 1992);~~
295 | and many crystals are also optically zoned. Other evidence for magma mixing is the common
296 | occurrence of rounded quartz blebs with dark reaction coronas, and ubiquitous opaque rims
297 | on primary hornblende crystals (Tepley et al., 1999; Supplementary Item 1). ~~The A~~ black
298 | dacite contains a few clinopyroxene glomerocrysts, but mostly consists of a fine-grained

299 groundmass dominated by prismatic to acicular feldspars. ~~Two photomicrographs from the~~
300 ~~Ridge Series are in Supplementary Item 1.~~ The Ridge Series included^s the only
301 ~~polycrystalline crustal~~ xenoliths noted from our sampling, ~~in a single sample from a single~~
302 ~~site~~ near Darik, north of Lake Arpi (Fig. 2). The xenoliths consist of a coarse-grained
303 groundmass of plagioclase, clinopyroxene, oxide, and rare iddingsite after olivine; and 2-3
304 mm phenocrysts of clinopyroxene and plagioclase, most consistent with inclusion of material
305 from the Valley Series. A slight chilled margin is observed within the host. ~~Based on~~
306 ~~petrographic similarities, we suggest that this xenolith has been derived from the Valley~~
307 ~~Series flows immediately underlying the ridge, and not the deeper crust. The host itself also~~
308 ~~contains some sub-rounded quartz xenocrysts (see Supplementary Item 1) and degraded~~
309 ~~plagioclase crystals with a speckled appearance, sometimes rimmed by new growth. The~~
310 ~~presence of quartz xenocrysts with reaction rims is taken to indicate assimilation of host~~
311 ~~rocks.~~

312

313 2.32.3. Cone Series

314

315 Scattered cinder cones are present in the Akhuryan valley near Lake Arpi (Fig. 2), often tens
316 of metres high and ~~reaching~~ several hundred metres across. ~~A notable lack of erosion of these~~
317 ~~cones suggests they represent the youngest volcanism in the area.~~ We have collected samples
318 from Sepasar, Eznasar, and Kaputkogh cones (Fig. 2). Most are composed of poorly welded
319 unsorted glassy or scoria~~eous~~ fragments ~~of various sizes~~, and more coherent scoria bombs
320 reaching a few tens of centimetres in diameter. The Cone Series compositions mirror the least
321 evolved of the ridge series, the majority of samples containing differing proportions of
322 plagioclase and clinopyroxene as phenocrysts and groundmass (Supplementary Item 1).
323 Bombs from Kaputkogh and Eznasar contain ubiquitous mm-scale rounded quartz

324 xenocrysts, whereas those at Sepasar appear more mafic, and devoid of foreign material. ~~A~~
325 ~~photomicrograph of a typical Cone Series sample is available in Supplementary Item 1.~~

326

327 **3. Analytical methods**

328

329 Samples were powdered in an agate ball mill at Durham University. Major element analysis
330 was conducted on fused glass beads using a PANalytical Axios Advanced X-Ray
331 Fluorescence (XRF) spectrometer at the University of Leicester. Leftover fractions of the
332 powder from XRF analysis were digested using a standard HF and HNO₃ technique prior to
333 trace element analysis. Solutions were run on a Thermo X2 inductively-coupled plasma mass
334 spectrometer (ICP-MS) at the Northern Centre for Isotopic and Elemental Tracing (NCIET)
335 at Durham University. Accuracy, precision, and reproducibility were monitored using blanks,
336 multi-run and within-run duplicates, Re-Rh spike solutions, and five international reference
337 standards. Standard W2 (n = 15) gave first relative standard deviations of 5% or better for
338 most transition metals (excepting 10% for Sc, 12% for Cr, 6% for Ni), the large ion lithophile
339 elements (LILE) and the rare earth elements (REE) (7% for La, 6% for Ce). Elemental results
340 are recorded in Table 1 and Supplementary Item 2, the latter also containing standard results.

341

342 Radiogenic Nd and Sr isotope analysis was conducted at NCIET, with column
343 chemistry for elemental pre-concentration based on the method of Dowall et al. (2007).
344 Powders were digested in HF and HNO₃, and solutions run through 1 ml pipettes containing
345 several drops of dilute Sr-spec resin to collect the Sr-bearing fraction. The high field strength
346 element (HFSE)- and rare earth element (REE)-bearing fraction from these columns was run
347 through 10 ml Bio-Rad polypropylene columns containing 1 ml of Bio-Rad AG1-X8 200-400
348 mesh anion-exchange resin. Neodymium was collected as part of a general rare earth element

349 fraction. Analysis was conducted on a Thermo Neptune Mass Collector ICP-MS. Strontium
350 was run in a single batch during which time blanks averaged 88 pg Sr (n = 6). International
351 reference standard NBS987 gave a mean of $^{87}\text{Sr}/^{86}\text{Sr} = 0.710263 \pm 0.000012$ (2σ , n = 12),
352 comparable to a preferred value of 0.710240, and providing a minimum uncertainty of
353 16 ppm (2σ). No correction was applied to the final results. Neodymium was run in two
354 separate batches, with blanks averaging 10 pg Nd (n = 6). During the first run, a combination
355 of the J&M standard and a Sm-doped version gave a mean $^{143}\text{Nd}/^{144}\text{Nd} = 0.511098 \pm$
356 0.000007 (2σ , n = 13), and a minimum uncertainty of 13 ppm (2σ). During the second run,
357 $^{143}\text{Nd}/^{144}\text{Nd} = 0.511100 \pm 0.000007$ (2σ , n = 13), giving an uncertainty of 14 ppm (2σ). For
358 consistency between the runs, all results were normalised to a preferred value of 0.511110.
359 Results are presented in Table 2.

360

361 **4. Geochemistry**

362

363 **4.1. Sample freshness**

364

365 We collected the freshest available samples at each locality, and this is reflected in loss-on-
366 ignition (LOI) values typically <1 wt.%, mostly un-weathered feldspars and mafic minerals,
367 and an overall lack of sericite and chlorite in thin section. Major and trace element data,
368 particularly element vs. SiO_2 plots (see Section 4.2), have trends consistent with magmatic
369 processes, particularly for CaO, MgO, K_2O , and Na_2O , as opposed to the widespread scatter
370 expected during sub-solidus alteration which easily mobilises these elements (e.g. Cann,
371 1970; Pearce, 1996). $^{87}\text{Sr}/^{86}\text{Sr}$ isotope results are commonly affected by hydrothermal
372 alteration, but here are depleted with no sign of a trend towards high $^{87}\text{Sr}/^{86}\text{Sr}$ at constant
373 $^{144}\text{Nd}/^{143}\text{Nd}$ (Table 2); nor is there a correlation between LOI and isotopic ratios.

374 Furthermore, the samples were erupted in an intra-continental high plateau so have not
375 interacted with high $^{87}\text{Sr}/^{86}\text{Sr}$ seawater or been exposed to tropical weathering.

376

377 4.2. Major and trace element characteristics

378

379 4.2.1. Valley Series

380

381 The Valley Series lavas (~49-55 wt.% SiO_2) are mostly mildly alkaline trachybasalts based
382 on the total alkali-silica classification (Le Bas et al., 1986; Fig. 3a), and belong to the
383 medium-K series of Peccerillo and Taylor (1976; Fig. 3b). They are evolved, with 4-7 wt.%
384 MgO and low molar Mg# from 46 to 58. Overall the samples have low TiO_2 , moderate-high
385 Al_2O_3 , and a sodic character ($\text{Na}_2\text{O}/\text{K}_2\text{O} = 2.7\text{-}4.1$) (Fig. 4). Trace element abundances and
386 trends can be seen on Figure 5. Also, the lavas have low Sc (<25 ppm), moderate Cr, Ni, and
387 large ion lithophile element (LILE) abundances (e.g. Ba = 280-450 ppm and Sr = 540-720
388 ppm). ~~Of the high field strength elements (HFSE), they have considerable enrichment in Zr~~
389 ~~(170-210 ppm), and super chondritic Zr/Hf (47-52), with Nb/Ta (17-22).~~ Chondrite-
390 normalised (CN) ~~Rare Earth Element (REE)~~REE abundances are light REE (LREE) enriched
391 ($\text{La}/\text{Yb}_{\text{CN}} = 5\text{-}9$; calc-alkaline), with flat heavy REE (HREE) patterns around 15-20 times
392 chondritic abundances (Fig. 6a). The patterns are split into two groups, one with lower LREE
393 and higher HREE concentrations and vice versa, the patterns crossing over at around Pr-Nd.
394 There are some very slight negative Eu anomalies relative to the ~~middle REE (MREE)~~. The
395 extended Primitive Mantle-normalised (PMN) plot (Fig. 6b) shows that the samples have
396 spiky LILE patterns (modest positive Ba, Rb, Th, Sr anomalies), prominent negative K, Nb-
397 Ta, and Ti anomalies and positive Zr-Hf anomalies relative to the REE, with super-chondritic
398 Zr/Hf ratios of 47-55.

399

400 *4.2.2. Ridge Series*

401

402 The more evolved Ridge Series (~57-68 wt.% SiO₂, 2-5 wt.% MgO, Mg# = 41-55) has a
403 wide range of sub-alkaline compositions from basaltic trachy-andesite through to dacite (Fig.
404 3a). Samples largely belong to the medium-K series, although two plot in the high-K field
405 (Fig. 3b). They have noticeably lower TiO₂, Fe₂O_{3(t)} and P₂O₅ concentrations compared to the
406 valley series, and are slightly less sodic (Na₂O/K₂O = 1.4-2.5) (Fig. 4). Transition metal
407 abundances are lower than the Valley Series, but the Ridge Series has higher Ba and Zr and
408 lower Sr and Nb concentrations compared to the mafic lavas (Fig. 5). Chondrite-normalised
409 LREE patterns (Fig. 6c) are similar to the Valley Series, again splitting into two groups with
410 higher or lower LREE concentrations. Ridge samples have La/Yb_{CN} from 8 to 18, with a
411 highly fractionated M-HREE distribution such that some samples have a U-shaped pattern.
412 There are small negative Eu anomalies. Primitive Mantle-normalised patterns (Fig. 6d) differ
413 slightly from the Valley Series in having positive Rb spikes, and more pronounced negative
414 Nb-Ta, P and Ti anomalies.

415

416 *4.2.3. Cone Series*

417

418 The Cone Series splits into three groups, the most mafic being the two cones at Sepasar (58
419 wt.% SiO₂, but low Mg# = 43), and the most felsic at Eznasar (62 wt.% SiO₂, Mg# = 52). The
420 large cone at Kaputkogh has intermediate silica content relative to the other cones, although it
421 has the highest Mg# of 54. The ~~inverted relationship between Mg# and silica content may be~~
422 ~~derived from the most primitive magmas happening to be contaminated by relatively higher~~
423 ~~proportions of associated felsic magmas or crustal components during ascent. This~~

424 | ~~relationship means that the Cone Series do not form a significant part of the discussion on~~
425 | ~~overall fractionation and contamination trends in Section 5.2. Finally, t~~The cones have higher
426 | Nb and Zr concentrations relative to the other series (Fig. 5); REE patterns for the Cone
427 | Series are clearly bimodal (Fig. 6e), whilst the Primitive Mantle-normalised plots look similar
428 | to the Valley Series (Fig. 6f).

429

430 4.3. Radiogenic isotope geochemistry

431

432 | Most samples span a narrow range from $^{87}\text{Sr}/^{86}\text{Sr} = 0.70416$ to 0.70446 and $^{143}\text{Nd}/^{144}\text{Nd} =$
433 | 0.51280 to 0.51287 , giving a range of values in epsilon notation from $\epsilon\text{Nd} = +3.1$ to $+4.6$. No
434 | age corrections were applied owing to the young age of the rocks. On Figure 7a, there is
435 | overlap between samples from the Valley, Ridge, and Cone series, and the samples display
436 | only a little isotopic enrichment with major element evolution (Fig. 7b). Overall, the samples
437 | lie on the mantle array between bulk silicate earth and depleted MORB mantle, and there is
438 | no clear evidence of any trends which might be related to mixing of different mantle end
439 | members (e.g. EMI or EMII) or old, isotopically enriched crustal contaminants. The ~~cones~~
440 | Cone and Valley-Ridge Series samples with-containing quartz xenocrysts are not isotopically
441 | different from the other samples.

442

443 | Regionally, the samples are significantly more depleted than most Pliocene-
444 | Quaternary centres in north-west Iran and Mount Damavand (Alborz), and Tendürek volcano
445 | in Eastern Anatolia (Fig. 7a). The Iranian volcanic rocks were erupted through thicker
446 | lithosphere than beneath Armenia (e.g. Liotard et al., 2008; Kheirkhah et al., 2009; Mirnejad
447 | et al., 2010; Davidson et al., unpublished data; Allen et al., in press 2013). Samples are also
448 | more depleted than asthenospheric melts from eastern Iran which have trends towards the

449 EM-II mantle end member (Saadat et al., 2011; Saadat and Stern, 2012). Instead, results are
450 closest to the few analyses conducted on the large stratovolcano, Mount Ararat, close to the
451 Armenian border (Pearce et al., 1990; Kheirkhah et al., 2009), and nearly identical in terms of
452 $^{143}\text{Nd}/^{144}\text{Nd}$ to six analyses of the ~3.25-2.05 Ma valley series lavas from southern Georgia,
453 and from eight Late Miocene sub-alkaline basalts in central Georgia (Lebedev et al., 2006;
454 2007). Radiogenic isotope results are not yet widely published from other Armenian
455 Pliocene-Quaternary centres, but Savov et al. (2007) and Lin et al. (2011) reported values
456 from $^{87}\text{Sr}/^{86}\text{Sr} = 0.7041$ to 0.7051 and $^{143}\text{Nd}/^{144}\text{Nd} = 0.5128$ to 0.5129 from ~~across much of~~
457 ~~the country various locations. This is a similar narrow range of results compared to our study,~~
458 ~~except for some $^{87}\text{Sr}/^{86}\text{Sr}$ values extending to more enriched compositions outside of the~~
459 ~~mantle array. The overall lack of enriched, continental crust like values and crustal or mantle~~
460 ~~xenoliths is an interesting feature of magmatism across the orogenic plateau in spite of varied~~
461 ~~basement compositions.~~

462

463 5. Discussion

464

465 5.1. Volcano-tectonic interaction

466

467 Before considering the petrogenesis of the magma series, we first address the location of
468 volcanic activity with respect to major crustal structures. The internal part of the orogenic
469 plateau is not undergoing contractile deformation (Jackson et al., 1995; Vernant et al., 2004),
470 but internal reorganisation of the plateau during the on-going convergence between Arabia
471 and Eurasia means that Eastern Anatolia, the Lesser Caucasus, and northwest Iran are criss-
472 crossed by numerous active strike-slip fault systems (Rebaï et al., 1993; Koçyiğit et al.,
473 2001). These systems, which often tally with pre-existing crustal discontinuities, have been

474 widely implicated in providing a locus for Quaternary magmatic activity through the
475 production of highly localised pull-apart zones (Dewey et al., 1986; Karakhanian et al., 1997,
476 2002; Avagyan et al., 2010; Shabanian et al., 2012).

477

478 In Armenia, the active Pambak-Sevan-Syunik right-lateral strike-slip fault system is
479 one such structure exploiting the existing discontinuity of the Sevan-Akera suture zone (Fig.
480 2). All of the magmatism described in this study originated just to the north of the fault zone,
481 and so we propose that this location sat over a region of localised upper crustal extension at
482 the time of magmatism. No active extension is recorded from the Shirak region from
483 earthquake focal mechanisms or geomorphic features. Blanket coverage of most pre-existing
484 fault structures by the Valley Series, and the absence of linear arrays of cinder cones (e.g.
485 Dewey et al., 1986), may have helped obscure this association between faulting and
486 magmatism. The south-eastern termination of the Pambak-Sevan-Syunik fault in the Syunik
487 region is characterised by widespread volcanism in the area south of the fault, with little
488 volcanism to the north (Kharakhanian et al., 2004). The Syunik centres therefore appear to
489 have developed along the complementary trailing imbricate fan (Woodcock and Fischer,
490 1986) to the Shirak volcanic rocks. The north-south trending volcanism along the Javakheti
491 Ridge is consistent with this idea.

492

493 Not all young Armenian centres fit a simple fault-control hypothesis: Aragats
494 volcano, the largest centre in the country, is situated in a region apparently not crossed by
495 presently-active faults (Kharakhanian et al., 2004). It is possible that older faults may be
496 obscured by lava flows, or that some other control on the location of Aragats may apply, such
497 as a local thin-spot in the lithosphere which focussed melting beneath the plateau.

498

499 5.2. Fractionation and contamination processes

500

501 *5.2.1. Fractional crystallisation – minerals involved*

502

503 | No sample ~~of~~from the mafic Valley Series lavas is close to a primary melt (MgO is typically
504 < 7 wt.%), so it is assumed that they have already evolved at depth involving a typical
505 fractionation assemblage of olivine and spinel. In the major element data, clear falling trends
506 for the Valley Series against typical indices of fractionation, such as SiO₂, TiO₂, MgO, and
507 CaO (Fig. 4), corroborate with the observed mineral assemblages in confirming that clino-
508 and orthopyroxene and Fe-Ti oxides were important in Valley Series evolution. Al₂O₃
509 concentrations cover a narrow range with no trends, indicating that feldspar fractionation was
510 not an important feature of the Valley Series; likewise with P₂O₅ concentrations and apatite.
511 Trace element abundances, such as Ba, Th, and La, display rising trends against SiO₂ in the
512 Valley Series, which confirms their incompatible behaviour (Fig. 5). In the more evolved
513 Ridge and Cone Series, clear falling trends emerge against SiO₂ for Al₂O₃, P₂O₅, Sr, Nb, Zr
514 and La, pointing to addition of plagioclase, along with small proportions of zircon and
515 apatite, to the fractionating assemblage.

516

517 The overall pattern of Shirak magmatism can be compared with Eastern Anatolia.
518 Volcanic centres that display either high- or low-Y trends relative to Rb, are associated with
519 fractionation of anhydrous (plagioclase, olivine, pyroxenes, and magnetite), or hydrous
520 assemblages (including amphibole, which is compatible with Y) respectively (Pearce et al.,
521 1990) (Fig. 8). The mafic Valley Series rocks in Shirak follow the same moderate to low-Y
522 trend as the Kars plateau/Mt. Ararat systems, which may indicate amphibole fractionation has
523 taken place at depth, given that amphibole is not seen in any of the Valley Series thin

524 sections. Another indication of amphibole fractionation is the compatible middle to heavy
525 REE (Sm-Lu) showing falling trends as the three series evolve (Fig. 6). The ridge series lavas
526 have a steeply falling trend for Y against Rb, which may reflect increased partition
527 coefficients for both clinopyroxene and amphibole for Y as these minerals fractionate from
528 more evolved rocks (Pearce et al., 1990).

529

530 5.2.2. Magma mixing

531

532 The petrographic evidence for magma mixing (zoned plagioclases, sieve textures,
533 reaction rims and quartz blebs) also needs to be reconciled with geochemical data. Major
534 element plots, especially TiO₂, CaO and MgO vs. SiO₂ (Fig. 4) have straight line trends
535 which are widely associated with mixing of two compositionally distinct magmas (Langmuir
536 et al., 1978), rather than the curved trends associated with fractional crystallisation. In the
537 field, the key observation is that the most evolved rocks found in the area, the obsidians at
538 Agvorik, underlie the mafic Valley Series, so felsic magmas had already been erupted by the
539 time of mafic magma injection.

540

541 5.2.32. Crustal contamination

542

543 Many models (e.g. Keskin et al., 1998) consider assimilation-fractional crystallisation (AFC)
544 processes to be important in magma genesis in the plateau. The extent to which crustal
545 contamination has affected primary magma compositions may vary widely across the
546 collision zone. Keskin et al. (1998) argues that recent mafic to felsic samples from Eastern
547 Anatolia have undergone significant amounts of combined assimilation-fractional
548 crystallisation (AFC) AFC coinciding with enriched ⁸⁷Sr/⁸⁶Sr ratios up to 0.7065 (Pearce et

549 al., 1990). In Shirak, ~~there are~~ samples have only ~~very a~~ slight variation in isotope ~~signatures~~
550 ~~ratios~~ relative to ~~silica concentration~~ SiO_2 (Fig. 7b) ~~in the Valley and Ridge Series~~, and
551 samples containing quartz xenocrysts ~~have neither higher~~ $^{87}\text{Sr}/^{86}\text{Sr}$ ~~nor lower~~ $^{143}\text{Nd}/^{144}\text{Nd}$
552 ~~ratios than do~~ not have different isotopic ratios to the other lavas - a feature that should
553 strongly support the hypothesis that fractionation and magma mixing were the dominant
554 processes. Also, preliminary results from elsewhere in Armenia, including the Aragats
555 volcanic system, show little clear isotopic evidence for contamination (Savov et al., 2007; Lin
556 et al., 2011) in spite of Aragats erupting through the SAB basement which has enriched
557 $^{87}\text{Sr}/^{86}\text{Sr}$ ratios of up to 0.7303 - any contamination should be easily identified (Bagdasaryan
558 and Gukasyan, 1985). However, along-strike from Shirak at Artvin in eastern Turkey, Eocene
559 rocks have measured $^{143}\text{Nd}/^{144}\text{Nd}$ of 0.512663 - 0.512854 and $^{87}\text{Sr}/^{86}\text{Sr}$ of 0.705148 -
560 0.704233 (Aydinçakir and Şen, in press). These values are very similar to the Shirak lavas
561 (Fig. 7), so partial melting or assimilation of similar Eocene crust may be very difficult to
562 decipher geochemically.

563

564 ~~In terms of trace element ratios, on~~ a Th/Yb vs. Ta/Yb plot (Pearce, 1983) (Fig. 9),
565 the ~~most mafic Valley Series lavas have enriched Ta/Yb ratios of 2.9-4.7, pointing to lower~~
566 ~~degrees of melting or a more fertile source than expected for mid-ocean ridge basalts~~
567 ~~(MORB) ($\text{Ta}/\text{Yb} = 0.9$; Sun and McDonough, 1989). The lavas also lie above the mantle~~
568 ~~array in the calc-alkaline field, indicative of a small subduction-related component (see~~
569 ~~Section 5.3). The three series form a consistent linear trend sub-parallel to the mantle array,~~
570 with the felsic rocks having compositions more enriched than those of typical continental
571 upper-crust (Rudnick and Gao, 2003). On this diagram, the fractional crystallisation trend for
572 a typical amphibole-bearing assemblage is shown. ~~An important consideration is that t~~
573 samples plot ~~both~~ to the left of the fractionation trend ~~and left of a direct mixing line with~~

574 ~~upper continental crust (Taylor and McLennan, 1985). This result~~ which suggests that AFC
575 processes may be operating - ~~although choice of mineral assemblages and partition~~
576 ~~coefficients can easily affect the FC trend.~~ AFC modelling (Powell, 1984) using the average
577 composition of the ~~Eocene Turkish Artvin rocks (Aydinçakir and Şen, in press)~~ quite
578 ~~reasonably reproduces the trend of the Shirak lavas, but the~~ and a ratio of assimilation to
579 fractionation ~~is high at~~ 0.8. ~~Results of modelling shown on Figure 9 indicate that this~~
580 ~~significant level of assimilation may produce a trace element trend more compatible with the~~
581 ~~composition of the Shirak rocks than attainable by pure FC processes. Unfortunately, isotopic~~
582 ~~analyses are not available for these Turkish rocks. Modelling thus shows that large volumes~~
583 ~~of isotopically similar material can be incorporated into the Shirak lavas without a significant~~
584 ~~effect on trace element evolution. Studies of disequilibrium textures and mineral chemistry~~
585 ~~might better elucidate the processes involved in magma evolution.~~

586

587 5.3. Mantle source and partial melting

588

589 5.3.1. ~~Overall nature of the m~~Mantle source of the *Shirak lavas Valley Series*

590

591 The presence of LILE and HFSE anomalies on normalised plots of mafic rocks (Fig. 6b) are
592 normally taken to indicate a subduction-modified mantle source owing to the retention of
593 HFSE in the slab, and the comparative mobility of the LILE/REE during slab heating and
594 dewatering into the overlying mantle wedge (e.g. Pearce and Peate, 1995). We have already
595 introduced the Th/Yb vs. Ta/Yb diagram (Fig. 9). The alkali basalts from Shirak plot above
596 the mantle array which is commonly taken to indicate the presence of a subduction-modified
597 source. However, they also have very much higher Ta/Yb ratios than many subduction-
598 related rocks. ~~We take this to indicate that t~~The Shirak lavas are therefore derived from an

599 | incompatible element-enriched mantle source, or ~~one that has undergone~~ are derived from a
600 | limited degree of melt extraction. As these lavas erupted >20 Myr after the end of Neo-
601 | Tethyan subduction, and there is no evidence for a slab at shallow depths beneath Eastern
602 | Anatolia and Armenia at the present day (Zor et al., 2008), it is improbable that a normal
603 | supra-subduction zone hydrated asthenospheric mantle wedge was involved in the origin of
604 | the Shirak lavas. Therefore, the subduction-like characteristics are likely to be derived from a
605 | fertile source within the mantle that had been inherited its slab-related geochemical
606 | component from earlier Neo-Tethyan subduction ~~processes~~. Crustal contamination is unlikely
607 | be responsible for the subduction-like characteristics of the Shirak lavas, as LILE and HFSE
608 | anomalies are significant in even the most mafic samples.

609

610 | Some of the trace element characteristics of the valley series may help constrain the
611 | mineralogy of the mantle source. Overall, the flat normalised HREE patterns (Fig. 6a)
612 | indicate a spinel-facies mantle source at <70 km, unless the degree of partial melting was
613 | very high (>25%) in order to completely consume any garnet present at depths of >70 km.
614 | This is unlikely given the overall LREE-enriched and Nb-Ta/HREE-enriched trace element
615 | patterns (Fig. 6b) which point towards modest degrees of partial melting of an enriched
616 | source. Low Sc concentrations (<25 ppm) in all Valley Series samples may indicate residual
617 | clinopyroxene, another indicator of a low degree of partial melting, but it is also possible that
618 | extensive pyroxene fractionation prior to eruption has resulted in these low values. Intra-
619 | LILE variations, including low Ba/Rb (<25) and Rb/Sr ratios (<0.05), do not point towards
620 | amphiboles or phlogopite playing an important role during melting (e.g. Furman and Graham,
621 | 1999). Melting therefore took place beneath the Armenian crust at depths of ~45-70 km.

622

623 One unusual feature of the Shirak lavas is high ocean island basalt (OIB)-like Zr
624 concentrations (~200 ppm) and Zr/Hf ratios (41-52) relative to MOR and arc basalts, the
625 latter having chondritic Zr/Hf ratios of 35-39 (Weaver et al., 1987; David et al., 2000;
626 Pfänder et al., 2007). Nb/Ta ratios range from 16-22 relative to the chondritic ratio of 19.9
627 (Pfänder et al., 2007). Mafic samples from other nearby centres in the plateau, including
628 Tendürek and Ararat, show similar features (Fig. 10). Lower ratios in the Ridge Series
629 compared to the Valley Series ~~might~~ be explained by contamination with crustal material
630 such as the Eocene basement (Fig. 10). However, the high Zr/Hf ratios of 47-52 in the less
631 evolved Valley Series are a primary feature of the magmas.

632

633 There is little correlation between Zr and Zr/Hf ratios (not shown), indicating that
634 zircon accumulation cannot be directly responsible for the high Zr-Zr/Hf character of the
635 Shirak lavas. HFSE fractionation in OIBs may be due to: (1) residual or fractionating
636 clinopyroxene (David et al., 2000); (2) fractionation of Ti-bearing phases such as rutile,
637 ilmenite, and amphibole (Foley et al., 2000; Tiepolo et al., 2001); (3) melting of recycled
638 eclogite or garnet pyroxenite (Pfänder et al., 2007); or (4) the occurrence of carbonate
639 metasomatism (Dupuy et al., 1992). For option (1), fractionation of clinopyroxene only has a
640 modest effect upon Zr/Hf ratios (Pfänder et al., 2000). Our modelling of pure clinopyroxene
641 fractional crystallisation from a starting composition with Zr/Hf and Nb/Ta of primitive
642 mantle shows that unrealistic amounts of ~~clinopyroxene~~-fractionation are required to generate
643 the Shirak samples (Fig. 10). In option (2), fractionation of titanate phases such as rutile and
644 ilmenite can generate very high Zr/Hf and Nb/Ta ratios, with $D_{Zr/Hf}$ and $D_{Nb/Ta}$ both <1
645 (Pfänder et al., 2000); however, titanate fractionation would also strongly reduce overall Nb
646 concentrations, a feature not seen in the Valley Series. Partial melting of garnet-bearing
647 lithologies (option 3) is invoked in many OIB examples (see Pfänder et al., 2007) but can be

648 ruled out here on the basis of flat normalised HREE patterns in the Shirak lavas – these are
649 not OIB-like magmas (Fig. 6b). Where carbonates are invoked in the mantle source (e.g.
650 Dupuy et al., 1992; Hoernle et al., 2002) (option 4), resultant alkaline melts or mantle
651 xenoliths have very high Sr and Ba of $\gg 1000$ ppm, and in spite of high Zr/Hf ratios many
652 carbonatites ~~have very low overall concentrations of these two~~have very low concentrations
653 of these elements (Ionov et al., 1993). This is not the signature of the Shirak samples hence
654 carbonate metasomatism is unlikely in this case. Several studies have shown that amphibole
655 and phlogopite fractionate the HFSE (Moine et al., 2001; Tiepolo et al., 2001;
656 Chakhmouradian, 2006), with Chakhmouradian (2006) demonstrating that low-Ti amphiboles
657 have high Zr/Hf ratios of ~60-200. Hence these minerals can impart high Zr/Hf on a melt; but
658 it is still unclear what the high overall Zr concentrations in the Shirak lavas are caused by -
659 this feature is normally attributed to ancient recycled oceanic crust in OIBs (Weaver, 1991).

660

661 *5.3.2. Modelling of partial melting*

662

663 Any model of partial melting conditions for Shirak has to be based on the HREE and HFSE,
664 making the assumption that neither set of elements were transported into the lithospheric
665 mantle source in a slab-derived fluid (Pearce and Peate, 1995). Therefore, we have
666 constructed non-modal batch melting curves using Dy, Yb and Nb (ignoring Zr owing to its
667 anomalous behaviour), in order to constrain the degree of partial melting needed to form the
668 Valley Series. We have taken the approach of Pearce et al. (1990) in assuming that hydrous
669 phases such as amphibole and phlogopite (if present) are completely consumed during
670 melting and do not contribute to the melt model. Given the high Ta/Yb ratios of even the least
671 evolved Valley Series samples (Fig. 9), it is reasonable to compare the melting of depleted
672 MORB mantle (DMM) (Workman and Hart, 2005) with a more incompatible-element

673 enriched source, in this case primitive mantle with 1% bulk continental crust extracted, as
674 used by Fitton and Godard (2004) for the Ontong Java oceanic plateau.

675

676 Although we can easily model HREE and HFSE ratios (see below), fractional
677 crystallisation of olivine, spinel, plagioclase and pyroxene versus fractionation of amphibole
678 from primary magma have competing effects on absolute REE and HFSE concentrations.
679 Often, elemental values for basalts in modelling are back-calculated to 9 wt.% MgO to negate
680 the effects of plagioclase and pyroxene crystallisation (Pearce & Parkinson, 1993). However,
681 valley series Dy and Yb concentrations are near-constant in spite of varying MgO and SiO₂
682 (Fig. 6a), probably due to the competing effects of amphibole and clinopyroxene
683 fractionation, so no realistic back-calculation can be applied. Therefore, we simply attempt to
684 model the elemental ratios of the last-evolved Valley Series lava (7 wt.% MgO) and assume
685 that this best reflects the conditions of partial melting.

686

687 Modelling results (Fig. 11) indicate that melting of a garnet peridotite cannot
688 reproduce the compositions of the Valley Series lavas, a finding consistent with the flat
689 normalised HREE patterns (Fig. 6a). Spinel peridotite partial melting curves do intersect the
690 valley series at low degrees of melting, with the DMM melting curve on Figure 11 giving
691 0.1-0.5% melting. In contrast the more fertile source gives 2-5% melting, which is perhaps
692 more realistic than the tiny proportion of melting required from a DMM source and the
693 difficulties of extracting such a small volume of melt (e.g. Hirth and Kohlstedt, 1995). This
694 spinel peridotite melting outcome is also consistent with geophysical surveys indicating a
695 seismically slow, ~~probably partially molten~~ mantle at depths of ~50 km beneath Armenia
696 (e.g. Koulakov et al., 2012).

697

698 5.4. Reconciliation with geophysical and geodynamic models

699

700 *5.4.1. Extent of lithospheric delamination*

701

702 Debate exists over the extent of lithospheric delamination beneath Eastern Anatolia following
703 the cessation of subduction beneath the Bitlis-Zagros suture (e.g. Keskin, 2003). Seismic
704 surveys indicate a crustal thickness of ~40-45 km, but with significant negative P- and S-
705 wave seismic velocity anomalies beneath, extending from ~50 to ~250 km depth, between
706 eastern Turkey, Armenia, the Black Sea and northwest Iran, concurrent with many Pliocene-
707 Quaternary volcanic centres (e.g. Piromallo and Morelli, 2003; Maggi & Priestley, 2005; Zor
708 et al., 2008; Koulakov et al., 2012). The anomaly has been used by these authors to argue for
709 the presence of hot, perhaps partially molten, asthenosphere, but several authors extend these
710 conclusions to the possibility that there is also no mantle lithosphere ‘lid’ beneath the
711 Anatolian crust (e.g. Keskin, 2003; Zor et al., 2008) and the Caucasus (Koulakov et al.,
712 2012). In this case, mafic magmatism in Shirak would have to have an asthenospheric source.

713

714 There are significant implications for magmatism in this scenario. The impact of hot
715 upwelling asthenosphere on the thickened Lesser Caucasus arc crust should result in
716 extensive lower crustal melting, as observed in the Puna Plateau of the Andes, and the Great
717 Basin Altiplano in the western U.S. (Allmendinger et al., 1997; Babeyko et al., 2002; Best et
718 al., 2009). Going back to our geochemical results, this model of whole-scale lithospheric
719 delamination proposed for the Puna Plateau is incompatible with the observed silica-
720 undersaturated magmatism in Shirak, which bears little evidence for large-scale crustal
721 interaction. We conclude that there is sufficient lithospheric mantle beneath the Armenian
722 crust to act as a thermal barrier between the asthenosphere and crust (Fig. 12), protecting the

723 crust from melting and infiltration by hot asthenospheric melts in the manner described by
724 Babeyko et al. (2002). ~~A Furthermore, an~~ asthenospheric source for the Shirak magmas ~~would~~
725 ~~not~~cannot have been influenced by a subducting slab, because subduction processes ended
726 ~~beneath the region~~ prior to the Miocene. Hence the Shirak magmas would not have
727 subduction-like trace element characteristics, and instead should closely resemble OIB. There
728 are asthenosphere-derived OIB-like lavas without subduction-related geochemical signatures
729 in Eastern Iran (Saadat et al., 2010; Saadat and Stern, 2012) and in the Arabian foreland
730 (Lustrino et al., 2010). The Iranian alkali olivine basalts show trends towards an EMII-like
731 isotope signature (particularly with respect to Pb isotope ratios) (Zindler and Hart, 1986).
732 They also and contain pyroxenite xenoliths from the lithospheric mantle, plagioclase
733 megacrysts of uncertain origin, and some lower crustal gabbroic xenoliths (Saadat and Stern,
734 2012). These lavas are ~~clearly~~ distinct in terms of xenolith content, trace element signatures
735 and isotope geochemistry from those erupted in Shirak.

736

737 5.4.2. Geodynamic model

738

739 Our geodynamic model is presented schematically in Figure 12. We propose that, upon the
740 termination of Neo-Tethyan subduction along the Bitlis-Zagros suture during the Oligocene,
741 Armenia lay in a continental back-arc position relative to the former subducting slab and
742 mantle wedge. Modelling studies have suggested that an old slab may be able to persist or
743 ‘stall’ in the upper mantle without breaking off for up to 20 Myr after terminal collision (van
744 Hunen and Allen, 2011). Delayed break-off of the Neo-Tethyan slab from Arabia beneath
745 Eurasia may thus be responsible for the upsurge in magmatism since 10 Ma, and particularly
746 in the Pliocene-Quaternary, across the orogenic plateau (e.g. Keskin, 2003), concurrent with
747 the influx of hot asthenosphere into the region the slab once occupied. In Eastern Anatolia,

748 the region immediately above the detached slab might lack mantle lithosphere, and
749 asthenospheric and crustal melting would combine to produce arc-like magmas (Fig. 12)
750 (Keskin, 2003). However, as we have already discussed, it is improbable that whole-scale
751 lithospheric mantle delamination occurred beneath Armenia because we do not see attendant
752 whole-scale lower crustal melting. The former asthenospheric mantle wedge of the Neo-
753 Tethyan arc system would be refrigerated by the presence of a stalled slab, and rapidly
754 converted into lithospheric mantle over the 15-25 Myr following terminal collision (c.f. Holt
755 et al., 2010). This depleted lithospheric mantle could be stable and buoyant enough to be at
756 least partially preserved following the eventual detachment of the underlying oceanic slab,
757 whilst the aforementioned influx of convecting asthenosphere would trigger partial melting in
758 the overlying lithospheric mantle, as well as providing a thermal support for the orogenic
759 plateau (Fig. 12).

760

761 Another potentially important consideration is that, although much of the LILE and
762 LREE budget of the southern Neo-Tethyan slab may have been delivered to the lithosphere
763 before continental collision, a stalled slab and associated sediments would continue
764 dewatering before break-off. This would contribute to the subduction-like signature on the
765 mantle frozen-in beneath Armenia. Other Pliocene-Quaternary centres in the collision zone,
766 such as the foreland volcanic system at Karacadağ, may result from asthenospheric melting
767 beneath thin spots in the lithosphere (Lustrino et al., 2010; Ekici et al., 2012). Mantle-derived
768 | volcanism is also apparent even in the 50+ km thick crust of the Elbrus region of the Greater
769 | Caucasus (Lebedev et al., 2006b; Koulakov et al., 2012), and it is here that magmatism may
770 | be related to melting during collisional thickening of lithospheric mantle and the breakdown
771 | of hydrous mineral phases such as micas and amphiboles (e.g. Pearce et al., 1990; Allen et

772 al., ~~in press~~2013) or to asthenospheric upwelling during lithospheric dripping (see Sosson et
773 al., 2010) (Fig. 12) ~~further work is required to distinguish these hypotheses.~~

775 6. Conclusions

- 776
777 • Mafic and more evolved Pliocene-Quaternary lavas in Shirak, NW Armenia, were
778 emplaced through a former continental margin arc sequence as a result of localised
779 extensional tectonics within the present-day Arabia-Eurasia collision zone.
- 780 • Magmas evolved from mafic through to dacitic compositions by fractional
781 crystallisation dominated by pyroxene, amphibole and plagioclase; and although
782 evolved samples contain quartz xenocrysts, none preserves clear isotopic evidence for
783 large-scale crustal assimilation - magma mixing appears to be the dominant
784 petrogenetic process. We conclude that if assimilation did occur, it was of local
785 ~~Mesozoic to Early Cenozoic~~ arc-related crust of a similar isotopic composition to the
786 ~~primary~~ Shirak melts.
- 787 • The least-evolved magmas preserve trace element evidence for derivation by
788 moderate degrees of melting (~3-4%) from a shallow, spinel-facies lithospheric
789 mantle source with an inherited subduction component probably related to earlier
790 Tethyan subduction processes. ~~Unusually,~~ they contain high Zr concentrations and
791 high Zr/Hf ratios which ~~cannot be explained by fractional crystallisation processes,~~
792 ~~and~~ are an intrinsic feature of the source or partial melting process.
- 793 • The presence of lithospheric mantle beneath Armenia is a requirement for
794 geodynamic models of the region; in order to prevent the occurrence of whole-scale
795 lower crustal melting.

797 **Acknowledgements**

798

799 This work is funded by the Natural Environment Research Council project, ‘Orogenic Plateau
800 Magmatism’ [NE/H021620/1]. Nick Marsh conducted the XRF analyses; Geoff Nowell and
801 Chris Ottley assisted with, and partly conducted, radiogenic isotope and trace element
802 analyses, respectively. We are grateful to *Lithos* guest editor Ioan Seghedi, along with
803 Evgenii Sharkov and an anonymous reviewer for their constructive comments. Ivan Savov
804 and Douwe van Hinsbergen are thanked for discussion on some of the ideas presented within.

805

806 **References**

807

808 Adamia, S.A., Chkhotua, T., Kekelia, M., Lordkipanidze, M., Shavishvili, I., 1981. Tectonics
809 of the Caucasus and adjoining regions: implications for the evolution of the Tethys ocean.
810 *Journal of Structural Geology* 3, 437-447.

811

812 Adamia, S.A., Zakariadze, G., Chkhotua, T., Sadradze, N., Tsereteli, N., Chabukiani, A.,
813 Gventsadze, S., 2011. Geology of the Caucasus: A Review. *Turkish Journal of Earth Sciences*
814 20, 489-544.

815

816 Agard, P., Omrani, J., Jolivet, L., Mouthereau, F., 2005. Convergence history across Zagros
817 (Iran): constraints from collisional and earlier deformation. *International Journal of Earth*
818 *Sciences* 94, 401-419.

819

820 Allen, M.B., Armstrong, H.A., 2008. Arabia-Eurasia collision and the forcing of mid
821 Cenozoic global cooling. *Palaeontology Palaeoclimatology Palaeoecology* 265, 52-58.

822

823 Allen, M.B., Kheirkhah, M., Emami, M.H., Jones, S.J., 2011. Right-lateral shear across Iran
824 and kinematic change in the Arabia-Eurasia collision zone. *Geophysical Journal International*
825 184, 555-574.

826

827 Allen, M.B., Kheirkhah, M., Neill, I., Emami, M.H., Mcleod, C., in press. Generation of arc
828 and within-plate chemical signatures in collision zone magmatism: Quaternary lavas from
829 Kurdistan Province, Iran. *Journal of Petrology*, doi: 10.1093/petrology/egs090.

830

831 Allmendinger, R.W., Isacks, B.L., Jordan, T.E., Kay, S.M., 1997. The evolution of the
832 Altiplano-Puna plateau of the Central Andes. *Annual Reviews of Earth Science* 25, 139-174.

833

834 Angus, D.A., Wilson, D.C., Sandvol, E., Ni, J.F., 2006. Lithospheric structure of the Arabian
835 and Eurasian collision zone in eastern Turkey from S-wave receiver functions. *Geophysical*
836 *Journal International* 166, 1335-1346.

837

838 Avagyan, A., Sosson, M., Karakhanian, A., Philip, H., Rebai, S., Rolland, Y., Melkonyan, R.,
839 Davtyan, V., 2010. Recent tectonic stress evolution in the Lesser Caucasus and adjacent
840 regions. In: Sosson, M., Kaymakci, N., Stephenson, R.A., Bergerat, F., Starostenko, V.
841 (Eds.). *Sedimentary Basin Tectonics from the Black Sea and Caucasus to the Arabian*
842 *Platform*. Geological Society of London Special Publications, v. 340, p.p. 393-408.

843

844 [Aydinçakir, E., Şen, C., 2013. Petrogenesis of the post-collisional volcanic rocks from the](#)
845 [Borçka \(Artvin\) area: Implications for the evolution of the Eocene magmatism in the Eastern](#)
846 [Pontides \(NE Turkey\). *Lithos*, in press, doi:10.1016/j.lithos.2013.04.007.](#)

847

848 Azizi, H., Moinevaziri, H., 2009. Review of the tectonic setting of Cretaceous to Quaternary
849 volcanism in northwestern Iran. *Journal of Geodynamics* 47, 167-179.

850

851 Babeyko, A.Yu., Sobolev, S.V., Trumbull, R.B., Oncken, O., Lavier, L.L., 2002. Numerical
852 models of crustal-scale convection and partial melting beneath the Altiplano-Puna plateau.
853 *Earth and Planetary Science Letters* 199, 373-388.

854

855 Baghdasaryan, G.P., Ghukasyan, R.Kh., 1985. Geochronology of magmatic, metamorphic
856 and ore formations of Armenian SSR. Publication of the Academy of Sciences of Armenian
857 Soviet Socialist Republic (in Russian).

858

859 Ballatto, P., Uba, C.E., Landgraf, A., Strecker, M.R., Sudo, M., Stockli, D.F., Friedrich, A.,
860 Tabatabaei, S.H., 2011. Arabia-Eurasia continental collision: Insights from late Tertiary
861 foreland-basin evolution in the Alborz Mountains, northern Iran. *Geological Society of
862 America Bulletin* 123, 106-131.

863

864 Berberian, F., Berberian M., 1981. Tectono-plutonic episodes in Iran. In: Gupta, H.K.,
865 Delany, F.M. (Eds.). *Zagros, Hindu Kush, Himalaya Geodynamic Evolution*. American
866 Geophysical Union Geodynamic Series v. 3, p.p. 5-32.

867

868 Best, M.G., Barr, D.L., Christiansen, E.H., Gromme, S., Deino, A.L., Tingey, D.G., 2009.
869 The Great Basin Altiplano during the middle Cenozoic ignimbrite flareup: insights from
870 volcanic rocks. *International Geology Review* 51, 589-633.

871

872 Bottrill, A.D., van Hunen, J., Allen, M.B., 2012. Insight into collision zone dynamics from
873 topography: numerical modelling results and observations. *Solid Earth* 3, 387-399.

874

875 Cann, J.R., 1970. Rb, Sr, Zr and Nb in some ocean floor basaltic rocks. *Earth and Planetary
876 Science Letters* 10, 7-11.

877

878 Chakhmouradian, A., 2006. High-field-strength elements in carbonatitic rocks:
879 Geochemistry, crystal chemistry and significance for constraining the source of carbonatites.
880 *Chemical Geology* 235, 138-160.

881

882 Chernyshev, I.V., Lebedev, V.A., Arakelyants, M.M., Jrbashyan, R.T., Ghukasyan, Y.G.,
883 2002. Geochronology of the Aragats volcanic centre, Armenia: Evidence from K-Ar dating.
884 *Doklady Earth Sciences* 384, 393-398 (in Russian).

885

886 Chernyshev, I.V., Lebedev, V.A., Arakelyants, M.M., 2006. K-Ar dating of Quaternary
887 volcanics: Methodology and interpretation of results. *Petrologiya (Petrology)* 14, 69-89.

888

889 [Chiu, H.-Y., Chung, S.-L., Zarrinkoub, M.H., Mohammadi, S.S., Khatib, M.M., Iizuka, Y.,
890 2013. Zircon U-Pb constraints from Iran on the magmatic evolution related to Neotethyan
891 subduction and Zagros orogeny. *Lithos* 162, 70-87.](#)

892

893 David, K., Schiano, P., Allégre, C.J., 2000. Assessment of the Zr/Hf fractionation in oceanic
894 basalts and continental materials during petrogenetic processes. *Earth and Planetary Science
895 Letters* 178, 285-301.

896

897 Davidson, J.P., Hassanzadeh, J., Berzins, R., Stockli, D.F., Bashukooh, B., Turrin, B.,
898 Pandamouz, A., 2004. The geology of Damavand volcano, Alborz Mountains, northern Iran.
899 Geological Society of America Bulletin 116, 16-29.

900

901 Dewey, J.F., Hempton, M.R., Kidd, W.S.F., Saroglu, F., Şengör, A.M.C., 1986. Shortening
902 of continental lithosphere: the neotectonics of Eastern Anatolia – a young collision zone. In:
903 Coward, M.P., Ries, A.C. (Eds.). Collision Tectonics. Geological Society of London Special
904 Publication, v. 19, p.p. 3-36.

905

906 Dilek, Y., Imamverdiyev, N., Altunkaynak, Ş., 2010. Geochemistry and tectonics of
907 Cenozoic volcanism in the Lesser Caucasus (Azerbaijan) and the peri-Arabian region:
908 collision-induced mantle dynamics and its magmatic signature.

909

910 Dowall, D.P., Nowell, G.M., Pearson, D.G., 2007. Chemical pre-concentration procedures for
911 high-precision analysis of Hf-Nd-Sr isotopes in geological materials by plasma ionisation
912 multi-collector mass spectrometry (PIMMS) techniques. In: Holland, J.G., Tanner, S.D.
913 (Eds.) Plasma Source Mass Spectrometry: Applications and Emerging Technologies.
914 Cambridge: The Royal Society of Chemistry, p.p. 321-337.

915

916 Drew, S.T., Ducea, M.N., Schoenbohm, L.M., 2009. Mafic volcanism on the Puna Plateau,
917 NW Argentina: Implications for lithospheric composition and evolution with an emphasis on
918 lithospheric foundering. Lithosphere 1, 305-318.

919

920 Dupuy, C., Liotard, J.M., Dostal, J., 1992. Zr/Hf fractionation in intraplate basaltic rocks:
921 Carbonate metasomatism in the mantle source. *Geochimica et Cosmochimica Acta* 56, 2417-
922 2423.

923

924 Ekici, T, Macpherson, C.G., Otlu, N, 2012. Polybaric melting of a single mantle source
925 during the Neogene Siverek phase of the Karacadağ Volcanic Complex, SE Turkey. *Lithos*
926 146, 152-163.

927

928 Fitton, J.G., Godard, M., 2004. Origin and evolution of magmas on the Ontong Java Plateau.
929 In: Fitton, J.G., Mahoney, J.J., Wallace, P.J., Saunders, A.D. (Eds.). *Origin and Evolution of*
930 *the Ontong Java Plateau. Geological Society of London Special Publication*, v. 229, p.p. 151-
931 178.

932

933 Foley, S.F., Barth, M.G., Jenner, G.A., 2000. Rutile/melt partition coefficients for trace
934 elements and an assessment of the influence of rutile on the trace element characteristics of
935 subduction zone magmas. *Geochimica et Cosmochimica Acta* 64, 933-939.

936

937 Furman, T., Graham, D., 1999. Erosion of lithospheric mantle beneath the East African Rift
938 System: geochemical evidence from the Kivu volcanic province. *Lithos* 48, 237-262.

939

940 Jackson, J., Haines, J., Holt, W., 1995. The accommodation of Arabia-Eurasia Plate
941 convergence in Iran. *Journal of Geophysical Research* 100, B8, P15205.

942

943 Johnson, C.M., 1991. Large-scale crust formation and lithosphere modification beneath
944 middle to late Cenozoic calderas and volcanic fields, western North America. *Journal of*
945 *Geophysical Research* 96, 13485-13507.

946

947 Jrbashian, R.T., Kazarian, G.A., Karapetian, S.G., Meliksetian, Kh.B., Mnatsakanian, A.,
948 Shirinian, K.G., 1996. Meso-Cenozoic basaltic volcanism in the northeastern part of
949 Armenian Highland. *Letters of the Armenian Academy of Sciences, Earth Sciences* 49, 19-32
950 (in Russian).

951

952 [Hirth, G., Kohlstedt, D.L., 1995. Experimental constraints on the dynamics of the partially](#)
953 [molten upper mantle: deformation in diffusion creep regime. *Journal of Geophysical*](#)
954 [Research 100, 1981-2001.](#)

955

956 Hoernle, K., Tilton, G., Le Bas, M.J., Duggan, S., Garbe-Schönberg, D., 2002. Geochemistry
957 of oceanic carbonatites compared with continental carbonatites: mantle recycling of oceanic
958 crustal carbonate. *Contributions to Mineralogy and Petrology* 142, 520-542.

959

960 Holt, P.J., Allen, M.B., van Hunen, J., Bjørnseth, H.M., 2010. Lithospheric cooling and
961 thickening as a basin forming mechanism. *Tectonophysics* 495, 184-194.

962

963 Ionov, D.A., Dupuy, C., O'Reilly, S.Y., Kopylova, M.G., Genshaft, Y.S., 1993. Carbonated
964 peridotite xenoliths from Spitsbergen: implications for trace element signature of mantle
965 carbonate metasomatism. *Earth and Planetary Science Letters* 119, 283-297.

966

967 Karapetian, S.G., Jrbashian, R.T., Mnatsakanian, A.Kh., 2001. Late collision rhyolitic
968 volcanism in the north-eastern part of the Armenian Highland. *Journal of Volcanology and*
969 *Geothermal Research* 112, 189-220.

970

971 Kharazyan, E.Kh., 1983. Geology of recent volcanism of north-west part of Armenian SSR
972 (basins of rivers Dzoraget and Akhuryan). PhD thesis, unpublished, ArmGeologia, Yerevan,
973 55 pp.

974

975 Kharazyan, E.Kh., 2005. Geological Map of Armenia. Ministry of Nature Protection of
976 Republic of Armenia.

977

978 Keskin, M., Pearce, J.A., Mitchell, J.G., 1998. Volcano-stratigraphy and geochemistry of
979 collision-related volcanism on the Erzurum-Kars Plateau, northeastern Turkey. *Journal of*
980 *Volcanology and Geothermal Research* 85, 355-405.

981

982 Keskin, M., 2003. Magma generation by slab steepening and breakoff beneath and
983 subduction-accretion complex: An alternative model for collision-related volcanism in
984 Eastern Anatolia, Turkey. *Geophysical Research Letters* 30, 1-4.

985

986 Keskin, M., 2007. Eastern Anatolia: a hot spot in a collision zone without a mantle plume. In:
987 Foulger, G.R., Jurdy, D.M. (Eds.) *Plates, Plumes, and Planetary Processes*. Geological
988 Society of America Special Paper, vol. 409, p.p. 1-25.

989

990 Keskin, M., Can Genç, Ş, Tüysüz, O., 2008. Petrology and geochemistry of post-collisional
991 Middle Eocene volcanic units in North-Central Turkey: Evidence for magma generation by
992 slab breakoff following the closure of the Northern Neotethys Ocean. *Lithos* 104, 267-305.
993

994 Karakhanian, A.S., Trifonov, V.G., Azizbekian, O.G., Hondkarian, D.G., 1997. Relationship
995 of late Quaternary tectonics and volcanism in the Khanarassar active fault zone, the
996 Armenian Upland. *Terra Nova* 9, 131-134.
997

998 Karakhanian, A., Djr bashian, R., Trifonov, V., Philip, H., Arakelian, S., Avagian, A., 2002.
999 Holocene-historical volcanism and active faults as natural risk factors for Armenia and
1000 adjacent countries. *Journal of Volcanology and Geothermal Research* 113, 319-344.
1001

1002 Karakhanian, A., Abgaryan, Y., 2004. Evidence of historical seismicity and volcanism in the
1003 Armenian Highland (from Armenian and other sources). *Annals of Geophysics* 47, 793-810.
1004

1005 [Kay, R.W., Kay, S.M., 1993. Delamination and delamination magmatism. *Tectonophysics*](#)
1006 [219, 177-189.](#)
1007

1008 Kheir khah, M., Allen, M.B., Emami, M.H., 2009. Quaternary syn-collision magmatism from
1009 the Iran/Turkey borderlands. *Journal of Volcanology and Geothermal Research* 182, 1-12.
1010

1011 Koçyiğit, A., Yilmaz, A., Adamia, S., Kuloshvili, S., 2001. Neotectonics of East Anatolian
1012 Plateau (Turkey) and Lesser Caucasus: implications for transition from thrusting to strike-slip
1013 faulting. *Geodinamica Acta* 14, 177-195.
1014

1015 [Langmuir, C.H., Vocke, R.D., Hanson, G.N., Hart, S.R., 1978. A general mixing equation](#)
1016 [with applications to Icelandic basalts. Earth and Planetary Science Letters 37, 380-392.](#)

1017

1018 Koulakov, I., Zabelina, I., Amanatashvili, I., Meskhia, V., 2012. Nature of orogenesis and
1019 volcanism in the Caucasus region based on results of regional tomography. Solid Earth 3,
1020 327-337.

1021

1022 Lebedev, V.A., Chernyshev, I.V., Chugaev, A.V., Dudauro, O.Z., Vashakidze, G.T., 2006a.
1023 K-Ar age and Sr-Nd characteristics of subalkali basalts in the Central Georgian neovolcanic
1024 region. Doklady Earth Sciences 408, 657-661.

1025

1026 Lebedev, V.A., Bubnov, S.N., Chernyshev, I.V., Gol'tsman, Y.V., 2006b. Basic magmatism
1027 in the geological history of the Elbrus neovolcanic area, Greater Caucasus: Evidence from K-
1028 Ar and Sr-Nd isotope data. Doklady Earth Sciences 406, 37-44.

1029

1030 Lebedev, V.A., Bubnov, S.N., Chernyshev, I.V., Chugaev, A.V., Dudauro, O.Z., Vashakidze,
1031 G.T., 2007. Geochronology and genesis of subalkaline basaltic lava rivers at the Dzhavakheti
1032 Highland, Lesser Caucasus: K-Ar and Sr-Nd isotopic data. Geochemistry International 45,
1033 211-225.

1034

1035 Lebedev, V.A., Bubnov, S.N., Dudauro, O.Z., Vashakidze, G.T., 2008a. Geochronology of
1036 Pliocene volcanism in the Dzhavakheti Highland (the Lesser Caucasus). Part 1: Western part
1037 of the Dzhavakheti Highland. Stratigraphy and Geological Correlation 16, 204-224.

1038

1039 Lebedev, V.A., Bubnov, S.N., Dudaury, O.Z., Vashakidze, G.T., 2008b. Geochronology of
1040 Pliocene volcanism in the Dzhavakheti Highland (the Lesser Caucasus). Part 2: Eastern part
1041 of the Dzhavakheti Highland. Regional geological correlation. Stratigraphy and Geological
1042 Correlation 16, 553-574.

1043

1044 Lebedev, V.A., Chernyshev, I.V., Chugaev, A.V., Gol'tsman, Y.V., Bairova, E.D., 2010.
1045 Geochronology of eruptions and parental magma sources of Elbrus volcano, the Greater
1046 Caucasus: K-Ar and Sr-Nd-Pb isotope data. Geochemistry International 48, 41-67.

1047

1048 Lebedev, V.A., Chernyshev, I.V., Yakushev, A.I., 2011. Initial time and duration of
1049 Quaternary magmatism in the Aragats neovolcanic area (Lesser Caucasus, Armenia).
1050 Doklady Earth Sciences 437, 532-536.

1051

1052 Le Bas, M.J., Le Maitre, R.W., Streckeisen, A., Zanettin, B., 1986. A chemical classification
1053 of volcanic rocks based on the total alkali-silica diagram. Journal of Petrology 27, 745-750.

1054

1055 Lin, Y.C., Chung, S.L., Karakhanian, A., Jrbashyan, R., Navasardyan, G., Galoyan, G., Chiu,
1056 H.Y., Lin, I.J., Chu, C.H., Lee, H.Y., 2011. Geochemical and Sr-Nd isotopic constraints on
1057 the petrogenesis of pre- to post-collisional volcanic rocks in Armenia. Geophysical Research
1058 Abstracts 13, EU2011-5422.

1059

1060 Liotard, J.M., Dautria, J.M., Bosch, D., Condomines, M., Mehdizadeh, H., Ritz, J.F., 2008.
1061 Origin of the absarokite-banakite association of the Damavand volcano (Iran): trace elements
1062 and Sr, Nd, Pb isotope constraints. International Journal of Earth Sciences 97, 89-102.

1063

1064 Lordkipanidze, M., 1980. Alpine volcanism and geodynamics of the central segment of the
1065 Mediterranean belt. Metsniereba, Tbilisi (in Russian).
1066
1067 Lordkipanidze, M., Meliksetian, B., Jrbashian, R., 1988. Mesozoic-Cenozoic magmatic
1068 evolution of the Pontian-Crimean-Caucasian region. Mémoire de la Société Géologique de
1069 France 154, 103-124.
1070
1071 Lustrino, M., Keskin, M., Mattioli, M., Lebedev, V.A., Chugaev, A., Sharkov, E., Kavak, O.,
1072 2010. Early activity of the largest Cenozoic shield volcano in the circum-Mediterranean area:
1073 Mt. Karacadağ, SE Turkey. European Journal of Mineralogy 22, 343-362.
1074
1075 Maggi, A., Priestley, K., 2005. Surface waveform tomography of the Turkish-Iranian plateau.
1076 Geophysical Journal International 160, 1068-1080.
1077
1078 McDonough, W.F., Sun, S.-S., 1995. The composition of the Earth. Chemical Geology 120,
1079 223-253.
1080
1081 McQuarrie, N., van Hinsbergen, D.J.J., 2013. Retrodeforming the Arabia-Eurasia collision
1082 zone: Age of collision versus magnitude of continental subduction. Geology 41, 315-318.
1083
1084 Mirnejad, H., Hassanzadeh, J., Cousens, B.J., Taylor, B.E., 2010. Geochemical evidence for
1085 deep mantle melting and lithospheric delamination as the origin of the inland Damavand
1086 volcanic rocks of northern Iran. Journal of Volcanology and Geothermal Research 198, 288-
1087 296.
1088

1089 Mitchell, J., Westaway, R., 1999. Chronology of Neogene and Quaternary uplift and
1090 magmatism in the Caucasus: constraints from K-Ar dating of volcanism in Armenia.
1091 Tectonophysics 304, 157-186.

1092
1093 ~~Mo, X., Hou, Z., Niu, Y., Dong, G., Qu, X., Zhao, Z., Yang, Z., 2007. Mantle contributions~~
1094 ~~to crustal thickening during continental collision: Evidence from Cenozoic igneous rocks in~~
1095 ~~southern Tibet. Lithos 96, 225-242.~~

1096
1097 Moine, B.N., Grégoire, M., O'Reilly, S.Y., Sheppard, S.M.F., Cottin, J.Y., 2001. High field
1098 strength element fractionation in the upper mantle: evidence from amphibole-rich composite
1099 mantle xenoliths from the Kerguelen Islands (Indian Ocean). Journal of Petrology 42, 2145-
1100 2167.

1101
1102 Morley, C.K., Kongwung, B., Julapour, A.A., Abdolghafourian, M., Hajian, M., Waples, D.,
1103 Warren, J., Otterdoom, H., Srisuriyon, K., Kazemi, H., 2009. Structural development of a
1104 major late Cenozoic basin and transpressional belt in central Iran: The Central Basin in the
1105 Qom-Saveh area. Geosphere 5, 325-362.

1106
1107 ~~Nelson, S.T., Montana, A., 1992. Sieve textured plagioclase in volcanic rocks produced by~~
1108 ~~rapid decompression. American Mineralogist 77, 1242-1249.~~

1109
1110 Okay, A.I., Zattin, M., Cavazza, W., 2010. Apatite fission-track data for the Miocene Arabia-
1111 Eurasia collision. Geology 38, 35-38.

1112

1113 Pagé, P., Bédard, J.H., Tremblay, A., 2009. Geochemical variations in a depleted fore-arc
1114 mantle: The Ordovician Thetford Mines Ophiolite. *Lithos* 113, 21-47.
1115

1116 Pearce, J.A., 1983. Role of the sub-continental lithosphere in magma genesis at active
1117 continental margins. In: Hawkesworth, C.J., Norry, M.J. (Eds.). *Continental Basalts and*
1118 *Mantle Xenoliths*. Shiva, Natwich, p.p. 230-249.
1119

1120 Pearce, J.A., Bender, J.F., Delong, S.E., Kidd, W.S.F., Low, P.J., Guner, Y., Sargolu, F.,
1121 Yilmaz, Y., Moorbath, S., Mitchell, J.G., 1990. Genesis of collision volcanism in eastern
1122 Anatolia, Turkey. *Journal of Volcanology and Geothermal Research* 44, 189-229.
1123

1124 Pearce, J.A., Parkinson, I.J., 1993. Trace element models for mantle melting: application to
1125 volcanic arc petrogenesis. In: Prichard, H.M., Alabaster, T., Harris, N.B.W., Neary, C.R.
1126 (Eds.). *Geological Society Special Publication* 76, 373-403.
1127

1128 Pearce, J.A., Peate, D.W., 1995. Tectonic implications of the composition of volcanic arc
1129 magmas. *Annual Review of Earth and Planetary Sciences* 23, 251-285.
1130

1131 Pearce, J.A., 1996. A users guide to basalt discrimination diagrams. In: Wyman, D.A. (Ed.).
1132 *Trace Element Geochemistry of Volcanic Rocks: Applications for Massive Sulphide*
1133 *Exploration*. Geological Association of Canada Short Course Notes 12, 79-113.
1134

1135 Peccerillo, R., Taylor, S.R., 1976. Geochemistry of Eocene calc-alkaline volcanic rocks from
1136 the Kastamonu area, northern Turkey. *Contributions to Mineralogy and Petrology* 58, 63-81.
1137

1138 Pfänder, J.A., Münker, C., Stracke, A., Mezger, K., 2007. Na/Ta and Zr/Hf in ocean island
1139 basalts – Implications for crust-mantle differentiation and the fate of Niobium. *Earth and*
1140 *Planetary Science Letters* 254, 158-172.

1141

1142 Piromallo, C., Morelli, A., 2003. P-wave tomography of the mantle under the Alpine-
1143 Mediterranean area. *Journal of Geophysical Research* 108, B2, doi:10.1029/2002JB001757.

1144

1145 Powell, R., 1984. Inversion of the assimilation and fractional crystallisation (AFC) equations;
1146 characterisation of contaminants from isotope and trace element relationships in volcanic
1147 suites. *Journal of the Geological Society of London* 141, 447-452.

1148

1149 Presnyakov, S.L., Belyaeva, E.V., Lyubin, V.P., Rodionov, N.V., Antonov, A.V., Saltykova,
1150 A.K., Berezhnaya, N.G., Sergeev, S.A., 2012. Age of the earliest Paleolithic sites in the
1151 northern part of the Armenian Highland by SHRIMP-II U-Pb geochronology of zircons from
1152 volcanic ashes. *Gondwana Research* 21, 929-938.

1153

1154 Priestley, K.F., McKenzie, D.P., 2006. The thermal structure of the literature from shear
1155 wave velocities. *Earth and Planetary Science Letters* 244, 285-301.

1156

1157 Rebaï, S., Philip, H., Dorbath, L., Borissoff, B., Haessler, H., Cisternas, A., 1993. Active
1158 tectonics in the Lesser Caucasus: coexistence of compressive and extensional structures.
1159 *Tectonics* 12, 1089-1114.

1160

1161 Richards, J.P., Spell, T., Rameh, E., Raziq, A., Fletcher, T., 2012. High Sr/Y magmas
1162 reflect arc maturity, high magmatic water content, and porphyry Cu ± Mo ± Au potential:

1163 examples from the Tethyan arcs of central and eastern Iran and western Pakistan. *Economic*
1164 *Geology* 107, 295-332.

1165

1166 Rolland, Y., Billo, S., Corsini, M., Sosson, M., Galoyan, G., 2009. Blueschists of the
1167 Amassia-Stepanavan suture zone (Armenia): linking Tethys subduction history from E-
1168 Turkey to W-Iran. *International Journal of Earth Sciences* 98, 533-550.

1169

1170 Saadat, S., Karimpour, M.H., Stern, C., 2010. Petrochemical characteristics of Neogene and
1171 Quaternary alkali olivine basalts from the western margin of the Lut Block, eastern Iran.
1172 *Iranian Journal of Earth Sciences* 2, 87-106.

1173

1174 Saadat, S., Stern, C.R., 2012. Petrochemistry of a xenolith-bearing Neogene alkali olivine
1175 basalt from northeastern Iran. *Journal of Volcanology and Geothermal Research* 225, 13-29.

1176

1177 Savov, I.P., Luhr, J., D'Antonio, M., Connor, C., Karakhanian, A., Ghukasyan, Y.,
1178 Djrbashian, R., 2007. Variable slab and subarc mantle signatures within dying arc setting –
1179 clues from the volcanology and geochemistry of Quaternary volcanic rocks from Armenia.
1180 *American Geophysical Union Spring Meeting Abstracts*, V53A-02.

1181

1182 Sen, P.A., Temel, A., Gourgaud, A., 2004. Petrogenetic modelling of Quaternary post-
1183 collisional volcanism: a case study of central and eastern Anatolia. *Geological Magazine* 141,
1184 81-98.

1185

1186 Şengör, A.M.C., Kidd, W.S.F., 1979. Post-collisional tectonics of the Turkish-Iranian plateau
1187 and a comparison with Tibet. *Tectonophysics* 55, 361-376.

1188

1189 Şengör, A.M.C., Özeren, M.S., Keskin, M., Sakiñ, M., Özbakir, A.D., Kayan, I., 2008.

1190 Eastern Turkish high plateau as a small Turkic-type orogen: Implications for post-collisional

1191 crust-forming processes in Turkic-type orogens. *Earth Science Reviews* 90, 1-48.

1192

1193 Shabanian, E., Acocella, V., Gioncada, A., Ghasemi, H., Bellier, O., 2012. Structural control

1194 on volcanism in intraplate post collisional settings: Late Cenozoic to Quaternary examples of

1195 Iran and Eastern Turkey. *Tectonics* 31, TC3013, doi:10.1029/2011TC003042.

1196

1197 Skhirtladse, N.N., 1958. Post-Paleogene Volcanism in Georgia (Postpaleogenovyi effuzivnyi

1198 vulkanizm Gruzii). Report of the Georgian Soviet Socialist Republic Academy of Sciences,

1199 Tblisi, 368 pp (in Russian).

1200

1201 Sosson, M., Rolland, Y., Müller, C., Danelian, T., Melkonyan, R., Kekelia, S., Adamia, A.,

1202 Babazadeh, V., Kangarli, T., Avagyan, A., Galoyan, G., Mosar, J., 2010. Subudctions,

1203 obduction and collision in the Lesser Caucasus (Armenia, Azerbaijan, Georgia), new insights.

1204 In: Sosson, M., Kaymakci, N., Stephenson, R.A., Bergerat, F., Starostenko, V. (Eds.).

1205 *Sedimentary Basin Tectonics from the Black Sea and Caucasus to the Arabian Platform.*

1206 *Geological Society of London Special Publications* 340, 329-352.

1207

1208 Stampfli, G.M., 2000. Tethyan oceans. In: Bozkurt, E., Winchester, J.A., Piper, J.D.A. (Eds.).

1209 *Tectonics and Magmatism in Turkey and the Surrounding Area.* Geological Society of

1210 London Special Publications 173, 1-23.

1211

1212 Sun, S.-S., McDonough, W.F., 1989. Chemical and isotopic systematics of oceanic basalts:
1213 implications for mantle composition and processes. In: Saunders, A.D., Norry, M.J. (Eds.)
1214 Magmatism in the Ocean Basins. Geological Society of London Special Publication, vol.42,
1215 p.p. 313-345.

1216

1217 [Tepley III, F.J., Davidson, J.P., Clyne, M.A., 1999. Magmatic interactions as recorded in](#)
1218 [plagioclase phenocrysts of Chaos Crags, Lassen Volcanic Centre, California. Journal of](#)
1219 [Petrology 40, 787-806.](#)

1220

1221 Tiepolo, M., Bottazzi, P., Foley, S.F., Oberti, R., Vannucci, R., Zanetti, A., 2001.
1222 Fractionation of Nb and Ta from Zr and Hf at mantle depths: the role of Titanian pargasite
1223 and kaersutite. Journal of Petrology 42, 221-232.

1224

1225 Tsachiyama, A., 1985. Dissolution kinetics of plagioclase in the melt system diopside-albite-
1226 anorthite, and origin of dusty plagioclase in andesites. Contributions to Mineralogy and
1227 Petrology 89, 1-16.

1228

1229 van Hunen, J., Allen, M.B., 2011. Continental collision and slab break-off: A comparison of
1230 3-D numerical models with observations. Earth and Planetary Science Letters 302, 27-37.

1231

1232 Verdel, C., Wernicke, B.P., Hassanzadeh, J., Guest, B., 2011. A Paleogene extensional arc
1233 flare-up in Iran. Tectonics 30, TC3008, doi:10.1029/2010TC002809.

1234

1235 Vernant, P., Nilforoushan, F., Hatzfeld, D., Abbassi, M., Vigny, C., Masson, F., Nankali, H.,
1236 Martinod, J., Ashtiani, A., Bayer, R., Tavakoli, F., Chery, J., 2004. Contemporary crustal

1237 deformation and plate kinematics in Middle East constraints by GPS measurements in Iran
1238 and northern Iran. *Geophysical Journal International* 157, 381-398.

1239

1240 Vincent, S.B., Allen, M.B., Ismail-Zadeh, A.D., Flecker, R., Foland, K.A., Simmons, M.B.,
1241 2005. Insights from the Talysh of Azerbaijan into the Paleogene evolution of the South
1242 Caspian region. *Geological Society of America Bulletin* 117, 1513-1533.

1243

1244 Weaver, B.L., Wood, D.A., Tarney, J., Joron, J.L., 1987. Geochemistry of ocean island
1245 basalts from the South Atlantic: Ascension, St. Helena, Gough and Tristan da Cunha. In:
1246 Fitton, J.G., Upton, B.G.J. (Eds.). *Alkaline Igneous Rocks*. Geological Society of London
1247 Special Publications 30, 253-267.

1248

1249 Weaver, B.L., 1991. The origin of ocean island basalt end-member compositions: trace
1250 element and isotope constraints. *Earth and Planetary Science Letters* 104, 381-397.

1251

1252 [Williams, H.M., Turner, S.P., Pearce, J.A., Kelley, S.P., Harris, N.B.W., 2004. Nature of the](#)
1253 [source regions for post-collisional, potassic magmatism in southern and northern Tibet from](#)
1254 [geochemical variations and inverse trace element modelling. *Journal of Petrology* 45, 555-](#)
1255 [607.](#)

1256

1257 Woodcock, N.H., Fischer, M., 1986. Strike-slip duplexes. *Journal of Structural Geology* 8,
1258 725-735.

1259

1260 Workman, R.K., Hart, S.R., 2005. Major and trace element composition of the depleted
1261 MORB mantle (DMM). *Earth and Planetary Science Letters* 231, 53-72.

1262

1263 Zindler, A., Hart, S., 1986. Chemical Geodynamics. Annual Reviews in Earth and Planetary
1264 Sciences 14, 493-571.

1265

1266 Zor, E., 2008. Tomographic evidence of slab detachment beneath eastern Turkey and the
1267 Caucasus. Geophysical Journal International 175, 1273-1282.

1268

1269

1270 **Table captions**

1271

1272 Table 1. Major and trace element data for selected samples from the valley, ridge, and cone
1273 series, Shirak. LOI = loss-on-ignition.

1274

1275 Table 2. Measured Nd and Sr isotope compositions of the valley, ridge, and cone series,
1276 Shirak.

1277

1278 **Supplementary Items**

1279

1280 Item 1. Selected photomicrographs of samples from the valley, ridge, and cone series, Shirak.

1281

1282 Item 2. Complete whole rock major and trace element data for the Shirak lavas, including
1283 trace element standards.

1284

1285

1286 **Figures**

1287

1288 Figure 1. Map of the Turkish- Iranian plateau with shaded digital topography, showing
1289 locations of Pliocene-Quaternary volcanic centres (cones) and the study area (rectangle).

1290

1291 Figure 2. Digital topography map of the study region with geological features simplified from
1292 work by Khachatur Meliksetian, Gevorg Navasardyan and Sergey Karapetyan of the Institute
1293 of Geology of the National Academy of Sciences of Armenia, plus outline map of Armenia
1294 showing administrative boundaries and regional coverage of Late Miocene-Quaternary
1295 magmatic products.

1296

1297 Figure 3. (a) Total alkali-silica classification (Le Bas et al., 1986) and (b) K_2O vs. SiO_2
1298 classification (Peccerillo and Taylor, 1976).

1299

1300 Figure 4. Major element variation diagrams for the Shirak lavas.

1301

1302 Figure 5. Minor and trace element variation in the Shirak lavas.

1303

1304 Figure 6. Rare earth element and extended trace element normalised plots. Chondrite
1305 normalisation values from McDonough and Sun (1995) and Primitive Mantle and OIB values
1306 from Sun and McDonough (1989).

1307

1308 Figure 7. (a) Nd-Sr isotope plot for Shirak lavas, compared to mafic centres within the
1309 collision zone. Pliocene-Pleistocene valley series in southern Georgia and Late Miocene
1310 mafic lavas from the Elbrus region of Southern Russia - Lebedev et al. (2007; 2010); NW

1311 Iran minor centres, Tendurek, Ararat, Kurdistan - Kheirkhah et al. (2009), Allen et al. (~~in~~
1312 ~~press~~2013); Damavand - Davidson et al. (unpublished data), Mirnejad et al. (2010); Artvin,
1313 Eastern Turkey - Aydiçakir and Şen, in press). Mantle end members and array - Zindler &
1314 Hart (1986). (b) Variation of Nd and Sr isotopes as a function of magmatic evolution.

1315

1316 Figure 8. Fractional crystallisation (FC) trends within the Shirak lavas (symbols as per
1317 previous diagrams). Data and FC vectors for basic to acidic rocks for Eastern Anatolia are
1318 from Pearce et al. (1990). pl = plagioclase; o = olivine; opx = orthopyroxene; cpx =
1319 clinopyroxene; hb = hornblende; gnt = garnet.

1320

1321 Figure 9. Th/Yb vs. Ta/Yb diagram (Pearce, 1983) for the Shirak lavas, showing a ~~fractional~~
1322 ~~crystallisation (FC)~~ an FC vector for a hydrous assemblage, taking into account increasing
1323 partition coefficients during magmatic evolution (after Keskin et al., 1998), and an
1324 ~~assimilation-FC~~ AFC vector as described on the figure. Eocene rocks from ~~North-~~
1325 ~~Central~~ Eastern Turkey, likely to be similar to those directly underlying the Shirak lava series,
1326 are plotted (~~Keskin et al., 2008~~ Aydiçakir and Şen, in press). ~~Upper crust - Taylor and~~
1327 ~~McLennan (1985), Crust (UCC: upper continental crust; MCC: middle crust; LCC: lower~~
1328 ~~crust; BCC: bulk continental crust, all from Rudnick and Gao, 2003).~~ Aactive margins -
1329 Pearce (1983). See text for discussion.

1330

1331 Figure 10. Zr/Hf vs. Nb/Ta plot for Shirak lavas and selected mafic Pliocene-Quaternary
1332 lavas from the Arabia-Eurasia collision. Ararat and Tendürek are from lithospheric mantle
1333 sources, Karacadağ in southern Turkey has an OIB source. Sources: ~~Eocene are rocks -~~
1334 ~~Keskin et al. (2008);~~ Tendürek, Ararat - Kheirkhah et al. (2009); Karacadağ - Sen et al.

1335 (2004), Lustrino et al. (2010); clinopyroxene fractionation based on partition coefficients of
1336 | Pagé et al. (2009); other references as per Figure 9.-

1337

1338 Figure 11. Non-modal batch partial melting models for the valley series lavas using depleted
1339 MORB mantle (Workman and Hart, 2005) and incompatible element enriched oceanic
1340 plateau (Fitton and Godard, 2004) sources. Source modes: spinel lherzolite - ol = 0.578, opx
1341 = 0.27, cpx = 0.119, sp = 0.033; garnet lherzolite - 0.598, 0.211, 0.076, gnt = 0.115. Melt
1342 modes: spinel lherzolite - 0.1, 0.27, 0.5, sp = 0.13; garnet lherzolite - 0.05, 0.2, 0.3, gnt =
1343 0.45. Partition coefficients are from the GERM Partition Coefficient Database
1344 (<http://earthref.org/KDD>).

1345

1346 Figure 12. A schematic cross-section through the present-day Arabia-Eurasia collision zone
1347 highlighting potential processes involved in Pliocene-Quaternary magmatism. Hatchings
1348 represent regions of partial melting. Crustal thicknesses estimated from Zor et al. (2008).

Figure 1

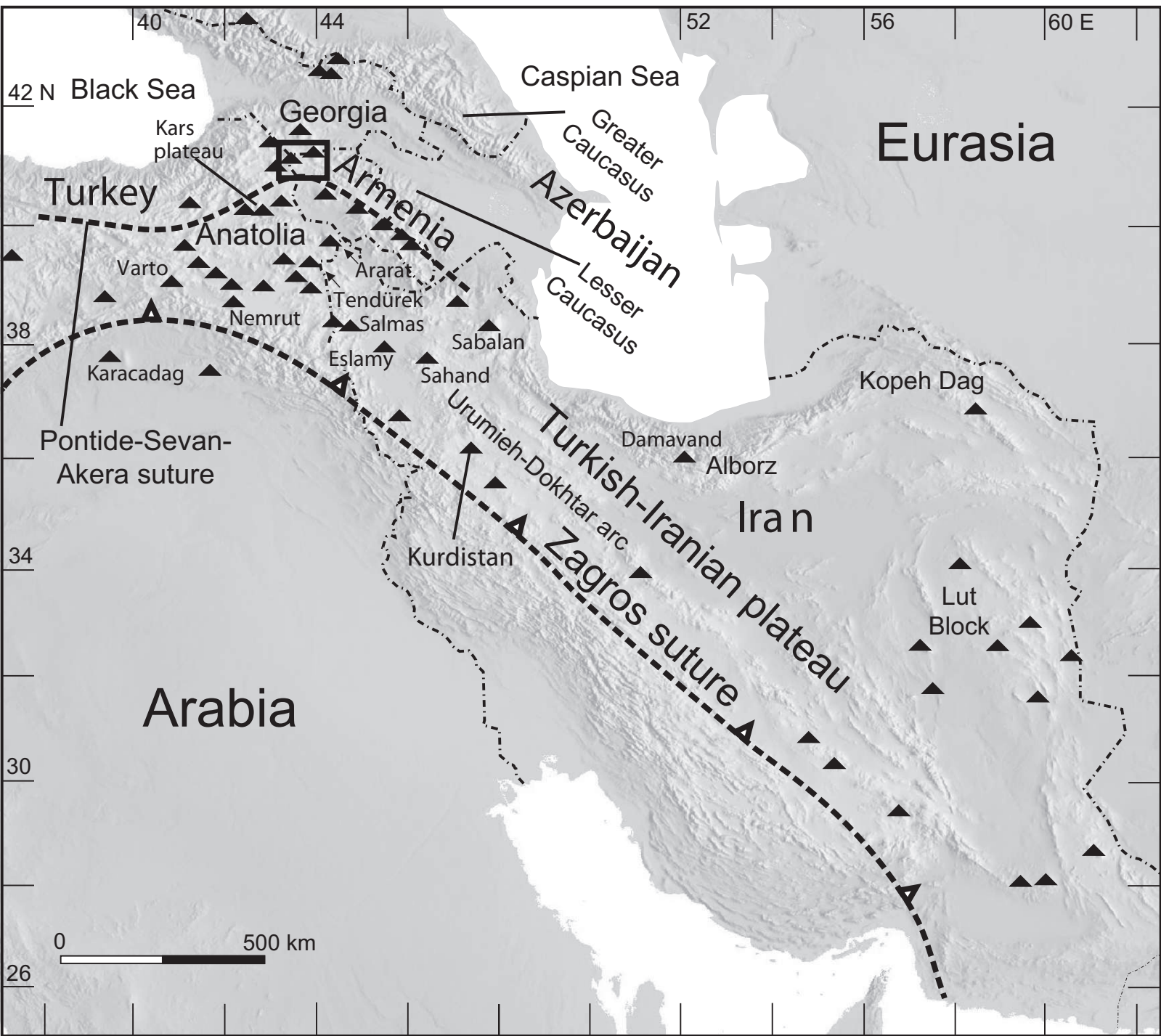


Figure 2

[Click here to download high resolution image](#)

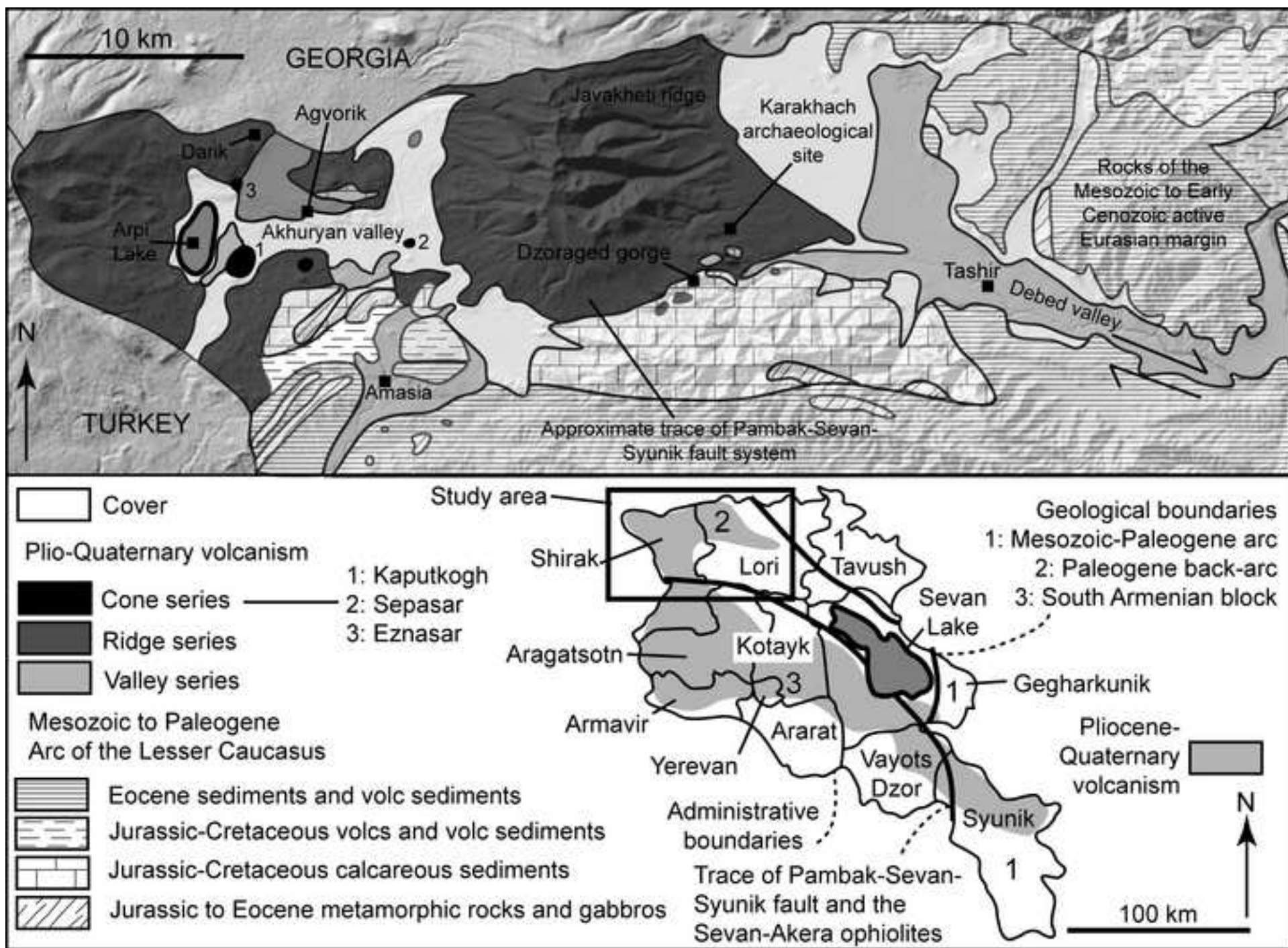


Figure 3

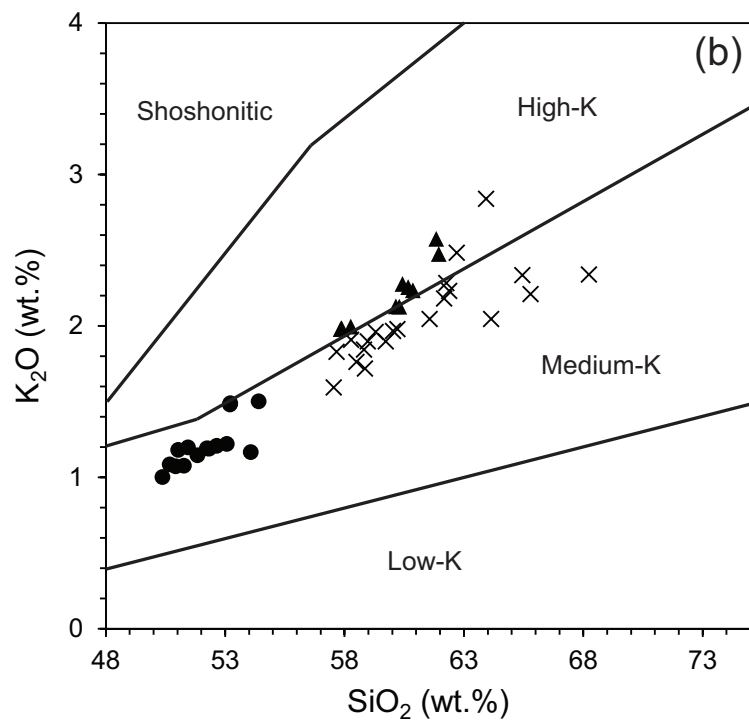
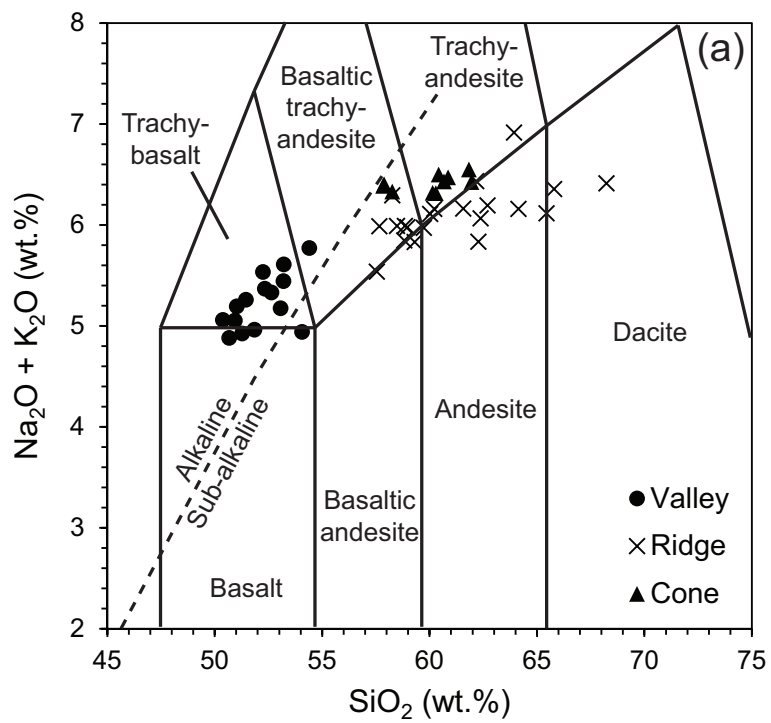


Figure 4

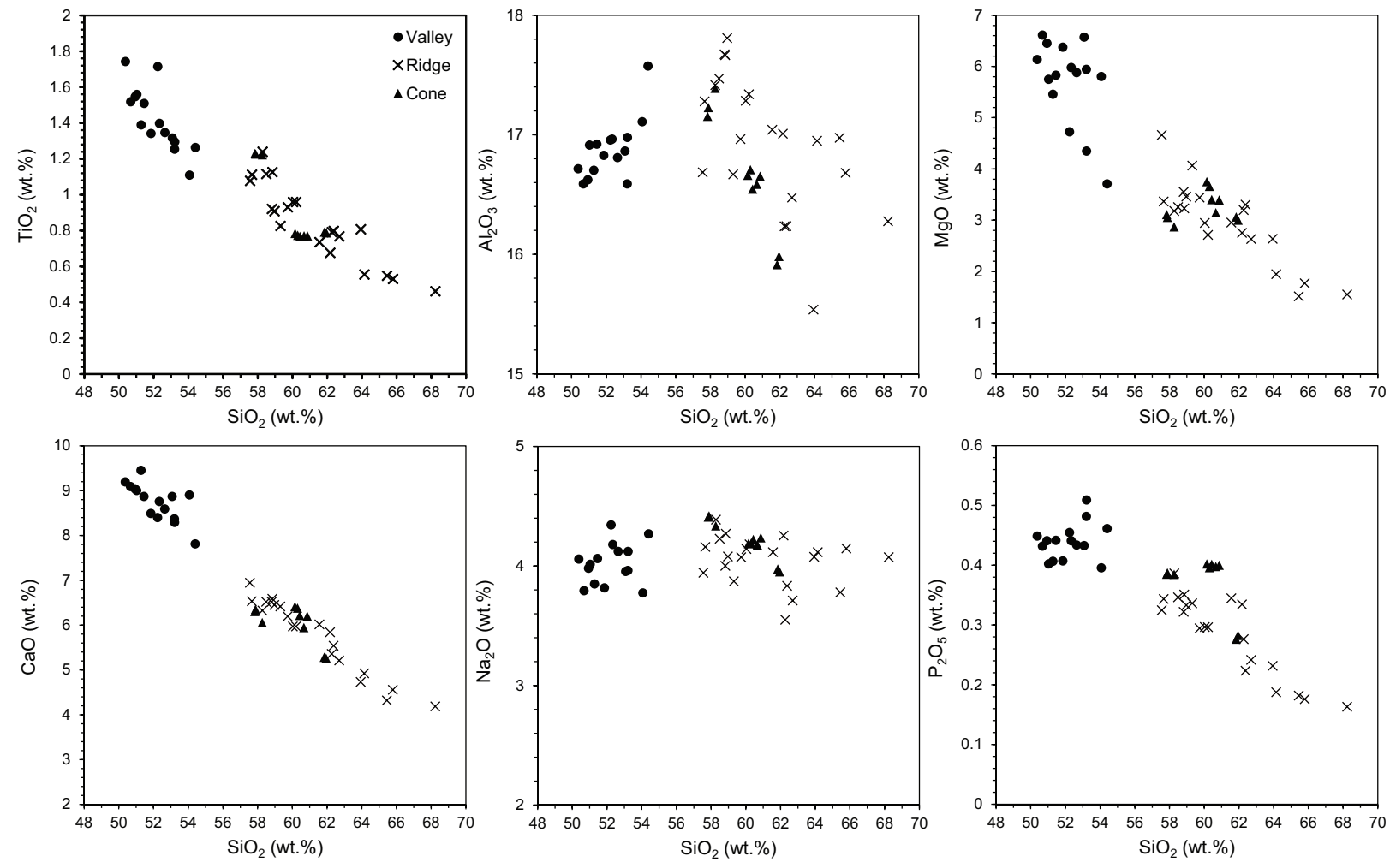


Figure 5

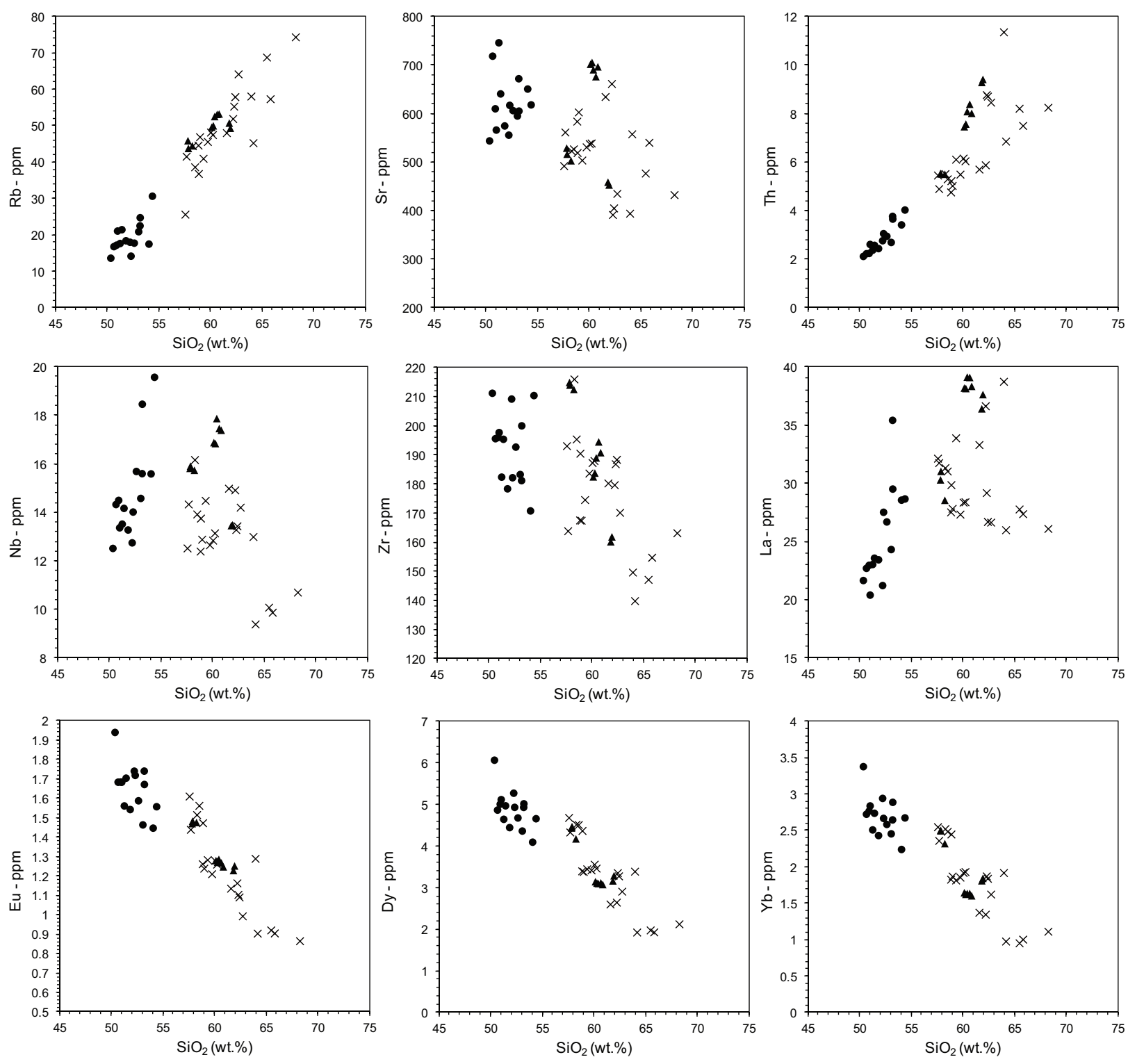


Figure 6

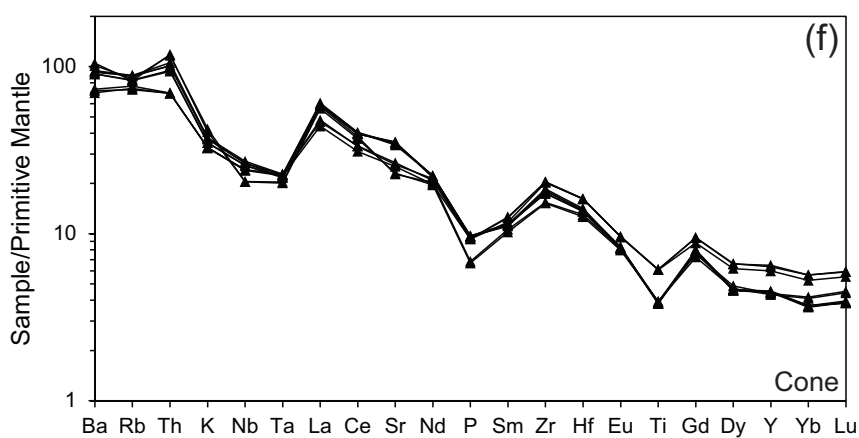
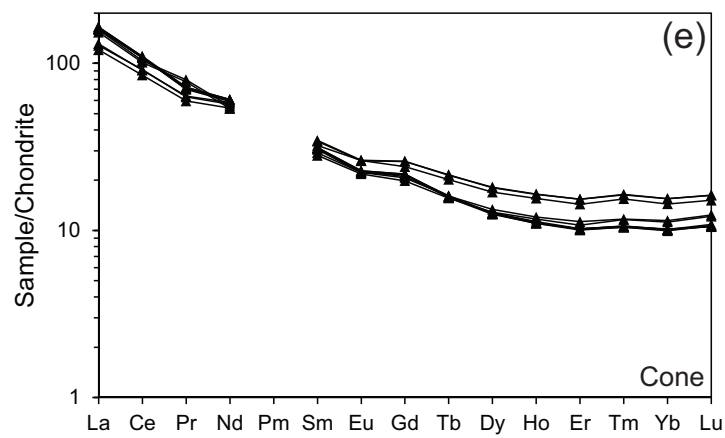
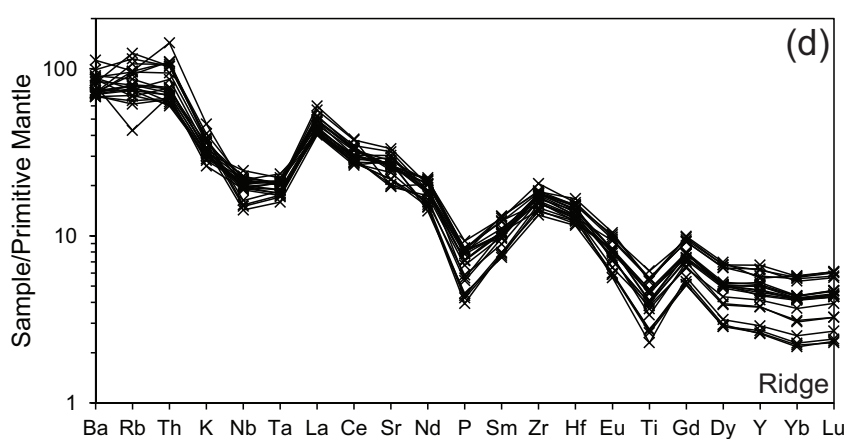
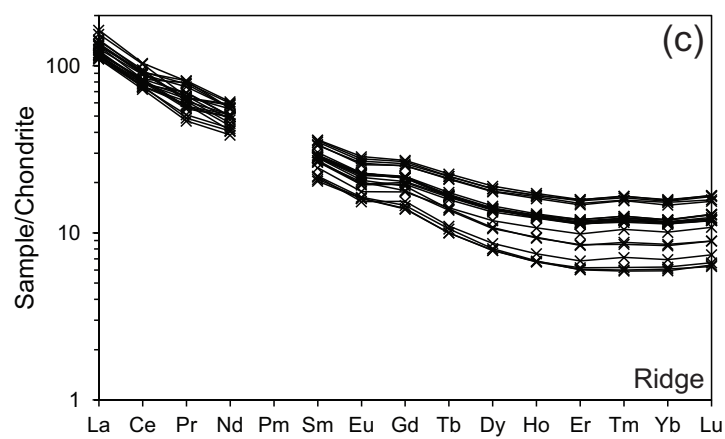
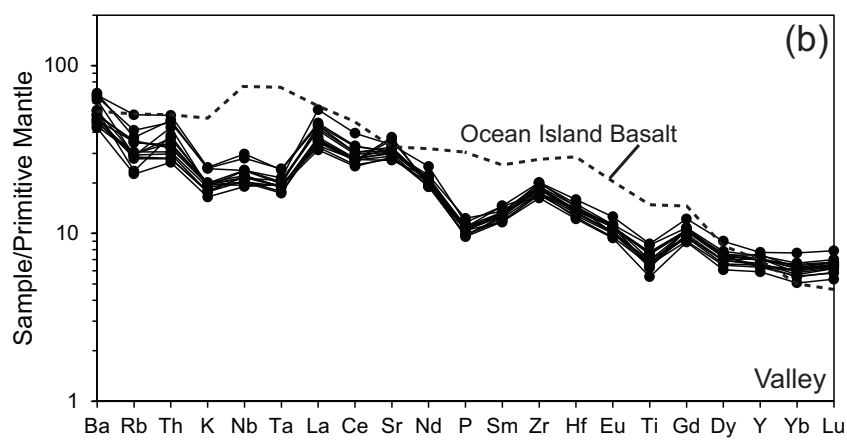
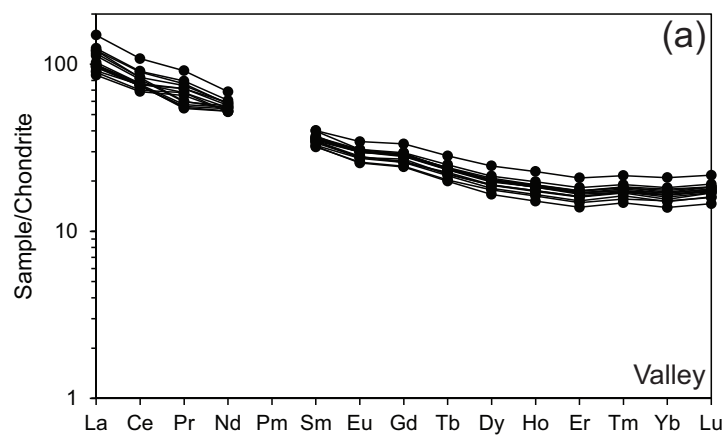


Figure 7

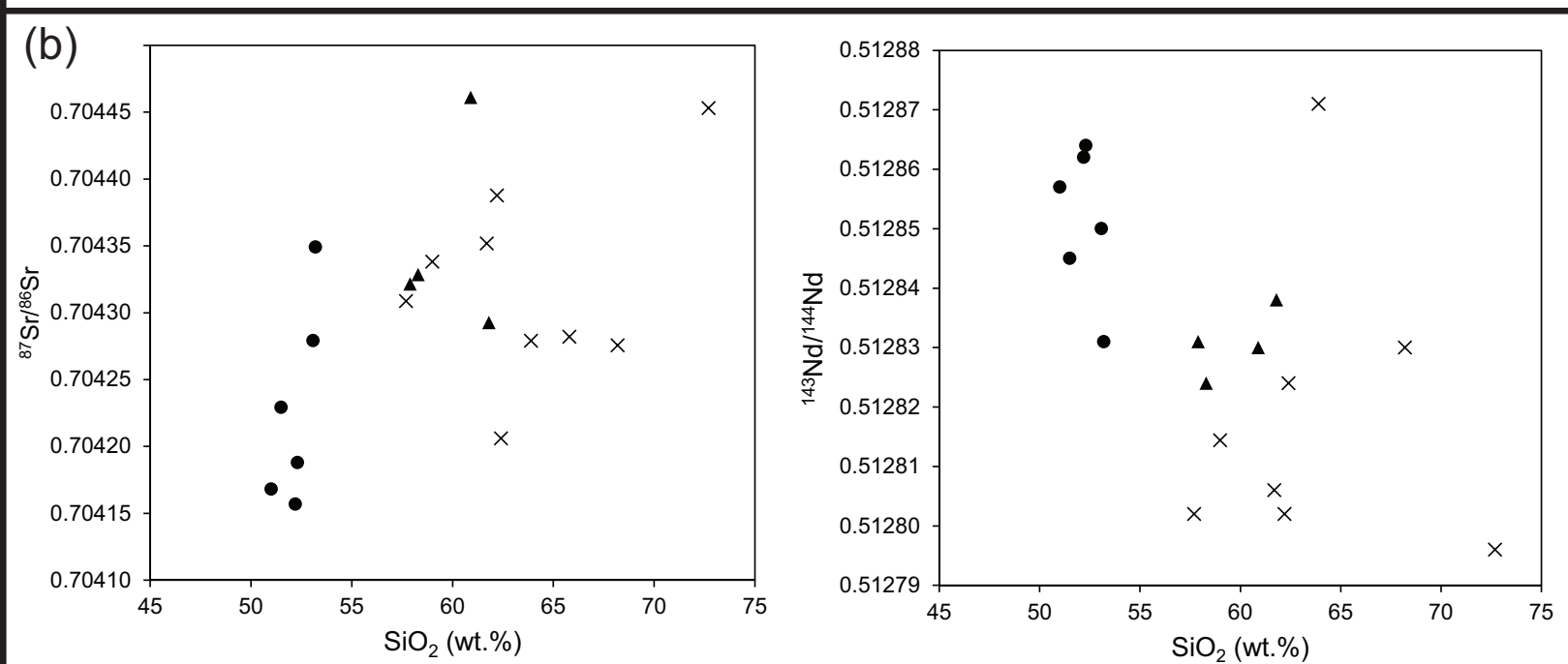
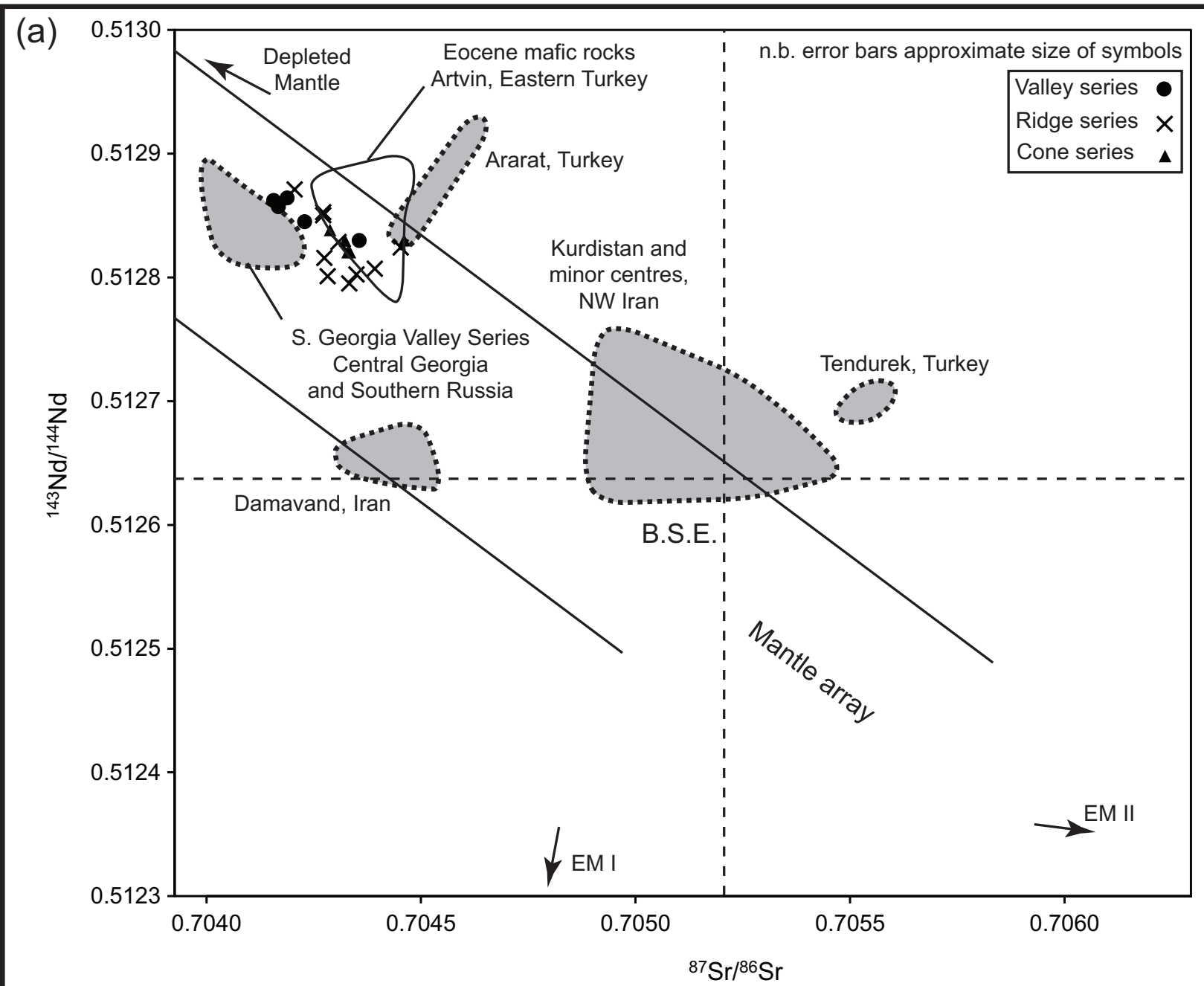


Figure 8

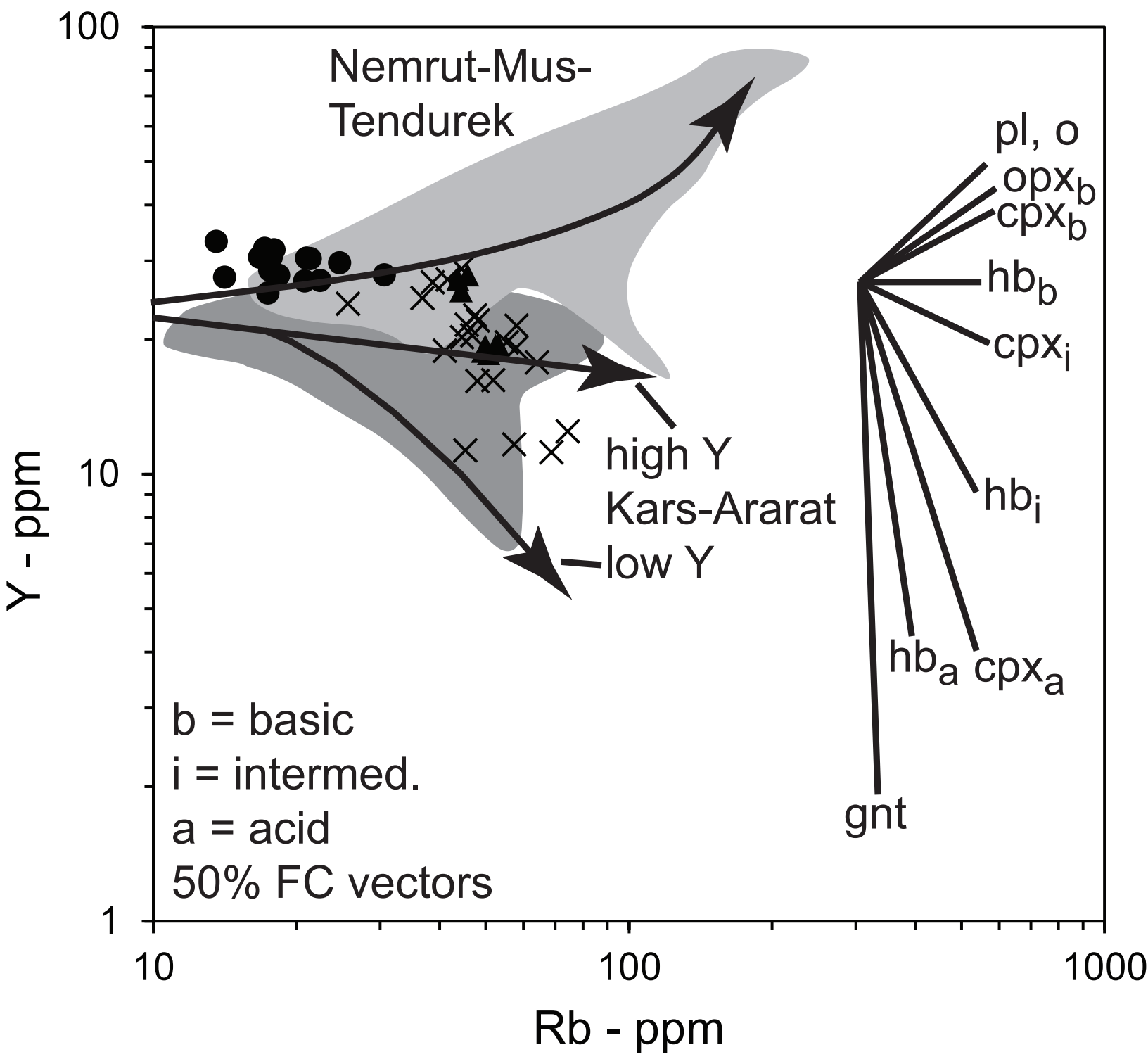


Figure 9

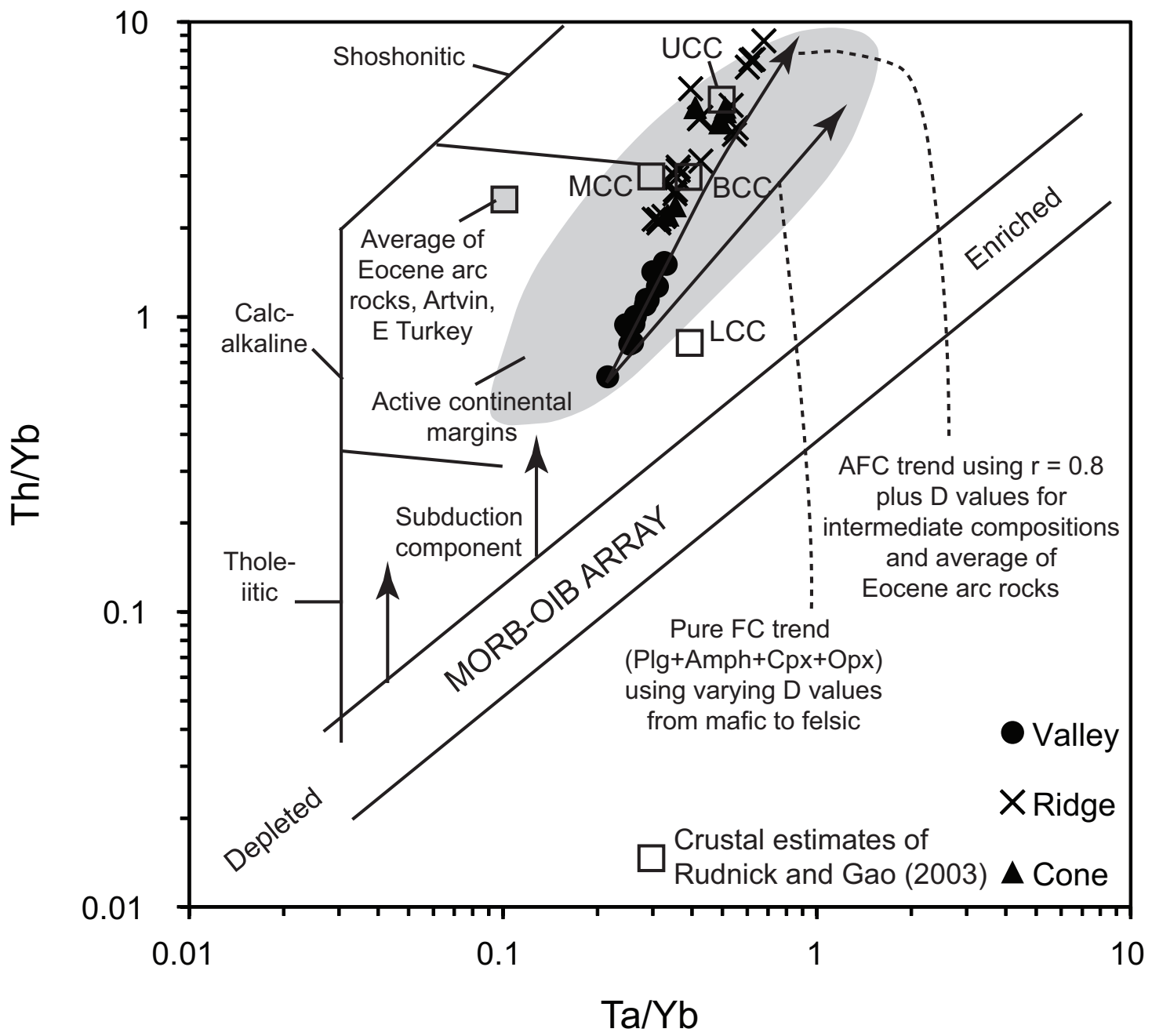


Figure 10

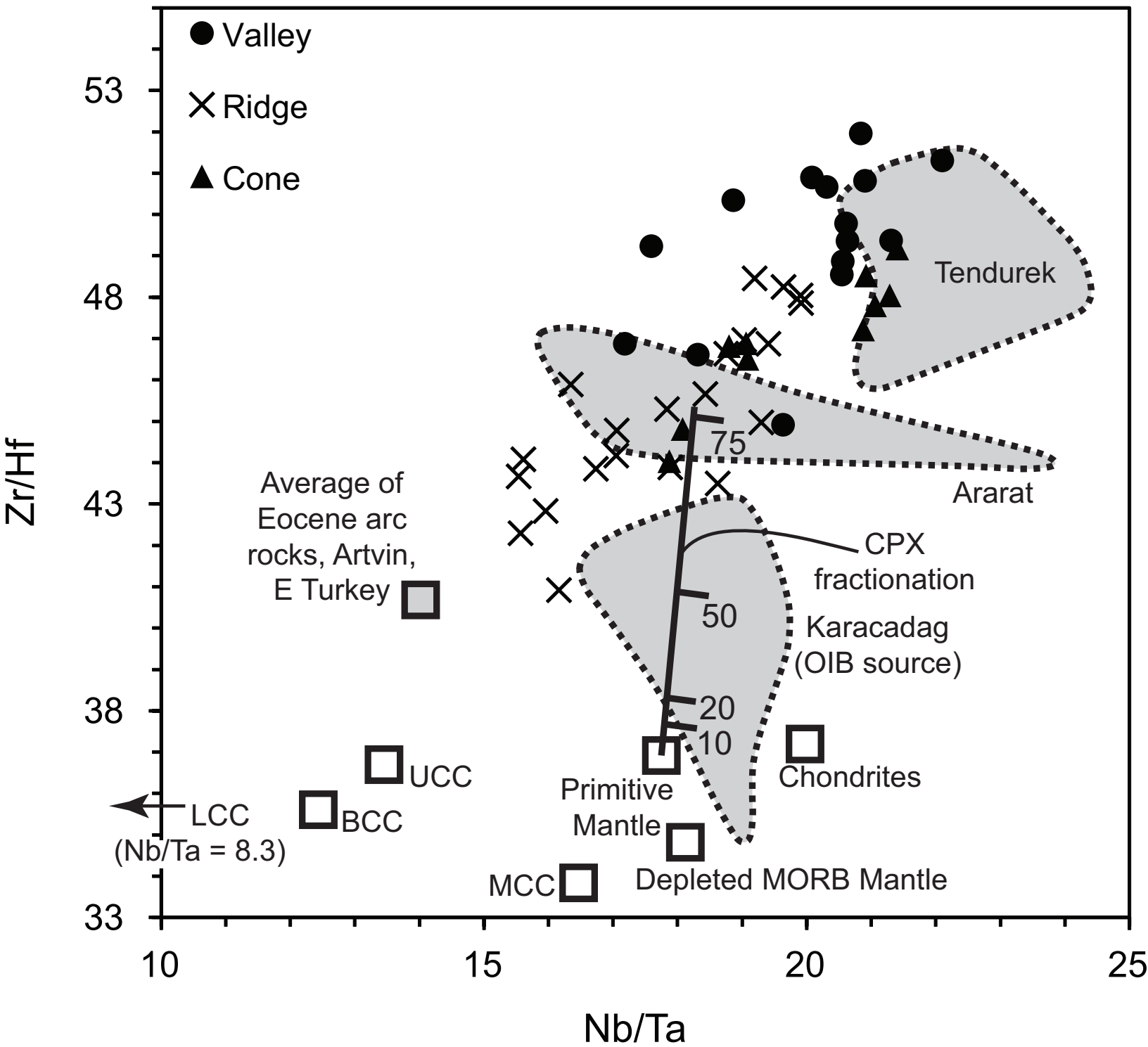


Figure 11

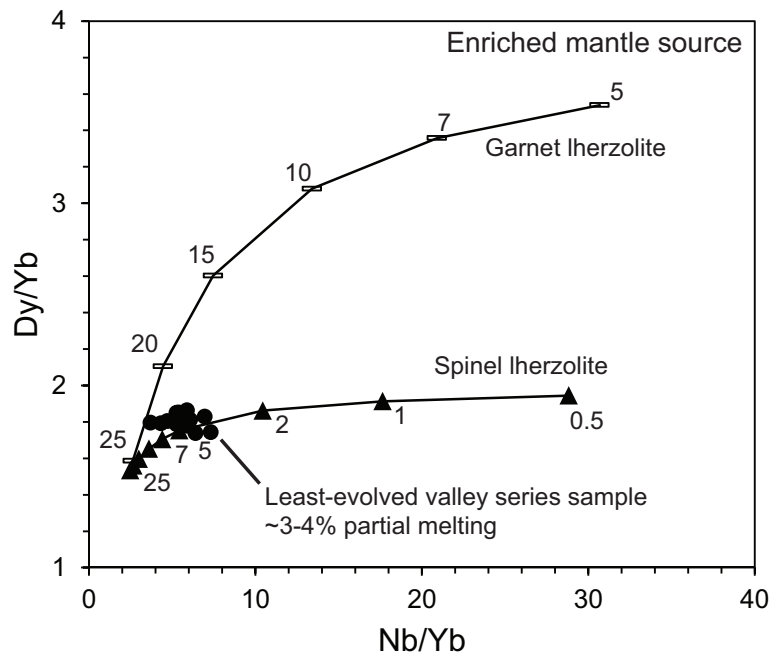
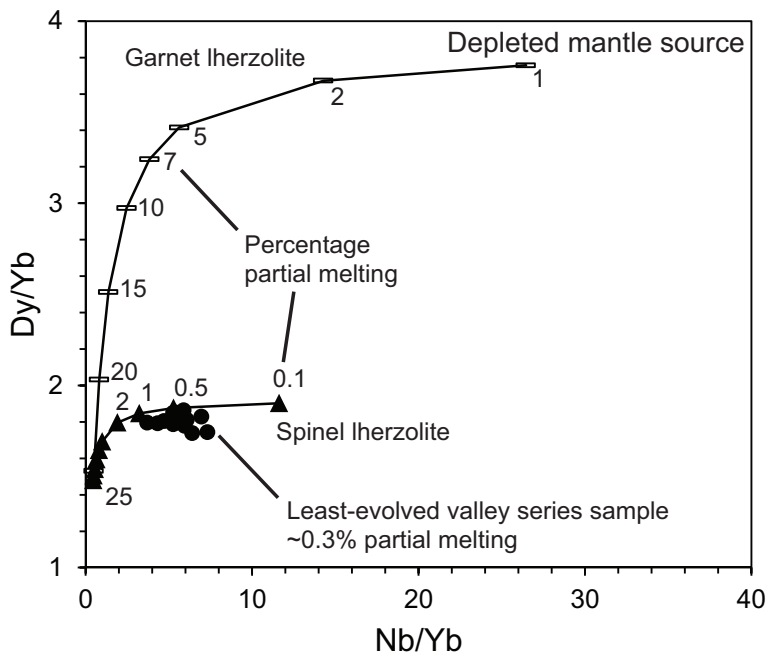


Figure 12

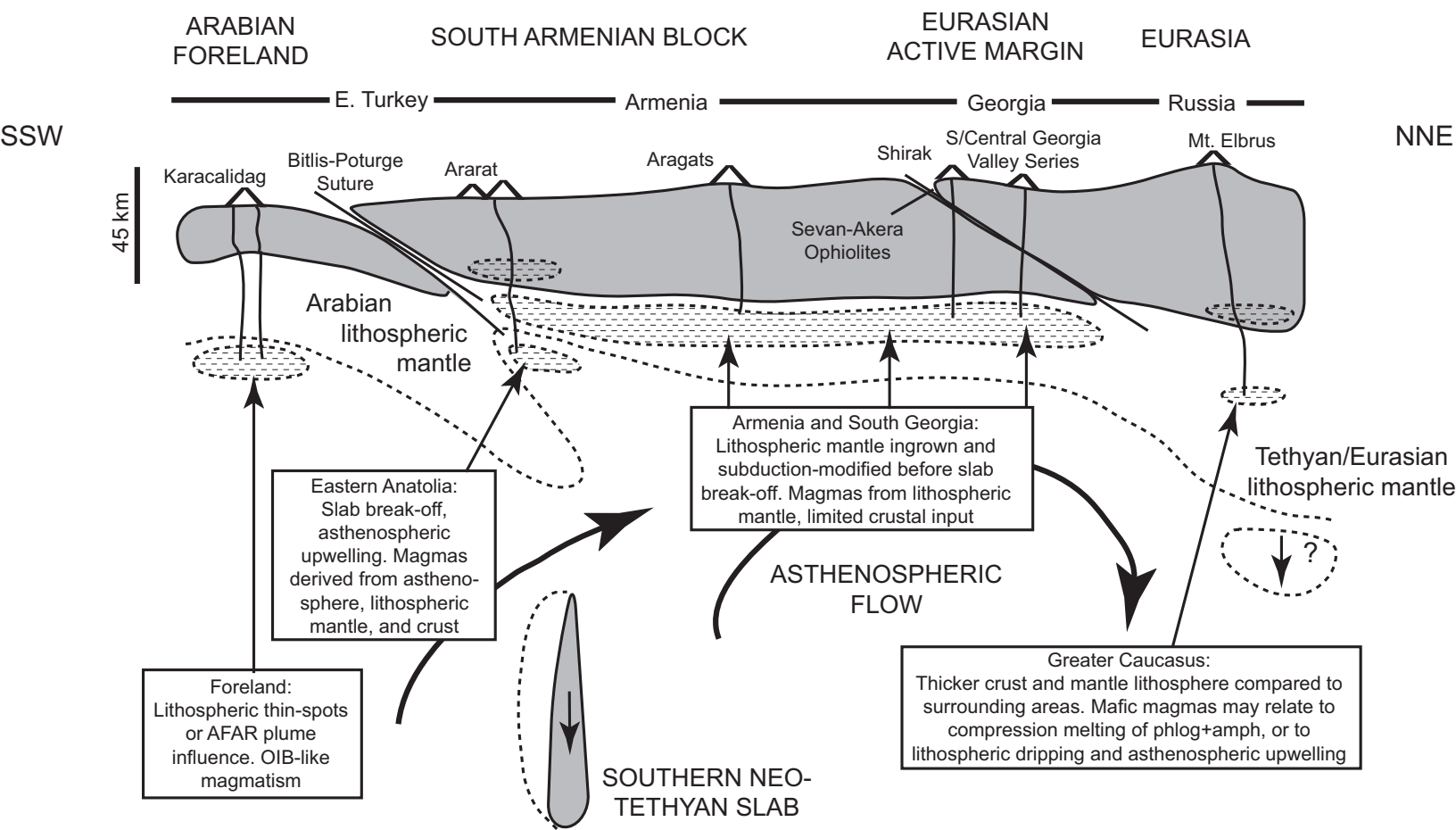


Table 1

[Click here to download Table: Neilletal Table1.docx](#)

Table I. Major and trace element data for selected samples from the valley (v), ridge (r), and cone (c) series, Shirak.

Number	S14.4	S14.5	S19.1	S25.2	S26.2	S28.1	S29.1	S4.2	S5.1	S6.1	S9.2	S21.1	S23.1	S30.2	S30.3	S1.1	S2.1	S7.3	S20.2
Series	V	V	V	V	V	V	V	R	R	R	R	R	R	R	R	C	C	C	C
SiO ₂	50.68	53.21	52.33	53.08	52.24	51.45	51.03	57.67	51.57	52.18	65.80	63.94	62.39	58.97	68.23	57.88	58.27	60.68	61.84
TiO ₂	1.52	1.25	1.40	1.32	1.71	1.51	1.56	1.11	0.73	0.68	0.53	0.81	0.80	0.91	0.46	1.23	1.22	0.77	0.79
Al ₂ O ₃	16.59	16.59	16.96	16.86	16.96	16.92	16.91	17.28	17.04	17.01	16.68	15.54	16.23	17.81	16.28	17.23	17.39	16.65	15.91
Fe ₂ O ₃ (T)	10.20	9.03	9.27	9.58	10.43	10.16	10.52	7.35	5.56	5.25	4.07	5.40	5.55	6.63	3.56	7.76	7.85	5.82	5.70
MnO	0.16	0.15	0.15	0.15	0.16	0.18	0.17	0.12	0.09	0.09	0.07	0.10	0.09	0.11	0.06	0.11	0.10	0.10	0.10
MgO	6.61	5.94	5.98	6.57	4.72	5.83	5.75	3.36	2.95	2.75	1.77	2.63	3.30	3.46	1.55	3.05	2.87	3.39	3.06
CaO	9.09	8.37	8.75	8.87	8.40	8.87	9.00	6.53	6.02	5.84	4.56	4.73	5.54	6.45	4.19	6.35	6.06	6.20	5.28
Na ₂ O	3.79	3.96	4.12	3.95	4.34	4.06	4.01	4.16	4.11	4.25	4.15	4.07	3.83	4.08	4.07	4.42	4.33	4.24	3.97
K ₂ O	1.09	1.48	1.19	1.22	1.19	1.20	1.18	1.83	2.05	2.18	2.21	2.84	2.23	1.90	2.34	1.94	2.00	2.24	2.58
P ₂ O ₅	0.43	0.48	0.44	0.43	0.46	0.44	0.40	0.34	0.35	0.33	0.18	0.23	0.22	0.33	0.16	0.39	0.39	0.40	0.28
LOI	0.73	-0.30	-0.14	-0.23	-0.09	0.05	-0.14	-0.07	0.45	-0.06	0.63	0.17	0.74	0.09	0.00	-0.06	0.11	-0.11	0.84
Total	100.89	100.16	100.52	101.81	100.56	100.67	100.40	99.68	100.92	100.50	100.64	100.47	100.94	100.74	100.91	100.34	100.58	100.55	100.37
Sc	15.6	23.1	19.3	20.3	21.7	22.1	22.2	bd	bd	bd	bd	bd	12.7	15.0	bd	bd	bd	bd	11.5
V	167	179	164	169	188	185	184	131	103	100	71	85	105	142	68	147	140	112	101
Cr	154	162	162	175	131	153	129	bd	45	44	bd	38	72	bd	bd	bd	bd	73	47
Co	37.6	33.0	36.5	36.5	35.0	41.4	42.2	22.9	16.1	15.3	9.8	18.9	19.0	23.1	9.5	20.6	20.3	18.1	17.6
Ni	106.8	113.8	113.5	125.6	65.4	106.3	101.5	bd	16.6	bd	bd	47.2	52.1	32.9	bd	bd	bd	39.2	36.7
Rb	16.7	22.5	14.1	20.8	17.9	21.4	21.0	41.6	48.1	51.9	57.4	58.1	57.9	46.9	74.4	43.7	44.4	53.2	50.7
Sr	718	671	617	595	555	640	566	562	635	662	540	395	405	603	433	516	503	696	458
Y	30.5	27.1	27.6	27.0	31.7	30.3	30.4	27.2	16.1	16.2	11.7	21.5	19.2	20.4	12.5	27.2	25.7	19.2	18.6
Zr	195.5	181.1	182.1	183.2	209.1	195.3	197.6	163.9	180.3	179.7	154.8	149.7	188.4	167.5	163.2	213.9	212.4	190.7	160.1
Nb	14.3	15.6	14.0	14.6	12.7	14.2	13.4	14.3	15.0	14.9	9.9	13.0	13.4	12.9	10.7	15.9	15.7	17.4	13.5
Ba	329	452	356	340	288	334	312	449	556	599	589	742	471	491	545	474	460	609	670
Hf	3.9	4.0	3.9	3.5	4.3	3.8	3.9	3.7	3.8	3.8	3.5	3.3	4.3	3.6	3.7	4.6	4.6	3.9	3.6
Ta	0.7	0.8	0.8	0.7	0.7	0.7	0.7	0.7	0.8	0.8	0.6	0.8	0.8	0.7	0.7	0.8	0.8	0.8	0.7
Pb	4.6	6.6	5.5	5.1	4.3	4.6	4.7	8.0	9.0	9.6	11.6	10.6	8.9	8.3	11.1	8.7	8.0	11.8	9.9
Th	2.2	3.8	3.1	2.7	2.8	2.6	2.6	4.9	5.7	5.9	7.5	11.4	8.7	5.0	8.3	5.5	5.5	8.0	9.3
U	0.7	0.9	0.3	0.8	0.3	0.8	0.6	1.2	1.3	1.4	1.9	2.0	2.2	1.3	2.2	1.5	1.4	1.8	1.7
La	22.7	35.4	27.5	24.3	21.2	23.6	20.4	31.8	33.3	36.6	27.4	38.7	26.7	27.8	26.1	31.0	28.5	38.3	26.4
Ce	45.6	66.2	51.1	47.1	43.0	47.0	42.1	54.6	58.1	62.7	46.3	63.6	48.2	50.9	46.0	55.8	52.1	66.3	62.0
Pr	5.2	8.5	6.9	6.3	6.3	6.6	6.0	5.9	5.7	6.1	4.5	7.5	5.9	6.4	5.5	5.9	5.5	6.6	7.2
Nd	24.7	31.3	26.8	23.7	25.1	26.0	23.9	26.6	23.3	25.2	18.6	25.4	20.7	22.7	18.7	26.7	24.7	27.7	24.5
Sm	5.3	5.9	5.3	4.7	5.4	5.4	5.2	5.0	3.9	4.2	3.1	4.3	3.9	4.2	3.2	5.1	4.8	4.5	4.2
Eu	1.7	1.7	1.7	1.5	1.7	1.7	1.7	1.4	1.1	1.2	0.9	1.3	1.1	1.2	0.9	1.5	1.5	1.3	1.2
Gd	5.6	5.8	5.6	4.9	5.9	5.7	5.7	5.0	3.6	3.8	2.8	4.2	3.9	4.3	3.1	5.2	4.8	4.3	3.9
Tb	0.8	0.9	0.9	0.7	0.9	0.9	0.9	0.8	0.5	0.5	0.4	0.6	0.6	0.6	0.4	0.8	0.7	0.6	0.6
Dy	4.9	4.9	4.9	4.3	5.3	5.0	5.1	4.3	2.6	2.7	1.9	3.4	3.3	3.4	2.1	4.5	4.2	3.1	3.2
Ho	1.0	1.0	1.0	0.9	1.1	1.0	1.0	0.9	0.5	0.5	0.4	0.7	0.7	0.7	0.4	0.9	0.9	0.6	0.6
Er	2.7	2.7	2.7	2.4	2.9	2.7	2.8	2.4	1.4	1.4	1.0	0.9	1.8	1.8	1.1	2.5	2.3	1.6	1.7
Tm	0.4	0.4	0.4	0.4	0.5	0.4	0.5	0.4	0.2	0.2	0.2	0.3	0.3	0.3	0.2	0.4	0.4	0.3	0.3
Yb	2.7	2.6	2.7	2.5	2.9	2.7	2.8	2.4	1.4	1.4	1.0	1.9	1.8	1.9	1.1	2.5	2.3	1.6	1.8
Lu	0.4	0.4	0.4	0.4	0.4	0.4	0.5	0.4	0.2	0.2	0.2	0.3	0.3	0.3	0.2	0.4	0.4	0.3	0.3

LOI = loss on ignition; b.d. = below detection

Table 2

[Click here to download Table: Neilletal Table2.docx](#)

Table 2. Measured Nd and Sr isotope compositions of the valley, ridge, and cone series, Shirak.

	$^{143}\text{Nd}/^{144}\text{Nd}$	$\pm 1\sigma$	ϵNd	$\pm 1\sigma$	$^{87}\text{Sr}/^{86}\text{Sr}$	$\pm 1\sigma$
Valley series						
S14.5	0.512831	0.000004	+3.76	0.08	0.704349	0.000009
S19.1	0.512864	0.000005	+4.41	0.10	0.704188	0.000007
S25.2	0.512850	0.000006	+4.14	0.12	0.704279	0.000007
S26.2	0.512862	0.000006	+4.37	0.12	0.704157	0.000008
S28.1	0.512845	0.000005	+4.04	0.10	0.704229	0.000008
S29.1	0.512857	0.000005	+4.27	0.10	0.704168	0.000007
Ridge series						
S4.2	0.512830	0.000007	+3.75	0.14	0.704309	0.000007
S5.1	0.512802	0.000007	+3.20	0.14	0.704352	0.000008
S6.1	0.512806	0.000005	+3.28	0.10	0.704388	0.000010
S9.2	0.512802	0.000005	+3.20	0.09	0.704282	0.000008
S21.1	0.512848	0.000004	+4.10	0.08	0.704279	0.000006
S23.1	0.512871	0.000005	+4.55	0.10	0.704206	0.000007
S30.2	0.512796	0.000005	+3.08	0.10	0.704338	0.000010
S30.3	0.512814	0.000005	+3.44	0.10	0.704276	0.000007
Cone series						
S1.1	0.512831	0.000005	+3.76	0.10	0.704321	0.000007
S2.1	0.512824	0.000005	+3.63	0.10	0.704329	0.000007
S7.3	0.512830	0.000003	+3.75	0.06	0.704461	0.000007
S20.2	0.512838	0.000004	+3.90	0.09	0.704293	0.000007

Supplementary Item 1

[Click here to download Background dataset for online publication only: NeilletalSUP1photomicrographs copy.pdf](#)

Supplementary Item 2

[Click here to download Background dataset for online publication only: Neilletal Shirak SUP 2.xlsx](#)